DENSITY MATRIX THEORY AND COMPUTATIONAL ASPECTS OF ATOMIC COLLISIONS INCLUDING SPIN-ORBIT RECOUPLING

By

ANDRÉS REYES

A DISSERTATION PRESENTED TO THE GRADUATE SCHOOL
OF THE UNIVERSITY OF FLORIDA IN PARTIAL FULFILLMENT
OF THE REQUIREMENTS FOR THE DEGREE OF
DOCTOR OF PHILOSOPHY

UNIVERSITY OF FLORIDA

2003

ACKNOWLEDGMENTS

I would like to thank my thesis adviser, Prof. David Micha, for giving me the opportunity to be a part of this project and for his support and guidance.

A boundless amount of gratitude must be expressed to my friends and colleagues in the group and in the office: Alberto Santana for his willingness to offer me his helping hand, for his advice and his friendship; Brian Thorndyke for his advice and Alex Pacheco for his friendship; Wilfredo Ortiz for his friendship, humor and his CDs.

I would like to express to gratitude to the two greatest: my "chief," Dr. Keith Runge, for his wise advice and resourceful insight, and Dr. Ajith Perera for his friendship and the helpful comments. I also want to acknowledge Dr. Jorge Morales for his friendship and advice when I was a new graduate student at QTP and Dr. Akbar Salam for his friendship.

A special appreciation goes to Prof. Samuel Trickey and Dr. Adrian Roitberg for their support and for being nice people to me.

I want to express my profound appreciation of Prof. Gustavo Sanchez at Universidad del Valle (Colombia) for teaching me that there was a way and for encouraging me to pursue graduate studies.

I thank Lina, my wife, for her love and support and Laura, my daughter, for being my source of inspiration. Thanks go to them for constantly reminding me that there are beautiful things in life outside of NPB 2323.

I do not want to forget to mention my friends in the neighborhood (Cali-Colombia) for their unconditional support.

TABLE OF CONTENTS

page

ACKNOWLEDGMENTS iii

LIST OF TABLES vii

LIST OF FIGURES viii

ABSTRACT xi

CHAPTER

1 INTRODUCTION 1

1.1 Overview of Experimental Work 1
1.2 Overview of Theory 2
1.3 Overview of Theoretical Studies in Alkali-Rare-Gas Interactions . 3
1.4 Our Approach 5
1.5 Systems To Be Studied 5
1.6 Outline of the Dissertation 6

2 PSEUDOPOTENTIAL THEORY FOR ALKALI-RARE-GAS ATOM SYSTEMS 8

2.1 Introduction 8
2.2 Pseudopotential Theory 9
2.3 Pseudopotential for Alkali-Rare Gas Atom Systems 11
2.3.1 Hamiltonian 11
2.3.2 Choice of Parameters 14
2.3.3 Choice of Basis Sets 14
2.3.4 Choice of the Core-Core Repulsion Function 16
2.4 Computational Aspects 18
2.4.1 Pseudopotential Matrix Elements in the Static Atomic Basis 18
2.4.2 Programming Details 19
2.5 Results and Discussion 20
2.5.1 Comparison of the LiHe Potential Energy Curves for Different Basis Sets 20
2.5.2 Comparison of LiHe Potential Energy Curves by Addition of Polarization Terms in the Hamiltonian 21
2.5.3 Calculation of the Potential Energy Curves of the LiNe, NaHe and NaNe Systems and Comparisons with Other Theoretical Results 22

3 DYNAMICS OF ALKALI ATOM-RARE GAS ATOM COLLISIONS IN THE KEV RANGE 33

3.1 Introduction 33
3.2 Eikonal/Time Dependent Molecular Orbital Method Including l-Dependent Pseudopotentials 33
3.2.1 Matrix Equations 37
3.2.2 Propagation of the Density Matrix 38
3.2.3 Physical Properties of Interest 40
3.3 Computational Aspects 43
3.3.1 Programming Details 43
3.3.2 Construction of the Density Matrix 43
3.4 Results and Discussion 45
3.4.1 Time-Dependent Study of the Li-He Collision 45
3.4.2 Basis Set Effects 47
3.4.3 Integral Cross Sections for the Li-Ne, Na-He and Na-Ne Systems 48

4 ALKALI ATOMS FINE-STRUCTURE TRANSITIONS INDUCED BY COLLISIONS WITH RARE GAS ATOMS 64

4.1 Introduction 64
4.2 Background 64
4.3 Spin-Orbit Coupling in Atoms 66
4.4 Spin-Orbit Coupling in Diatomic Molecules 68
4.4.1 Spin-Orbit Coupling in Terms of Pseudopotentials 68
4.4.2 Choice of Parameters 70
4.5 The Eik/TDMO Method with Spin-Orbit Coupling 71
4.6 Eik/TDMO-SO in Terms of a General Basis Set 71
4.7 Matrix Equations in the Traveling Atomic Basis 74
4.8 Transformation from the Static to the Traveling Basis Set 75
4.9 Physical Properties of Interest 75
4.10 Computational Aspects 78
4.10.1 Spin-Orbit Integrals 78
4.10.2 Structure of the Program 82
4.10.3 Choice of Initial Conditions 82
4.11 Results and Discussion 85
4.11.1 Pseudopotential Results 85
4.11.2 Pictures of the Evolution of Electronic Angular Momenta . 86
4.12 Fine-Structure Cross Sections 89

5 CONCLUSION 97

5.1 Pseudopotentials 97
5.2 The Eikonal-Time Dependent Molecular Orbital Method Including Pseudopotentials 98

5.3 Spin-Orbit Recoupling 99
5.4 Computational Aspects 100
5.5 Future Work 100

APPENDIX

A FLOW CHART FOR THE EIKTDMOPPSO PROGRAM 101

A.1 Program Features 101
A.2 Subroutine Description 102
A.3 eiktdmoppso Flow Diagram 103

B SUBROUTINE POLAR.F90 107

B.1 Subroutine polar.f90 107
B.1.1 Evaluation of the r^K Integral 107
B.1.2 Special Case b=0 115

C SUBROUTINE SHORT_RANGE.F90 117

C.1 Subroutine short_range.f90 117
C.2 Special Cases 118
C.2.1 $k_A, k_B = 0$ 118
C.2.2 k_A or $k_B = 0$ 119
C.3 Evaluation of the Integrals 120
C.3.1 Angular Integrals 120
C.3.2 Radial Integral 120

REFERENCE LIST 127

BIOGRAPHICAL SKETCH 132

LIST OF TABLES

Table		page
2–1	Pseudopotential parameters for alkali atoms (au)	15
2–2	Pseudopotential parameters for He and Ne (au)	15
2–3	Li atom ionization energies (au) for different basis sets	17
2–4	Alkali-atom ionization energies (au)	17
4–1	Parameters (in au) of the spin-orbit operators for Li and Na.	70
4–2	Spin-orbit splitting for ^2P states (cm^{-1}).	85
4–3	Calculated fine-structure cross sections $\sigma_{j,m_j \to j',m'_{j'}}$ at v^*(400 K)	93
4–4	Calculated fine-structure cross sections $\sigma_{j,m_j \to j',m'_{j'}}$ at v^*(450 K)	95
4–5	Theoretical and experimental results for the total and multipole relaxation cross sections (in $\AA^2$) at 400 and 450 K	96

LIST OF FIGURES

Figure page

2–1 V_{cc} curve for LiHe: A=16.016 and b= 2.4402. 23

2–2 LiHe potential energy curves using basis set II. 24

2–3 LiHe potential energy curves using basis set III. 25

2–4 LiHe potential energy curves using basis set IV. Note that it is almost identical to figure 2–3 within the graphics accuracy. 26

2–5 LiHe potential energy curves comparison: Our results (basis set IV) vs. pseudopotential results from Czuchaj. 27

2–6 LiHe potential energy curves comparison: Our results (basis set IV) vs. ab initio from Behmenburg. 28

2–7 Comparison of the potential energy curves of LiHe. (a) results obtained keeping all the terms of the Hamiltonian; (b) results obtained neglecting the cross-terms; (c) results obtained neglecting all the polarization terms. 29

2–8 LiNe potential energy curves comparison: Our results (basis set IV) vs. ab initio from Behmenburg. 30

2–9 NaHe potential energy curves comparison: Our results vs. ab initio results from Theodorakopoulos. 31

2–10 NaNe potential energy curves comparison: Our results vs. pseudopotential results from Czuchaj. 32

3–1 The collision is taken to occur in the $x - z$ plane, the alkali atom is chosen to be the projectile and we assume that the rare-gas atom is initially at rest. 49

3–2 Trajectories for a 1.0 keV Li atom incident on a He atom target. Comparison of results for three different impact parameters, b = 0.5, 0.75 and 1.0 au. The He target is initially sitting at rest at the origin of coordinates. 50

3–3 Populations of the Li 2s and 2p orbitals vs. time in a 1.0 keV Li-He collision, at b = 1.0 au. 51

3–4 Final orbital populations of Li 2s and 2p orbitals vs. impact parameter in 1.0 keV Li-He collisions. 52

3–5 Alignment parameter vs. time in a Li-He collision (E_{lab} = 1.0 keV, b = 0.5 au). 53

3–6 Alignment parameter vs. time in a Li-He collision (E_{lab} = 1.0 keV, b = 1.0 au). 54

3–7 Alignment parameter vs. time in a Li-He collision (E_{lab} = 1.0 keV, b = 2.0 au). 55

3–8 Orientation parameter vs. time in a Li-He collision (E_{lab} = 1.0 keV, b = 0.5 au). 56

3–9 Orientation parameter vs. time in a Li-He collision (E_{lab} = 1.0 keV, b = 1.0 au). 57

3–10 Orientation parameter vs. time in a Li-He collision (E_{lab} = 1.0 keV, b = 2.0 au). 58

3–11 $2s \rightarrow 2p$ Integral cross sections vs. E_{lab} for Li-He collisions. Comparison of our results using different basis set choices with experiment. 59

3–12 $2s \rightarrow 2p$ Integral cross sections for collisions of Li-He (E_{lab} = 1.0-10.0 keV). Our results (using basis set III) compared with other theories. 60

3–13 $2s \rightarrow 2p$ Integral cross sections in Li-Ne collisions. Comparison of our results with experimental results from Olsen and theoretical results from Manique. 61

3–14 $3s \rightarrow 3p$ Integral cross sections in collisions of Na-He. We present our results and those from Olsen (exp.) and Kimura(theory). 62

3–15 $3s \rightarrow 3p$ Integral cross sections for Na-Ne collisions. We show our theoretical results and those from Olsen (exp.). 63

4–1 Diatomic potential energy curves of Na(^2P)-He, including(solid line) and neglecting (dotted line) spin-orbit interactions. Energies are relative to the asymptotic values neglecting spin-orbit interactions. I: Our results, II: Ab initio results. 87

4–2 Population of the Na($^2P_{j,m_j}$) states as a function of time. 88

4–3 Evolution of $\langle \mathbf{l} \rangle$ for a straight line trajectory. The initial state is Na($^2P_{3/2,3/2}$) 90

4–4 Evolution of $\langle \mathbf{s} \rangle$ for a straight line trajectory. The initial state is Na($^2P_{3/2,3/2}$) 91

4–5 Evolution of $\langle \mathbf{j} \rangle$ for a straight line trajectory. The initial state is $Na(^2P_{3/2,3/2})$ 92

4–6 Transition probabilities vs. impact parameter in a $Na_{3/2.3/2}$+He collision, $v*(450K) = 6.74 \times 10^4$ au 94

A–1 Cycle for printing energies and initializing dynamics. 104

A–2 Relax-and-drive cycle. 105

A–3 Update and continue. 106

Abstract of Dissertation Presented to the Graduate School
of the University of Florida in Partial Fulfillment of the
Requirements for the Degree of Doctor of Philosophy

DENSITY MATRIX THEORY AND COMPUTATIONAL ASPECTS OF ATOMIC COLLISIONS INCLUDING SPIN-ORBIT RECOUPLING

By

Andrés Reyes

May 2003

Chair: David A. Micha
Major Department: Chemistry

A first principles description of electronic excitation and spin-orbit recoupling in alkali-rare-gas atom colliding pairs is developed introducing l-dependent pseudopotentials and including two and three-body polarization terms and the spin-orbit interatomic potential. The treatment combines an eikonal (or short wavelength) approximation for the nuclear motion and time-dependent molecular orbitals to provide interatomic potentials, their non-adiabatic couplings, and state populations during interactions.

Our pseudopotential choice is adequate for these systems in terms of accuracy. A description of the matrix equations and computational details of the pseudopotential code are presented. Results on ionization energies of the Li and Na atoms and the potential energy functions of distance for LiHe, LiNe, NaHe and NaNe are presented. Our results are in excellent agreement with experiment and other theories.

The theory of the eikonal time-dependent molecular orbital (Eik/TDMO) method in terms of pseudopotentials is presented as well as a detailed description of the computational approach. We study the time-dependence of orbital alignment, orientation and population. We discuss the effects of the basis set size on the calculations,

and compare our results with experiment and other calculations. Our integral cross sections for LiHe, LiNe, NaHe and NaNe, obtained with a large basis set, are in excellent agreement with experiment.

The theory for recoupling of angular momenta in alkali-rare-gas atom thermal collisions is developed and the computational aspects of the spin-orbit coupling code in terms of pseudopotentials are presented. Results for the spin-orbit splitting of the ^2P states of Li and Na are presented along with fine-structure cross sections for collisions at 400 and 450 K. The agreement with experiment and other theories is very good.

CHAPTER 1
INTRODUCTION

This study is part of a broader effort to bring new insights into the time-dependence of collision of quasi-one-electron systems. We are particularly interested in studying the time-dependence of electronic excitation and the time-dependence of spin-orbit coupling in slow alkali-rare gas atom collisions.

The work developed in this dissertation is related to phenomena of experimental interest, such as pressure broadening of spectra in condensed matter and kinetics in hot gases and plasmas.[1–5] In a related area, the optical spectroscopy of alkali atoms in rare gas atom clusters has been the focus of recent research, particularly in connection with spectra in liquid helium.[6–9]

It is of conceptual value to gain a fundamental understanding of the most basic time-dependent aspects of the rearrangement phenomena in simple systems where detailed studies can be carried out.

Alkali-rare gas atom collisions constitute a particularly important subject of study. In addition to the fundamental interesting questions they pose, they are at the heart of a large number of applications in such areas as laser systems, surface interactions, chemical reactions, energy transfer and others.[10]

In particular, we are interested here in studying the time-evolution of electronic excitation and spin-orbit recoupling of Li and Na in collisions with He and Ne in terms of a formalism developed to consider our many electron system as a one-active electron system.

1.1 Overview of Experimental Work

Over the last thirty years, several experimental results for these systems have improved our current understanding of the electronic rearrangement phenomena.

Overviews of those studies are available in the literature.[11,12] Experimentalists have been able to select the initial states of colliding species to perform collisions at specific energies. The level of control in experiments has reached the point at which theoretical results from first principles calculations can be of help in the interpretation of experiments.[5]

Excitation of the alkali projectile in the energy range from a fraction of a keV to 100 keV has been investigated. Representative studies for emission cross sections, alignment and polarization[13–16] have partly revealed the mechanisms responsible for the observed excitations.

The literature on experimental aspects of spin-orbit effects in gas-phase chemical reactions done before mid-80's has been reviewed.[17,18] More recently, some experimental work has been done to understand the role of spin-orbit coupling in the stereochemical behavior of larger systems. The use of spin-polarized beams is bringing new insights because collisions can be studied in specific spin states. The use of coincidence detection allows observation of a larger number of parameters. The ability to use the polarization of lasers to prepare highly aligned, or directional, reagents has opened new possibilities in the area of orbital stereochemistry. Recent advances in laser pump-probe techniques have been applied to the study fine-structure changing in collisions of alkali atoms with rare gases.[19,20] Important advances in experimental spectroscopic studies of alkali atoms attached to large rare-gas atom clusters have allowed probing and modeling as the alkali atom is excited or deexcited.[6–9]

1.2 Overview of Theory

The field of quantum molecular dynamics has seen unparalled development over the last three decades. Methods for the solution of the time-dependent Schrödinger equation for atomic collisions process abound in the literature. However the majority of these methods make use of the central dogma in both time-dependent and

time-independent calculation of molecular properties and reaction rates: the Born-Oppenheimer (BO) approximation. The BO approximation is invoked to separate the Schrödinger equation for the whole system into two separate equations to be solved independently: one for the electrons and another one for the nuclei. Time-dependent methods can be classified in two groups based on the way that they approximate the molecular time-dependent Schrödinger equation. The first group consists of methods that solve the time-dependent Schrödinger equation for the nuclear degrees of freedom subject to known potential energy surfaces (PES), while in the second group the electronic and nuclear degrees of freedom are propagated simultaneously. This is different from finding the solution for the electronic problem along a nuclear trajectory. The eikonal time-dependent Hartree-Fock method (Eik/TDHF) method[21–24] and the electron nuclear dynamics method (END)[25] can be cataloged in the second group.

Because of the success of methods in the first group for the study of collisional systems, explicit time-dependent calculations for both electrons and nuclei have not become common practice. However, there is a lot to gain from these approaches as a much clearer picture of excitation mechanism can be drawn from time-dependent simulations. For example, in collisions involving excitation or charge transfer, following how charge changes with nuclear configuration over time can offer insight into mechanisms.

First principles methods of full dynamics have some obvious advantages when compared to other methods: there is no need to use inconvenient coordinate systems because atomic cartesian coordinates are used throughout and there is also no need to construct potential energy surfaces.

1.3 Overview of Theoretical Studies in Alkali-Rare-Gas Interactions

A complete and rigorous theory of these processes involves calculation of the full quantum wave function ψ describing the motion of the nuclei and active electron

with solutions of close-coupling scattering equations. This formulation has been implemented by different authors.[4,26–31]

The atomic-state expansion method was used by Andersen and Nielsen[32] for Li and Na with He and Ne collision. There, they adopted various semiempirical model potentials or the pseudopotential proposed by Bottcher[33] and Baylis[34] to obtain electronic wavefunction with which to carry out the close-coupling calculations. They also used a frozen core Hartree-Fock potential. Their calculated integral cross sections agree well with experiment. However the shape of the cross sections differs from the experimental measurements in the low-energy region.

More recent calculations by Kimura and Pascale[35] present results for the integral cross sections of the alkali atom-He system in the low keV energy regime. Their results are obtained with a close-coupling method including electron translation factors and straight line trajectories. The agreement with experiment is good for LiHe and NaHe. For KHe and CsHe the results are only qualitatively good. More recently Archer et al[2] presented results on the orientation and alignment of LiHe and NaHe collisions.

The close-coupling method is known to give accurate cross sections; however it has some disadvantages because the formulation of the theory and the long numerical codes are complex, and physical insight can be lost when many states are coupled. A more intuitive, though less rigorous, semiclassical model has successfully been used to study these systems.

A strong coupling approximation to obtain analytic formulas for the cross sections of fine-structure transitions in the Na-Ar system is presented in Nikitin.[36] Some authors preferred to numerically solve equations for the Na-He system using a semiclassical impact parameter method,[37,38] later refined[39] to take into account trajectory effects. More recently[40] a semiclassical formalism was used to monitor the expectation values of the orbital and spin angular momentum vectors.

1.4 Our Approach

The Eik/TDMO method developed in our group is a semi-classical method that uses a combination of the eikonal and the TDMO approximations. Starting with an eikonal representation of the total wave function, a wave function is constructed from the classical trajectories and the TDMO formulation is developed in terms of a density operator. The coupling of the density operator to nuclear motions is solved with a "relax and drive" procedure[21,22] that couples the fast (electronic) and slow (nuclear) degrees of freedom. We have made this one-electron method capable of studying the quasi-one electron system where the valence electron has been described explicitly while its interaction with the alkali core and the rare gas atom has been described with l-dependent atomic pseudopotentials.[41,42]

1.5 Systems To Be Studied

This dissertation studies the first-principles molecular dynamics of the alkali-rare-gas atom colliding pair. We will concentrate on two different energy regimes:

A high energy regime (with collision energies between 500 eV and 30 keV) in which we study the electronic excitation of the alkali atom M from the ground state to any excited state

$$M(nl) + Rg \rightarrow M(n'l') + Rg,$$

where n and l are the principal and orbital quantum numbers and M = Li, Na and Rg = He, Ne. We will monitor the time-dependence of the atomic populations and orbital alignment and orientation and we will also calculate final state-to state integral cross sections. The terms orientation and alignment refer to parameters related to the shape and dynamics of an excited atomic or molecular level, as it is manifested in a non-statistical population of the magnetic sublevels.

Hyperthermal energy regime (with energies of only a fraction of an eV) where we will study the recoupling of angular momenta in collisions of excited Na with He.

These collisions may result either in reorientation

$$Na^*(^2P_{J,M_J}) + He \rightarrow Na^*(^2P_{J,M'_J}) + He \tag{1.1}$$

or in intramultiplet transitions

$$Na^*(^2P_{J,M_J}) + He \rightarrow Na^*(^2P_{J',M'_{J'}}) + He \tag{1.2}$$

with energy transfer

$$\Delta E = E_{J,M_J} - E_{J',M'_{J'}}, \tag{1.3}$$

where we have used the labels J for the total electronic angular momentum and M_J for its projection. At these low energies these are the only processes which occur with appreciable probability.[11] Spin-orbit coupling plays an important role in both processes. To get a complete picture of the collisional processes, we we will monitor the expectation values of the electronic orbital $\langle \mathbf{l} \rangle$, spin $\langle \mathbf{s} \rangle$ and total $\langle \mathbf{j} \rangle$ angular momentum vectors along a trajectory.

1.6 Outline of the Dissertation

Chapter 2 gives a general introduction to the pseudopotential theory and discusses in more detail the pseudopotential method used in this dissertation. In that chapter, we concentrate on the evaluation of the hamiltonian matrix elements. We also discuss the effects of the basis set size on the calculated energies. We explain the computational aspects of the pseudopotential code and finally compare our calculated ionization energies for Li and Na with other theories and experiments as well as the potential energy curves of the alkali-rare-gas atom systems: LiHe, LiNe, NaHe and NaNe.

Chapter 3 generalizes the eikonal time-dependent molecular orbital (Eik/TDMO) method[23,24] to include pseudopotentials (Eik/TDMO-PP). Theory and computational details are introduced in this chapter. The calculation of some time-dependent

physical properties such as electronic populations and orientation and alignment parameters are reviewed here too. Calculations of time-dependent properties and also of the excitation integral cross sections are presented along with their comparison to experiments and other theories.

In Chapter 4, the problem of recoupling of angular momenta in thermal alkali-rare-gas atom collisions is formulated within a formalism based on the Eik/TDMO-PP method that includes spin-orbit coupling (Eik/TDMO-PP-SO). The evaluation of the spin-orbit coupling matrix elements, and related computational aspects are exposed. Results for the spin-orbit coupling splitting of alkali atoms and the potential energy curve of the Na-He system are presented as well as some encouraging results on the fine-structure cross sections at 400 and 450 K. Pictures of the time evolution of the angular momenta vectors are presented here too.

Chapter 5 summarizes the main conclusions obtained in this dissertation.

Appendix A presents the flow diagram of the Eik/TDMO code, which includes pseudopotentials and spin-orbit coupling. It also contains some information about the main modules of the program.

Appendix B explains in detail the procedure we used to solve the polarization interaction integrals of our pseudopotential.

Appendix C gives a detailed explanation of the solution of the short-range interaction integrals in terms of Cartesian Gaussian functions present in our choice of pseudopotential.

CHAPTER 2
PSEUDOPOTENTIAL THEORY FOR ALKALI-RARE-GAS ATOM SYSTEMS

2.1 Introduction

Much experimental and theoretical work has been devoted in the last forty years to the study of various processes occurring in collisions between ground state or excited state alkali atoms and ground state rare-gas (Rg) atoms at a wide range of energies. From the experimental perspective, the processes of interest have been inter-doublet and intra-doublet transitions, quenching, redistribution, pressure spectral line broadening, etc.

Because the interatomic interactions are the main physical quantities needed for a good understanding of these collisional processes, much effort has been devoted to calculating or experimentally determining the adiabatic potentials of the alkali-Rg systems.

Standard ab initio all-electron calculations of the adiabatic potentials, which in principle can be very accurate when enough electronic configurations are included in the calculation, become rapidly difficult to perform as the number of electrons in the atomic cores increase. Calculations using pseudopotentials offer a very interesting alternative to treat the problem. They take advantage of the fact that the alkali core and Rg atom have closed-shell structures to reduce the problem of the alkali-Rg interaction to a three-body problem.

This chapter gives a general introduction to the pseudopotential theory and discusses in detail the pseudopotential method to be used in this work. It also reports some encouraging results for the ionization energies of Li and Na and for the potential energy curves (PECs) of some alkali-rare gas (alkali-Rg) diatomic systems. Details on the implementation of the computer code are also included.

2.2 Pseudopotential Theory

In many problems of atomic and molecular physics the electrons of the system can be divided into valence and core electrons. It is natural to try to reduce those problems from a mathematical N-electron problem, where the N is the total number of electrons, to an n-electron problem, where n is the number of valence electrons. Since in many cases $n \ll N$, such reductions mean a significant conceptual and mathematical simplification.

Hellmann,[43] Hellmann and Kassatotschkin[44] and Gombas[45] were the first to demonstrate, using the Thomas -Fermi model, that the Pauli exclusion principle for the valence electrons can be replaced with an effective potential. Since the requirement that the valence orbital be orthogonal to the core orbital is equivalent to the Pauli exclusion principle, they replaced the need for orthogonality by the effective potential. The introduction of the effective potential represents a considerable mathematical simplification, since the orthogonality requirement between valence and core wave functions may lead to difficulties, especially in the case of large cores.[46]

Later, in 1959, Phillips and Kleinman[47] provided a rigorous basis for replacing the explicit core-valence orthogonality constraints by a modification of the valence Hamiltonian. The usefulness of the Hellmann and the Phillips-Kleinman approaches is that they provide the theoretical basis for the subsequent development of effective potentials.

From a mathematical point of view the pseudopotential methods can be divided into two groups: ab initio and model methods. The ab initio methods differ from the model methods in that parametric functional forms are not assumed for the potential. Rather, its form is abstracted directly from the atomic Hartree-Fock equations upon use of a specific pseudo-orbital transformation. Examples for ab initio methods are those proposed by Kahn et al.,[48] later improved by Hay et al.[49] Model

pseudopotentials are effective potentials that appear from simplifications made on ab initio pseudopotentials. In general, they can be semi-empirical when they contain adjustable parameters determined from experimental data, or non-empirical when they do not require experimental data for their construction, as in the case of density-dependent pseudopotentials.[50]

Regardless of their differences, all the pseudopotential methods have in common:

1) The potential should be asymptotically correct for large electron-nucleus distance r, at least to the order of $1/r$ and preferably higher orders.

2) The Hamiltonian operator eigenvalues should accurately reproduce the observed spectra of the appropriate single-valence electron system. There should be no eigenvalues corresponding to the core orbitals of the physical system.

3) The potential should be simple so that it can be easily constructed. An analytic form involving a small number of parameters is most convenient. This analytic form should be applicable to many atomic systems, through suitable choice of the parameters.

4) The potential should not be large in magnitude in the core region. This is desirable to avoid computational difficulties, and is particularly important for molecular applications. In the case of l-dependent pseudopotentials, where l is the orbital angular momentum of the core electrons, for each value of l one introduces one or two adjustable parameters and so can reproduce exactly the experimental energy for two levels. With two parameters for each l-value it is usually possible to obtain an excellent fit to all valence state energies.

The true utility of effective potentials is that they provide a method for reducing substantially the number of calculations, making possible calculation on large molecules and on molecules containing heavy atoms. We have taken advantage of

that feature in the study of electronic excitations and electronic angular recoupling in collisions of alkali (Li and Na) and Rg (He and Ne) atoms.

Extensive pseudopotential molecular-structure calculations for all the alkali-Rg systems have been done using l-independent Gombas-type statistical pseudopotentials.[34,51–53] Although these calculations yielded reasonable potentials for the systems involving heavy Rg atoms, they fail badly in the case of He and Ne. An improvement was achieved by applying the l-dependent pseudopotential technique[42,54] for LiHe,[3,42] LiNe[31,41] and NaNe.[41,54,55] Encouraged by the accuracy of those results we applied the l-dependent pseudopotential method for the calculation of the adiabatic potentials and couplings of alkali-Rg systems.

2.3 Pseudopotential for Alkali-Rare Gas Atom Systems

The fact that an alkali core and an Rg atom have closed-shell structures allows us to reduce a many-body problem to a three-body problem (alkali core, valence electron and Rg atom). The interaction between the valence electron and both the alkali core and the Rg atom is then represented by a pseudopotential and if desired, it can also include polarization terms in order to account for the valence electron-core correlation effects. In the approach that we have chosen, the effect of the core electrons of both the alkali atom and the Rg atom is simulated by an l-dependent semi-empirical pseudopotential including core polarization.[41] This pseudopotential is composed of two parts: the l-dependent short-range term, and the polarization potential containing a cutoff parameter.

2.3.1 Hamiltonian

Let us recall that the alkali-Rg atomic pair is represented by a three-body system (alkali core, Rg atom and alkali valence electron). The Hamiltonian for the one electron alkali-Rg system at a given internuclear distance R and without

spin-orbit coupling is (in atomic units)

$$\hat{H}_{el}^{PP} = -\frac{1}{2}\nabla_{r_A}^2 + \hat{V}_{el}^{PP}, \tag{2.1}$$

$$\hat{V}_{el}^{PP} = V_A(\mathbf{r}_A) + V_{AB}(\mathbf{r}_A, \mathbf{R}), \tag{2.2}$$

where, in general, $\mathbf{r}_X$ $(X = A, B)$ is the position vector of the alkali valence electron e^- with respect to the alkali core (A) or the Rg atom (B), and $\mathbf{R}$ is the position vector of B with respect to A. The term $V_A(\mathbf{r}_A)$ describes the interaction between the valence electron and the alkali core and is given by

$$V_A(\mathbf{r}_A) = \frac{Z_A^c}{r_A} + V_A^{pol}(r_A) + V_A^{sr}(\mathbf{r}_A). \tag{2.3}$$

Here Z_A^c is the net charge of the alkali core seen by e^- at an infinite distance and V_A^{pol} is the polarization potential,

$$V_A^{pol}(r_A) = -\frac{\alpha_A^c}{2r_A^4} w(r_A, \delta_c)^2, \tag{2.4}$$

where α_A^c is the dipole polarizability of the alkali core and w stands for a cutoff function defined by

$$w(r, \delta_c) = 1 - \exp(-\delta_c r^2), \tag{2.5}$$

with an adjustable cutoff parameter δ_c. The last term in Eq. 2.3 is the so-called semi-local (l-dependent) pseudopotential, which is given here as

$$V_X^{sr}(\mathbf{r}_X) = \sum_{l,i} B_{l,i} \exp(-\beta_{l,i} r_X^2) P_{l,X}, \tag{2.6}$$

where B_{li} and $\beta_{l,i}$ are pseudopotential parameters adjusted to experimental data and $P_{l,X}$ stands for the projection operator on angular symmetry l,

$$P_{l,X} = \sum_m |\, Y_{lm}(\hat{\mathbf{r}}_X)\rangle\langle Y_{lm}(\hat{\mathbf{r}}_X)\,|\,. \tag{2.7}$$

The vector $|\, Y_{lm}(\hat{\mathbf{r}}_X)\rangle$ represents a spherical-harmonic function centered on the core X ($\hat{\mathbf{r}}_X = \mathbf{r}_X/r_X$) . In turn, the term V_{AB} in Eq. 2.2 describes the interaction between the alkali atom and the Rg atom and is represented as

$$V_{AB}(\mathbf{r}_A, \mathbf{R}) = V_B(\mathbf{r}_B) + V_{ec}(\mathbf{r}_A, \mathbf{R}) + V_{cc}(R). \tag{2.8}$$

The term $V_B(\mathbf{r}_B)$ ($\mathbf{r}_B = \mathbf{r}_A - \mathbf{R}$) describes the interaction between the valence electron and the Rg atom and is given by

$$V_B(\mathbf{r}_B) = V_B^{sr}(\mathbf{r}_B) - \frac{\alpha_B^d}{2r_B^4} w(r_B, \delta)^4 - \frac{\alpha_B^{q\,\prime}}{2r_B^6} w(r_B, \delta)^6. \tag{2.9}$$

The parameter $\alpha_B^{q\,\prime}$, is defined as $\alpha_B^{q\,\prime} = \alpha_B^q - 6\beta_1$, where β_1 is the dynamical correction to the static quadrupole polarizability of the Rg atom. The short-range term $V_B^{sr}(\mathbf{r}_B)$ is defined as by Eq. 2.6. In turn, the term V_{ec} in Eq. 2.8 is the so-called cross-term, which arises from the polarization of B by both e^- and A, and is given by

$$V_{ec}(\mathbf{r}_A, \mathbf{R}) = Z_A^c \alpha_B^d \frac{P_1(\cos\theta)}{R^2 r_B^2} w^2(r_B, \delta) + Z_A^c \alpha_B^q \frac{P_2(\cos\theta)}{R^3 r_B^3} w^3(r_B, \delta), \tag{2.10}$$

where P_1, and P_2, are the Legendre polynomials and θ is the angle between the vectors $\mathbf{R}$ and $\mathbf{r}_B$.

Finally, the core-core interaction is assumed to have the form

$$V_{cc}(R) = V_{cc}^{sr}(R) - \frac{1}{2}\frac{\alpha_B^d}{(R^2 + d_B^2)^2} - \frac{1}{2}\frac{\alpha_B^{q\,\prime}}{(R^2 + d_B^2)^3}, \tag{2.11}$$

where the short-range part $V_{cc}^{sr}(R)$ can be calculated with different methods.[34,42,56,57] Our choice for the V_{cc}^{sr} was based on a more practical approach discussed later in this chapter. The parameters α_B^d , $\alpha_B^{q\,\prime}$ and d_B for He and Ne are available in the literature. In more sophisticated calculations the V_{cc} term can include exchange effects, Coulomb interaction as well as the dispersion forces.

2.3.2 Choice of Parameters

The pseudopotential parameters for alkali atoms employed for (Li, Na) were taken from Fuentealba et al.[58] (see Table 2–1). These parameters were determined by adjusting the calculated atomic energies to the corresponding experimental ionization energies.[59] The pseudopotential parameters of the Rg atoms (He, Ne) were obtained from Czuchaj et al.[41] (see Table 2–2). They were determined by fitting the experimental l-wave scattering phase shifts together with the scattering length, considered currently to be the best available, for e^-–He (Ne, Ar) elastic scattering in the very low energy region.

The long-range polarization potentials contain the cutoff functions. They are simply expressed as suitable powers of the function defined by Eq. 2.5 with the cutoff parameter δ assumed to be the same for both the dipole and quadrupole interaction terms.

The Gaussian form of the short-range part $V_B^{sr}(\mathbf{r}_B)$ of the effective potential is one of the most widely encountered in the literature. Because the term $V_B^{sr}(\mathbf{r}_B)$ represents an effective potential acting between the scattered electron and the atom in the core region, its precise form is not essential for reproducing experimental scattering phase shifts. Rather the form of $V_B^{sr}(\mathbf{r}_B)$ is motivated by subsequent use of the pseudopotentials in molecular calculations.

2.3.3 Choice of Basis Sets

We have chosen Cartesian Gaussian functions $g_{lk}(\mathbf{r};\alpha_{jl,k})$, $j = 1, 2, \ldots, N_l$, to represent static atomic functions with quantum number (l) and s-, p-, and d-symmetry given by a k index,

$$\chi_{jlk}(\mathbf{r},\alpha_{jl,k}) = \sum_{k=1}^{K_{jl}} d_{jl,k} g_{lk}(\mathbf{r};\alpha_{jl,k}), \tag{2.12}$$

providing segmented contracted combinations of Gaussians with exponents α and coefficients d obtained from the literature. There are several choices of Cartesian

Table 2–1: Pseudopotential parameters for alkali atoms (au)

	α_A^c	δ_c	l	B_l	β_l
Li	0.1915	0.831	0	5.786	1.276
			1	- 1.065	1.607
Na	0.9947	0.62	0	10.839	1.378
			1	2.303	0.6639
			2	- 1.777	0.9249
K	5.354	0.29	0	13.564	0.853
			1	2.648	0.3696
			2	-4.517	0.6639

Table 2–2: Pseudopotential parameters for He and Ne (au)

	α_B^d	α_B^q	β_1	δ	l	i	B_l	β_l
He	1.3834	2.3265	0.706	0.79	0	1	0.83	1.30
					0	2	2.27	0.50
					1	1	-0.12	0.75
					1	2	-1.87	1.00
Ne	2.663	6.458	1.27	1.00	0	1	2.50	0.71
					1	1	10.00	5.20
					1	2	1.22	0.41
					2	1	-4.50	1.00

Gaussian basis sets available in the literature, but they are not accurate in all of the cases. The basis sets we have used for Li and Na were optimized in the pseudopotential calculation of the ionization energies of the ground and several excited states of s-, p- and d- symmetries of those alkali atoms. For Li, we found two finite basis sets, in the usual notation (uncontracted/contracted) Cartesian Gaussian functions of s-, p- and d-type, optimized for our pseudopotential: a small (4s4p/2s2p) basis was taken from the MOLPRO webpage and a big (9s9p5d/7s7p5d) basis taken from Czuchaj et al.[3] For Na we found a (13s12p4d/10s8p4d) basis in Czuchaj et al.[41] The small basis sets obtained from the MOLPRO webpage are meant to reproduce well only the ground state energy and the first excited state of the alkali atom.

As a first numerical test of the accuracy of our pseudopotential we present some results for the ionization energies of Li and Na. Table 2–3 shows the dependence of the ionization energies of Li on the basis sets. Basis set (4s4p/2s2p) reproduces well the ground state energy of Li. For the other calculations we started with a contracted (9s9p5d/7s7p5d) basis set[3] and the remaining choices were obtained by removing functions from that original basis.

In Table 2–4 we summarize our best ionization energies for Li and Na. Our results are in excellent agreement with the experiment.

2.3.4 Choice of the Core-Core Repulsion Function

Finally, we consider the alkali ion-Rg interaction, which is necessary to obtain the true adiabatic potentials. The short-range term $V_{cc}^{sr}(R)$ occurring in Eq. 2.11 is the most difficult one for evaluation and seems to be the main source of error in the estimation of $E_i(R)$ in the intermediate range of the internuclear separation. It can be experimentally deduced from mobility and beam scattering measurements. Theoretically it is calculated mainly on the basis of the electron-gas model. In previous calculations it has been obtained on the basis of the statistical Gombas-Baylis

Table 2–3: Li atom ionization energies (au) for different basis sets

Term	Exp.[59]	7s6p3d	6s6p5d	5s5p4d	4s4p3d	2s2p
Li(2s) ^2S	0.198142	0.198030	0.198029	0.198026	0.198023	0.198067
Li(2p) ^2P	0.130236	0.130197	0.130197	0.130197	0.130197	0.130078
Li(3s) ^2S	0.074182	0.074086	0.074086	0.074053	0.032669	0.040740
Li(3p) ^2P	0.057236	0.057169	0.057168	0.057162	0.056870	-.0687640
Li(3d) ^2D	0.055606	0.055548	0.055548	0.055493	0.043098	
Li(4s) ^2S	0.038616	0.038514	0.038510	0.038517	0.015093	
Li(4p) ^2P	0.031975	0.031895	0.031891	0.031652	-0.14235	

Table 2–4: Alkali-atom ionization energies (au)

Li term	9s9p5d	Exp.[59]	Na term	10s8p4d	Exp.[59]
Li(2s) ^2S	0.198115	0.198142	Na(3s) ^2S	0.188837	0.188858
Li(2p) ^2P	0.130127	0.130236	Na(3p) ^2P	0.111559	0.111560
Li(3s) ^2S	0.074176	0.074182	Na(4s) ^2S	0.071579	0.071579
Li(3p) ^2P	0.057111	0.057236	Na(3d) ^2D	0.055786	0.055941
Li(3d) ^2D	0.055482	0.055606	Na(4p) ^2P	0.050944	0.050938
Li(4s) ^2S	0.038614	0.038616	Na(5s) ^2S	0.037483	0.037585
Li(4p) ^2P	0.031886	0.031975	Na(5p) ^2P	0.028008	0.029199

model.[34] In more recent calculations Kim and Gordon[56] and Patil[57] reproduced the minima of the $^2\Pi$ term very well.

We have opted instead to use a pragmatic approach to calculate the $V_{cc}^{sr}(R)$ term: first, we subtract our ground state PEC of the alkali-Rg system (omitting the energy contribution from the V_{cc}) from the most accurate curve available in the literature. The curve we obtain, which represents the core-core contribution, is then fitted using a function of adjustable parameters A and b

$$V_{cc}^{sr}(R) = \frac{Ae^{-bR}}{R}. \tag{2.13}$$

Here R is a scalar that stands for the internuclear distance between the two atoms. Figure 2–1 shows how the parameters were obtained for the Li-He pair. The energy curve $2s\sigma$ without V_{cc} corresponds to the molecular ground state curve of the Li-He without the core-core contribution; $2s\sigma$ Behmenburg is the ground state curve for the Li-He system taken from an ab initio calculation by Behmenburg et al.;[4] $2s\sigma$ with V_{cc} is the energy curve of the molecular ground state including the core-core energy contribution.

2.4 Computational Aspects

2.4.1 Pseudopotential Matrix Elements in the Static Atomic Basis

The Hamiltonian matrix elements including pseudopotential (neglecting spin-orbit coupling) are obtained projecting the Hamiltonian operator on the left and right by $\langle\chi_p \mid$ and $\mid \chi_q\rangle$ respectively:

$$\begin{aligned} H_{pq} &= \langle\chi_p \mid \hat{H}_{el}^{PP} \mid \chi_q\rangle \\ &= \langle\chi_p \mid -\frac{1}{2}\nabla_{\mathbf{r}_A}^2 + V_A(\mathbf{r}_A) + V_{AB}(\mathbf{r}_A, \mathbf{R}) \mid \chi_q\rangle. \end{aligned} \tag{2.14}$$

The first term in the above equation is the kinetic energy whereas the second term describes the electron-core interaction which is composed of

$$\mathcal{V}_{pq}^{A} = \langle \chi_p \mid V_A(\mathbf{r}_A) \mid \chi_q \rangle = \langle \chi_p \mid \frac{Z_A^c}{r_A} + V_A^{pol}(r_A) + V_A^{sr}(\mathbf{r}_A) \mid \chi_q \rangle. \tag{2.15}$$

The first element in Eq. 2.15 gives the electron-core coulombic attraction. The third term in Eq. 2.14 is

$$\mathcal{V}_{pq}^{AB} = \langle \chi_p \mid V_{AB}(\mathbf{r}_A, \mathbf{R}) \mid \chi_q \rangle = \langle \chi_p \mid V_B(\mathbf{r}_B) + V_{ec}(\mathbf{r}_A, \mathbf{R}) + V_{cc}(R) \mid \chi_q \rangle \tag{2.16}$$

The short-range matrix elements found in Eq. 2.15 and also in the $V_B(\mathbf{r}_B)$ term of Eq. 2.16 (as shown in Eq. 2.9) can be written as:

$$\langle \chi_p \mid V_X^{sr}(\mathbf{r}_X) \mid \chi_q \rangle = \langle \chi_p \mid \sum_{l,i} B_{l,i} \exp(-\beta_{l,i} r_X^2) P_{l,X} \mid \chi_q \rangle, \tag{2.17}$$

with $X = A, B$.

2.4.2 Programming Details

The molecular-structure calculations reported in the next section have been carried out using a series of subroutines we coded in Fortran 90.

Following a recursive algorithm proposed by Obara and Saika[60] we coded the routines `gkineticg.f90` and `gnuclearg.f90` to calculate the kinetic energy and electron-core attraction matrices respectively.

The routine `short_range.f90` based on a procedure described by McMurchie and Davidson[61] with some additions from Pitzer and Winter[62] allowed us to calculate the short-range matrix elements in Eqs. 2.15-2.16.

The polarization terms of Eq. 2.15, the $V_B(\mathbf{r}_B)$ term of Eq. 2.16 and the cross terms of $V_{ec}(\mathbf{r}_A, \mathbf{R})$ were calculated with the `polar.f90` routine. Here we followed the formalism presented by Schwerdtfeger.[63]

The procedure we have developed to calculate the adiabatic potentials is part of the `eiktdmo.f90` program. See appendix A for the flow diagram of the program

and for a detailed explanation of the subroutines. Complete derivations of the integrals in the `polar.f90` and the `short_range.f90` are found in appendices B and C respectively.

Similar routines for the calculation of these matrix elements are used by other quantum chemistry packages like MOLPRO[64] and COLUMBUS.[65]

2.5 Results and Discussion

The present calculations of the interatomic potentials were performed for the internuclear separation interval between 3.0 and 20.0 au with different step sizes. The PECs have been calculated for the LiHe, LiNe, NaHe and NaNe diatomic systems. To test the validity of the pseudopotential method, our PECs are compared with other theoretical and experimental results. The simplest system of that series, LiHe, is studied in detail to determine the effect of the basis sets size of the PEC. The energy contribution of the polarization terms is also analyzed.

2.5.1 Comparison of the LiHe Potential Energy Curves for Different Basis Sets

An optimal basis set is one that minimizes the computational effort without sacrificing the quality of the PECs of the excited molecular states of interest. To choose a good basis set, several preliminary calculations with different basis sets need to be run until the balance effort-quality is reached. As an example we have done this in the case of the LiHe system. For a detailed comparison we have chosen the basis sets:

Basis II : (6s5p3d/4s4p3d).

Basis III : (7s6p4d/5s5p4d).

Basis IV : (9s9p5d/7s7p5d).

Figures 2–2–2–4 show the PECs of LiHe (for the states up to 3d term) obtained using the basis sets II, III and IV respectively. The general shape of the potential curves can be characterized as follows. All states except $2s\sigma$ and the $2p\sigma$ exhibit

pronounced minima in the vicinity of 4 au. The $2s\sigma$ and the $2p\sigma$ are purely repulsive. A close comparison of figures 2–2-2–4 shows that basis set III gives converged results up to the 3d-curves.

In figure 2–5 our LiHe PECs (basis set IV) and those from Czuchaj et al.[3] are compared. Their PECs were obtained with a l-dependent pseudopotential for the Li core, while the He electrons were described explicitly. The agreement of the curves is good except in the region between 3 and 4 au where the repulsive term of the Hamiltonian plays an important role.

Figure 2–6 compares our results with basis set IV with the most current ab initio results from Behmenburg et al.[4] The agreement is good although there are some deviations. For the $2p\pi$ state our $D_e = 1200\ cm^{-1}$ and $R_e = 3.3$ au are different from the ab initio values $D_e = 868\ cm^{-1}$ and $R_e = 3.42$ au. The calculated D_e is compared with the experimental $800\ cm^{-1}$ by Lee et al.[66]

Later in the chapter, the PECs for the other alkali-Rg systems will be presented.

2.5.2 Comparison of LiHe Potential Energy Curves by Addition of Polarization Terms in the Hamiltonian

We now turn our attention to the polarization terms of the Hamiltonian and their impact on the PECs. All calculations were performed with the basis set IV on Li and as shown in figure 2–7, where all the PECs have been labeled as either (a), (b) of (c). The (a) curves were obtained with the full Hamiltonian, the (b) curves were calculated neglecting the polarization cross-terms and the (c) were produced neglecting all polarization terms and cross-terms. From the figure we conclude that the contribution of the polarization terms to the PECs is appreciable and that of the cross-terms negligible. Therefore, it is possible to neglect the cross-terms from our calculations without affecting the accuracy of our results.

2.5.3 Calculation of the Potential Energy Curves of the LiNe, NaHe and NaNe Systems and Comparisons with Other Theoretical Results

Molecular structure calculations have been performed to obtain the adiabatic potentials for the ground state and several excited states of the LiNe, NaHe and NaNe systems. Internuclear separations ranging from 3.0 to 25.0 au with different step sizes were considered. The atomic basis sets were kept constant for all values of distance R. The precision of our calculations can only be estimated by comparison with spectroscopic data and ab initio results.

LiNe: We have calculated the PECs with the basis set IV for Li. In figure 2–8 we show our results for the lower states of Li up to the Li(3s) term along with those from an ab initio calculations by Behmenburg et al.[31] The agreement of the curves is good since our potential curves present minima in the vicinity of 4 au. There are some minor discrepancies specially in our $2p\sigma$ potential curve which is more repulsive than the ab initio one.

NaHe: We have obtained the PECs with the basis set (10s10p3d/7s6p3d) of Na. Our results up the Na(4s) state are compared to other ab initio calculations by Theodorakopoulos and Petsalakis[67] in Fig. 2–9. Our calculated PECs are in good agreement with the ab initio ones over the entire distance range, except our $3p\sigma$ curve which is more repulsive .

NaNe: The PECs were produced with the same basis set with used for NaHe. In figure 2–10 we present our results of the lowest states of the system up to the $3p\sigma$ state. Pseudopotential results by Czuchaj et al.[41] obtained with a basis set (13s12p4d/10s8p4d) are also reported in that figure. There were no ab initio results available. The agreement of the curves is good over the entire range of distances.

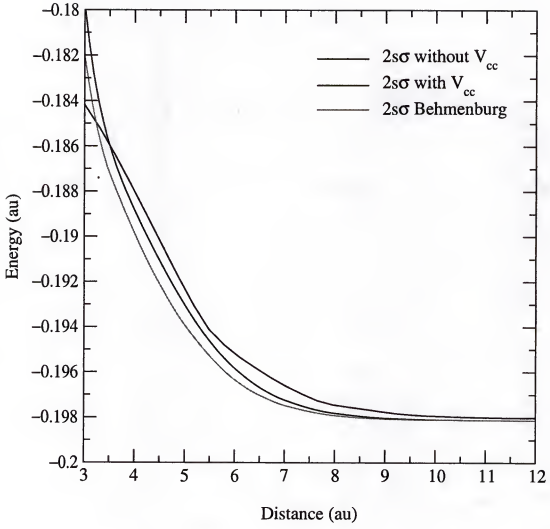

Figure 2–1: V_{cc} curve for LiHe: A=16.016 and b= 2.4402.

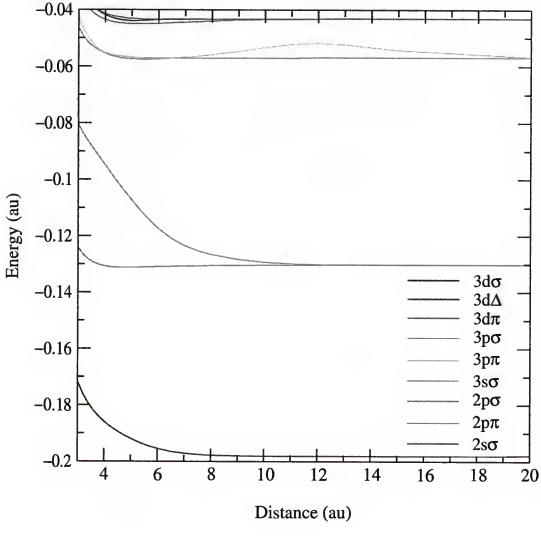

Figure 2–2: LiHe potential energy curves using basis set II.

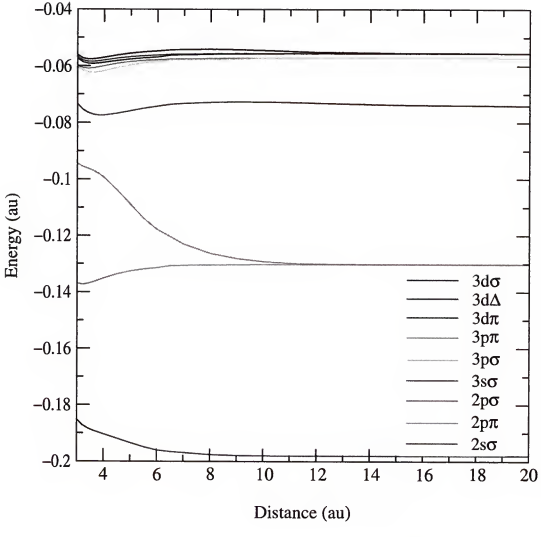

Figure 2–3: LiHe potential energy curves using basis set III.

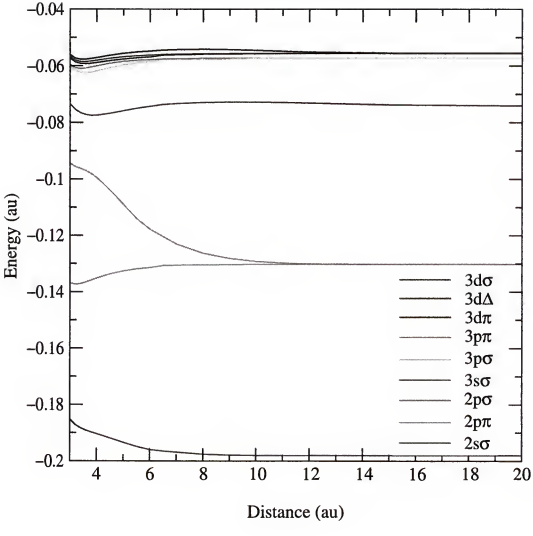

Figure 2–4: LiHe potential energy curves using basis set IV. Note that it is almost identical to figure 2–3 within the graphics accuracy.

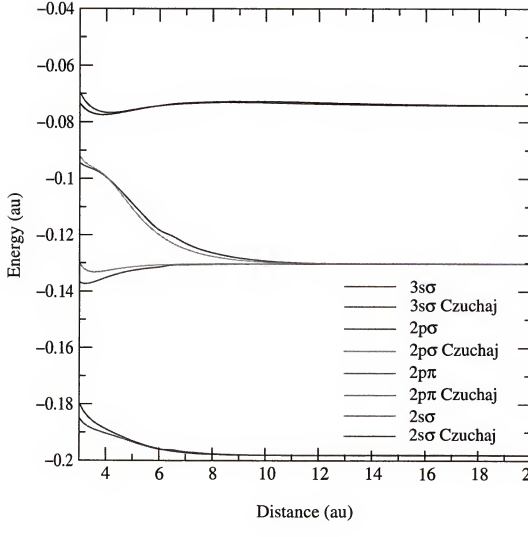

Figure 2–5: LiHe potential energy curves comparison: Our results (basis set IV) vs. pseudopotential results from Czuchaj.

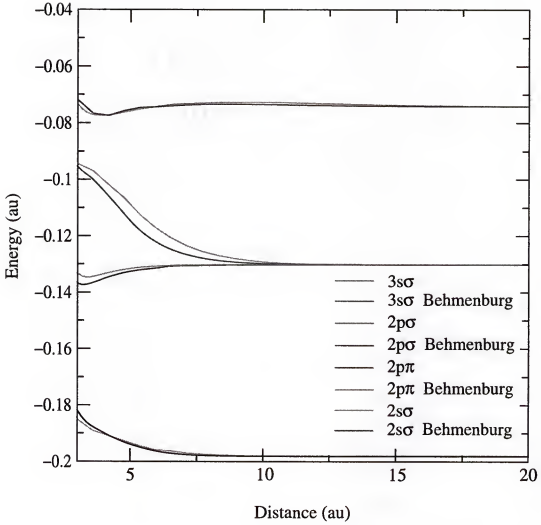

Figure 2–6: LiHe potential energy curves comparison: Our results (basis set IV) vs. ab initio from Behmenburg.

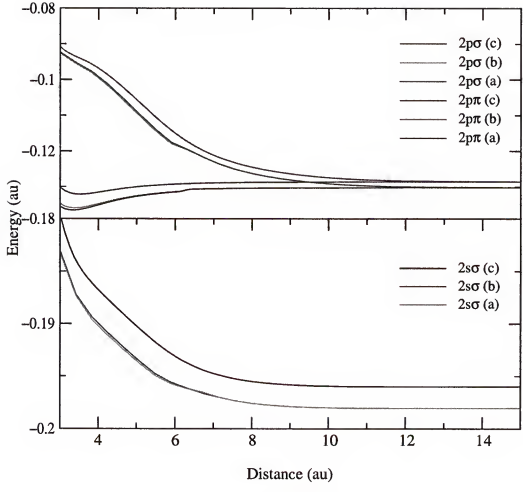

Figure 2–7: Comparison of the potential energy curves of LiHe. (a) results obtained keeping all the terms of the Hamiltonian; (b) results obtained neglecting the cross-terms; (c) results obtained neglecting all the polarization terms.

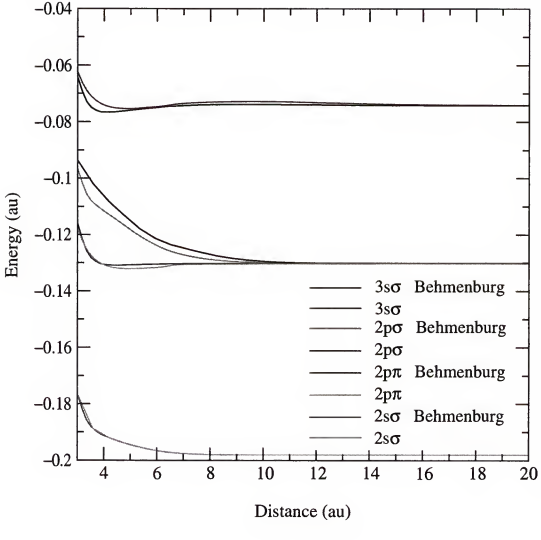

Figure 2–8: LiNe potential energy curves comparison: Our results (basis set IV) vs. ab initio from Behmenburg.

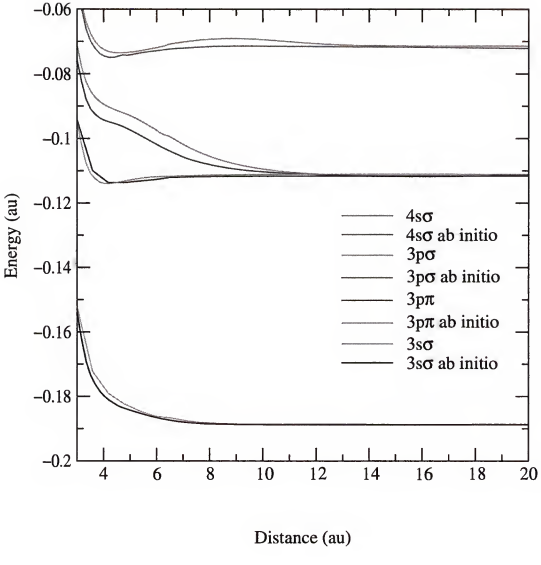

Figure 2–9: NaHe potential energy curves comparison: Our results vs. ab initio results from Theodorakopoulos.

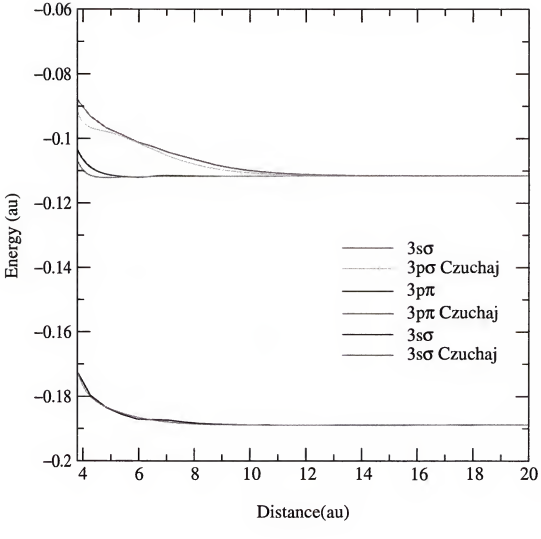

Figure 2–10: NaNe potential energy curves comparison: Our results vs. pseudopotential results from Czuchaj.

CHAPTER 3
DYNAMICS OF ALKALI ATOM-RARE GAS ATOM COLLISIONS IN THE KEV RANGE

3.1 Introduction

We introduce here a new first principles treatment to study the time evolution of electronic transitions in collisions of alkali atoms with Rg atoms. Our approach combines the l-dependent pseudopotential method (described in the previous chapter) and the eikonal/time dependent molecular orbital (Eik/TDMO) method[24] to reduce our many electron alkali-Rg atom problem into a three-body problem (alkali-metal core, valence electron, and Rg atom), simplifying dramatically the theory and decreasing the computational effort.

We begin this chapter by showing the derivation of the Eik/TDMO method in terms of l-dependent pseudopotentials (Eik/TDMO-PP). We then continue presenting a general description of the computational aspects of the method and a brief explanation of the program. It is of interest to describe what is occurring during the collisions. Among the possible quantities of interest we present in this chapter results for the orbital populations and the alignment and orientation parameters of the collisional system. Later, to check the validity of our method, we compare our calculated integral cross sections (ICSs) with other experimental and theoretical results.

3.2 Eikonal/Time Dependent Molecular Orbital Method Including l-Dependent Pseudopotentials

The Eik/TDMO method is the version of the more general eikonal/time dependent Hartree-Fock (Eik/TDHF) method to study one-active-electron systems. The implementation of Eik/TDHF and EIk/TDMO methods has been described in

great detail in references[23,24,68] and therefore, we only summarize the most relevant equations of the Eik/TDMO method and present them in the context of l-dependent pseudopotentials.

We consider the collision of an alkali atom A with an Rg atom B. The total wave function for the system Ψ is a solution of the Schrödinger equation for total energy E

$$\hat{H}\Psi(\mathbf{X},\vec{R}) = E\Psi(\mathbf{X},\vec{R}), \tag{3.1}$$

where $\mathbf{X}$ is the collection of coordinates of the active electron and $\vec{R}$ the relative position of the atomic centers.

The Hamiltonian operator $\hat{H}$ of the atomic pair can be written as

$$\hat{H} = -\frac{\hbar^2}{2M}\frac{\partial^2}{\partial\vec{R}^2} + H_{\vec{R}}\left(\frac{\hbar}{i}\frac{\partial}{\partial\mathbf{X}},\mathbf{X}\right), \tag{3.2}$$

where M is the reduced mass of the nuclei and $H_{\vec{R}}$ is the Hamiltonian term for fixed nuclear positions. In what follows, we have replaced $H_{\vec{R}}$ by the Hamiltonian $\hat{H}_{el}^{PP}$ (Hamiltonian including the pseudopotential).

It is convenient to write the total wave function in the Eikonal representation

$$\Psi(\mathbf{X},\vec{R}) = \chi(\mathbf{X},\vec{R})\exp\left[iS(\vec{R})/\hbar\right], \tag{3.3}$$

where S is real mechanical action and χ is the complex electronic wave function.

Replacing Ψ in Eq. 3.1, we obtain

$$\left[\frac{1}{2M}\left(\frac{h}{i}\frac{\partial}{\partial\vec{R}} + \frac{\partial S}{\partial\vec{R}}\right)^2 + \hat{H}_{el}^{PP} - E\right] \mid \chi(\vec{R})\rangle = 0. \tag{3.4}$$

Taking the real part of the projection of χ on the right of Eq. 3.4 gives

$$\frac{1}{2M}\left(\frac{\partial S}{\partial\vec{R}}\right)^2 + V_{qu}\left(\frac{\partial S}{\partial\vec{R}},\vec{R}\right) = E, \tag{3.5}$$

where V_{qu} is a quantum potential

$$V_{qu} = V + V' + V'', \tag{3.6}$$

$$V = \frac{\langle \chi \mid \hat{H}_{el}^{PP} \mid \chi \rangle}{\langle \chi \mid \chi \rangle}, \tag{3.7}$$

$$V' = \frac{i\hbar}{2M} \frac{\partial S}{\partial \vec{R}} \cdot \left[\left\langle \frac{\partial \chi}{\partial \vec{R}} \middle| \chi \right\rangle - \left\langle \chi \middle| \frac{\partial \chi}{\partial \vec{R}} \right\rangle \right] \Big/ \langle \chi \mid \chi \rangle, \tag{3.8}$$

$$V'' = -\frac{\hbar^2}{2M} \frac{1}{2} \left[\left\langle \frac{\partial^2 \chi}{\partial \vec{R}^2} \middle| \chi \right\rangle - \left\langle \chi \middle| \frac{\partial^2 \chi}{\partial \vec{R}^2} \right\rangle \right] \Big/ \langle \chi \mid \chi \rangle. \tag{3.9}$$

The first term of the quantum potential V_{qu} is identified as the Ehrenfest potential for core motions, while the second and third terms give quantal corrections due to nuclear displacements.

The trajectories of the nuclei can be obtained for a fixed energy E introducing position and momentum functions of the time t, satisfying the Hamiltonian equations

$$H_{qu}(\vec{P}, \vec{R}) = \frac{\vec{P} \cdot \vec{P}}{2M} + V_{qu}(\vec{P}, \vec{R}), \tag{3.10}$$

$$\frac{d\vec{R}}{dt} = \frac{\partial H_{qu}}{\partial \vec{P}}, \tag{3.11}$$

$$\frac{\partial \vec{P}}{dt} = -\frac{\partial H_{qu}}{\partial \vec{R}}, \tag{3.12}$$

where we defined the momentum

$$\vec{P} = \frac{\partial S}{\partial \vec{R}}, \tag{3.13}$$

and the total mechanical action along the trajectory

$$S(\vec{R}) = S(\vec{R}_i) + \int_{\vec{R}_i}^{\vec{R}} d\vec{R} \cdot \vec{P}. \tag{3.14}$$

The eikonal approximation for short de Broglie wavelengths $\lambda = h/ \mid \vec{P}_R \mid$ is introduced by neglecting the second and third terms in the quantum potential that

involve the gradient and Laplacian of the electronic wave functions:

$$\left|\left\langle \chi \left| \frac{\partial \chi}{\partial \vec{R}} \right\rangle\right| \Big/ \mid \langle \chi \mid \chi \rangle \mid \ll \lambda^{-1}, \tag{3.15}$$

and

$$\left|\left\langle \chi \left| \frac{\partial^2 \chi}{\partial \vec{R}^2} \right\rangle\right| \Big/ \left|\left\langle \chi \left| \frac{\partial \chi}{\partial \vec{R}^2} \right\rangle\right| \ll \lambda^{-1}, \tag{3.16}$$

which allows us to neglect V' and V'' so that $V_{qu} \approx V$. Hence, we propagate the nuclei under the influence of the Ehrenfest potential.

Returning to the description of the electronic states, the time-dependent electronic wave function for our one-electron system χ is reduced to a single (complex valued) molecular orbital ψ. The time evolution of the molecular orbitals can be obtained by either solving a differential equation in time in terms of the molecular orbitals ψ or equivalently by solving one in terms of the electronic density operator $\hat{\rho}$[23]

$$\hat{\rho}(t) = \mid \psi(t)\rangle\langle\psi(t) \mid . \tag{3.17}$$

The collision dynamics is carried out solving the Hamiltonian equations 3.11-3.12 coupled to time-dependent differential equation for the density operator $\hat{\rho}$

$$\hat{H}_{el}^{PP}\hat{\rho} - \hat{\rho}\hat{H}_{el}^{PP} = i\hbar\partial\hat{\rho}/\partial t. \tag{3.18}$$

The quantum potential in terms of the density matrix is therefore approximated by

$$V_{qu} = \frac{\mathrm{tr}[\hat{\rho}\hat{H}_{el}^{PP}]}{\mathrm{tr}[\rho]} \tag{3.19}$$

and becomes a function of time.

3.2.1 Matrix Equations

The time evolution of electronic densities and nuclear positions and momenta, within the framework of the Eik/TDMO-PP method, requires the choice of a basis set. We expand the time-dependent molecular orbitals ψ in terms of linear combinations of static atomic functions (AFs) $\{\chi\}$, which are centered on the alkali atom. It is well known that, by replacing these AFs in Eq. 3.18, spurious asymptotic couplings appear in the form of $\langle \chi_\mu \mid \partial \chi_{\mu'}/\partial t \rangle$ terms.[23] These spurious couplings are avoided by expanding each TDMO ψ as a linear combination of the traveling atomic functions ξ:

$$\psi_i(\vec{r},t) = \sum_p \xi_p(\vec{r},t) c_{ip}(t), \tag{3.20}$$

$$\xi_\mu(\vec{r},t) = \chi_\mu(\vec{r}) T_m(\vec{r},t), \tag{3.21}$$

here the c's are complex expansion coefficients, $\chi_\mu(\vec{r})$ is an atomic orbital centered at core position $\vec{R}_m(t)$ for the electron with position $\vec{r}$. The electron translation factor (ETF) $T_m(\vec{r},t)$ is defined by

$$T_m(\vec{r},t) = \exp\left[i m_e \left(\vec{v}_m(t) \cdot \vec{r} - \int_{t_i}^{t} dt' v_m^2(t') \Big/ 2 \right) \right], \tag{3.22}$$

where $\vec{v}_m$ is the velocity vector of core m, t_i is the initial time, and m_e is the electron mass. In what follows we are setting $\hbar = 1$.

The density operator in the basis of traveling atomic orbitals is written as

$$\hat{\rho}(t) = \sum_{pq} \mid \xi_p \rangle P_{pq}(t) \langle \xi_q \mid = \mid \xi \rangle \mathbf{P} \langle \xi \mid, \tag{3.23}$$

where the $\mathbf{P}$ is the density matrix. The matrix elements of $\mathbf{P}$ are

$$P_{pq}(t) = \sum_{occ\ i} c_{pi}^*(t) c_{qi}(t). \tag{3.24}$$

Equation 3.18 can be written in terms of the density matrix by projecting on the left and right by $\langle \xi \mid$ and $\mid \xi \rangle$ respectively and gives

$$i\dot{\mathbf{P}} = \mathbf{S}^{-1}\mathbf{H}_T\mathbf{P} - \mathbf{P}\mathbf{H}_T\mathbf{S}^{-1}. \tag{3.25}$$

Here $\mathbf{S}^{-1}$ is the inverse of the overlap matrix and in more detail, $(\mathbf{H_T})_{\mu\nu}$ is written as

$$(\mathbf{H}_T)_{\mu\nu} = \langle \xi_\mu \mid T_m \hat{H}_{el}^{PP} T_m^{-1} \mid \xi_\nu \rangle, \tag{3.26}$$

where T_m is the ETF on center m. It is now clear that we have to calculate the one-electron integrals, present in the matrix form of Eq. 3.18, in a basis of traveling atomic functions.

We discuss now the transformation of matrices from a static basis χ (in which they are originally calculated) to the traveling basis ξ. We define the transformation matrix

$$B_{\mu\nu} = \sum_k (\mathbf{S}^{(\chi)})^{-1}_{\mu k} (\mathbf{S}^{(\chi\xi)})_{k\nu}, \tag{3.27}$$

$$(\mathbf{S}^{(\chi\xi)})_{\mu\nu} = \langle \chi_\mu \mid \xi_\nu \rangle, \tag{3.28}$$

so that the relationship between a matrix in the static basis $\mathbf{O}^{(\chi)}$ and one in the traveling basis $\mathbf{O}^{(\xi)}$ is given by

$$\mathbf{O}^{(\xi)} = \mathbf{B}^\dagger \mathbf{O}^{(\chi)} \mathbf{B}. \tag{3.29}$$

3.2.2 Propagation of the Density Matrix

The propagation of the density matrix is carried out using the relax-and-drive procedure.[23,68] Let us begin by rewriting equation 3.25 in the form

$$i\dot{\mathbf{P}}(t) = \mathbf{W}(t)\mathbf{P}(t) - [\mathbf{P}(t)\mathbf{W}(t)]^\dagger, \tag{3.30}$$

where $\mathbf{W} = \mathbf{S}^{-1}(t)\mathbf{H}(t)$.

The density matrix $\mathbf{P}$ is then separated into two matrices: The first matrix, $\mathbf{P}^{(0)}$, describes the electronic relaxation for fixed nuclei, and the second matrix, $\mathbf{Q}$, describes the density-matrix change due to the driving forces of the nuclear motions:

$$\mathbf{P}(t) = \mathbf{P}^{(0)}(t) + \mathbf{Q}(t). \tag{3.31}$$

The reference density $\mathbf{P}^{(0)}$ is defined by its time propagation

$$i\dot{\mathbf{P}}^{(0)}(t) = \mathbf{W}(t_0)\mathbf{P}^{(0)}(t) - \mathbf{P}^{(0)}(t)[\mathbf{W}(t_0)]^\dagger, \tag{3.32}$$

or equivalently,

$$\mathbf{P}^0(t) = \mathbf{U}_0(t, t_0)\mathbf{P}^0(t_0)\mathbf{U}_0(t, t_0)^\dagger, \tag{3.33}$$

where $\mathbf{U}_0$ is the time evolution operator defined as

$$\mathbf{U}_0(t, t_0) = \exp[-i(t - t_0)\mathbf{W}_0]. \tag{3.34}$$

The reference density at the beginning of a time interval is given by

$$\mathbf{P}(t_0) = \mathbf{P}^{(0)}(t_0) + \mathbf{Q}(t_0). \tag{3.35}$$

Given this choice of the reference density, the time propagation of the density-matrix change $\mathbf{Q}$ follows from

$$i\dot{\mathbf{Q}}(t) = \mathbf{W}(t_0)\mathbf{Q}(t) - \mathbf{Q}(t)[\mathbf{W}(t_0)]^\dagger + \mathbf{D}(t), \tag{3.36}$$

where $\mathbf{D}$ is the driving term

$$\mathbf{D}(t) = \Delta\mathbf{W}(t)\mathbf{P}^0(t) - \mathbf{P}^0(t)[\Delta\mathbf{W}(t)]^\dagger, \tag{3.37}$$

$$\Delta\mathbf{W}(t) = \mathbf{W}(t) - \mathbf{W}_0(t_0), \tag{3.38}$$

and gives

$$\mathbf{Q}(t) = \int_{t_0}^{t} dt' \mathbf{U}_0(t,t') \mathbf{D}(t') \mathbf{U}_0(t,t')^{\dagger}. \tag{3.39}$$

The propagation of the above differential equations requires the choice of a time step $\Delta t = t_1 - t_0$ which is chosen so that the condition

$$\epsilon_{lower} \leq \frac{\| \mathbf{Q} \|}{\| \mathbf{P} \|} \leq \epsilon_{higher} \tag{3.40}$$

is satisfied. The lower tolerance ϵ_{lower} allows for larger time steps in the adiabatic region, where the evolution of the density matrix is nearly equal to the evolution of the reference density. The higher tolerance ϵ_{higher}, restricts the procedure to smaller time steps in the diabatic region where the change in the density matrix is relatively large. The relax-and-drive procedure is able to adjust the time step size automatically in order to maximize the performance of the method by minimizing the number of steps taken for the maximum accuracy in the integration the density matrix equations.

3.2.3 Physical Properties of Interest

It is of interest to describe in some way what is occurring during collisional electronic excitation and rearrangement. Among the possible quantities of interest are the alignment and orientation parameters and the electronic population of the atomic orbitals.

The Eik/TDMO-PP method allows us to propagate the density matrix over time and from the density matrix it is possible to examine the expectation values of an operator $\hat{O}$ by using the general expression

$$\langle \hat{O} \rangle = \frac{\mathrm{tr}[\mathbf{P}\hat{\mathbf{O}}]}{\mathrm{tr}[\mathbf{P}]}. \tag{3.41}$$

In this study, as shown in Fig. 3–1, we consider the plane of the collision to be on the x-z plane with the z-direction being the incoming direction of the projectile and

the x-direction being the direction of the impact parameter, so that the y-direction is always perpendicular to the plane.

Having chosen this particular geometry, we move on to the definition of the alignment and orientation parameters. In general, one may describe the orbital polarization of a system by examining the anisotropy of the orbital angular momentum of the electrons. A state of given angular momentum L is said to be:[69]

1) Isotropic, if all its magnetic substates are equally populated.
2) Oriented, if the magnetic substates have differing populations.
3) Aligned, if substates with magnetic quantum numbers of equal magnitude but opposite signs are equally populated.

To illustrate these definitions let us consider a system with angular momentum $\vec{L}$. We introduce the spherical irreducible tensor operators $\hat{L}_q^{(n)}$, where we consider $n = 1,2$ and $-n \leq q \leq n$

$$\begin{aligned}
\hat{L}_0^{(1)} &= \hat{L}_z, \\
\hat{L}_{\pm 1}^{(1)} &= \mp\frac{1}{\sqrt{2}}\hat{L}_{\pm}, \\
\hat{L}_0^{(2)} &= \frac{1}{\sqrt{6}}(3\hat{L}_z^2 - \hat{L}^2), \\
\hat{L}_{\pm 1}^{(2)} &= \mp\frac{1}{2}\hat{L}_{\pm}(2\hat{L}_z \pm 1), \\
\hat{L}_{\pm 2}^{(2)} &= \frac{1}{2}\hat{L}_{\pm}^2,
\end{aligned} \tag{3.42}$$

where we define in Cartesian coordinates

$$\hat{L}_{\pm} = \hat{L}_x \pm i\hat{L}_y. \tag{3.43}$$

Let us define now the orientation vector $O_q^{(1)}$ and the alignment tensor $A_q^{(2)}$ at time t,

$$O_q^{(1)}(L,t) = \frac{1}{\sqrt{L(L+1)}} Re\langle \hat{L}_q^{(1)} \rangle_t, \tag{3.44}$$

$$A_q^{(2)}(L,t) = \frac{\sqrt{6}}{L(L+1)} Re\langle \hat{L}_q^{(2)} \rangle_t, \tag{3.45}$$

where the quantities in angle brackets are the expectation values which can be expressed in terms of the density matrix and hence may be calculated as functions of time in our method

$$\langle \hat{L}_q^{(n)} \rangle_t = \frac{\mathrm{tr}[\mathbf{P}\mathbf{L}_q^{(n)}]}{tr[\mathbf{P}]} \tag{3.46}$$

In our geometry the only alignment parameter with nonzero value is[70]

$$A_0^{(2)}(L) = \frac{\sqrt{6}}{L(L+1)} Re\langle \hat{L}_0^{(2)} \rangle_t, \tag{3.47}$$

$$\hat{L}_0^{(2)} = \frac{1}{\sqrt{6}}(3\hat{L}_z^2 - \hat{L}^2). \tag{3.48}$$

The time evolution of the atomic orbital population can be obtained from the density matrix introducing the Löwdin populations

$$n_a^L(t) = \sum_{\nu \in a} \sum_{\kappa\lambda} [\mathbf{S}(t)^{1/2}]_{\nu\kappa} [\mathbf{P}(t)]_{\kappa\lambda} [\mathbf{S}(t)^{1/2}]_{\lambda\rho}. \tag{3.49}$$

for atomic orbital a.

The alignment parameter may also be written in terms of Löwdin populations as

$$A_0^{(2)}(t) = n_{2p_z}^L(t) - 2n_{2p_x}^L(t). \tag{3.50}$$

We are also interested in reporting final physical quantities that can be compared with other theories and experiments such as state-to-state integral cross sections (ICSs). The ICS from an initial atomic orbital p to a final orbital q for projectile

energy E is defined by

$$\sigma_{p\to q}(E) = 2\pi \int db\ b\ P_{qq}^{(p)}(E,b) \tag{3.51}$$

where $P_{qq}^{(p)}(E,b)$ is the transition probability for a transition $p \to q$ and b is the impact parameter.

3.3 Computational Aspects

3.3.1 Programming Details

The pseudopotential code was entirely written in Fortran 90 (F90). To make possible the further integration of the pseudopotential routines into the original `eiktdmo` code, available in our group, it was necessary to rewrite many of the original Fortran 77 routines into Fortran 90.

We present in appendix A a flow diagram for the algorithm of the `eiktdmopp` program along with an explanation of the main features of each subroutine.

3.3.2 Construction of the Density Matrix

The matrix representation of the density, overlap and Hamiltonian operators requires a set of basis functions in which the atomic and molecular orbitals for the ground and several other excited states may be expanded accurately.

Our TDMOs $\{\psi\}$ are written as combinations of atomic Cartesian functions $\{\phi^c\}$

$$|\ \psi\rangle\ = |\ \phi^c\rangle \mathbf{C}^c, \tag{3.52}$$

where $\mathbf{C}^c$ is the matrix of the expansion coefficients. Here we have assumed that the atomic functions are normalized but not orthogonal to each other. The matrix $\mathbf{C}^c$ is the matrix of eigenvectors obtained by diagonalizing the $\mathbf{W}^c$ matrix (in the $\{\phi^c\}$ basis) at initial time

$$\mathbf{W}^c\mathbf{C}^c\ =\ \mathbf{C}^c\mathbf{E}. \tag{3.53}$$

Once we have selected the initial state of the system ψ_i (with $i = 2s,\ 2p_z$, etc.), which in our calculations corresponds the ground state of the alkali atom, we construct the initial density matrix $\mathbf{P}^{\psi}$ (in the basis of molecular orbitals ψ) setting all its matrix elements to zero except the element $\mathbf{P}^{\psi}_{ii}$ which is set to one. Because all the matrices we use in the propagation are calculated in the basis of Cartesian Gaussian functions ϕ^c, we need to take the density matrix we have constructed in the ψ basis to the ϕ^c basis in which the calculation are carried out. The procedure we have developed to do this transformation is discussed below.

The density operator $\hat{\rho}$ can be expanded in terms of either the TDMOs ψ or the basis of atomic Cartesian functions ϕ^c (the basis in which the calculations are run)

$$\hat{\rho} \quad = \quad |\ \psi\rangle \mathbf{P}^{\psi} \langle \psi\ | = |\ \phi^c\rangle \mathbf{P}^{c} \langle \phi^c\ | \ . \tag{3.54}$$

We transform the density matrix from the ψ basis to ϕ^c basis by projecting the second and third terms of Eq. 3.54 on the left by $\langle \phi^c\ |$ and on the right by $|\ \phi^c\rangle$ to get

$$\langle \phi^c\ |\ \phi^c\rangle \mathbf{P}^{c} \langle \phi^c\ |\ \phi^c\rangle = \langle \phi^c\ |\ \psi\rangle \mathbf{P}^{\psi} \langle \psi\ |\ \phi^c\rangle \tag{3.55}$$

$$\mathbf{S}^{c}\mathbf{P}^{c}\mathbf{S}^{c} = \langle \phi^c\ |\ \psi\rangle \mathbf{P}^{\psi} \langle \psi\ |\ \phi^c\rangle \tag{3.56}$$

and replacing the ψ's in 3.56 using their expansions shown in 3.52 we get

$$\begin{aligned} \mathbf{S}^{c}\mathbf{P}^{c}\mathbf{S}^{c} \quad &= \quad \langle \phi^c\ |\ \phi^c\rangle \mathbf{C}^{c}\mathbf{P}^{\psi}\mathbf{C}^{c\dagger} \langle \phi^c\ |\ \phi^c\rangle \\ &= \quad \mathbf{S}^{c}\mathbf{C}^{c}\mathbf{P}^{\psi}\mathbf{C}^{c\dagger}\mathbf{S}^{c}. \end{aligned} \tag{3.57}$$

Multiplying on the left and right of Eq. 3.57 by $(\mathbf{S}^{c})^{-1}$ we get the expression we were looking for $\mathbf{P}^{c}$ in terms of $\mathbf{P}^{\psi}$

$$\mathbf{P}^{c} \quad = \quad \mathbf{C}^{c}\mathbf{P}^{\psi}\mathbf{C}^{c\dagger}, \tag{3.58}$$

where $\mathbf{P}^c$ is the density matrix in the Cartesian Gaussian basis.

Once the propagation has ended, we take the density matrix from the ϕ^c basis to the ψ basis to analyze the results, using the transformation

$$\mathbf{P}^{\psi} = (\mathbf{C}^c)^{-1}\mathbf{P}^c(\mathbf{C}^{c\dagger})^{-1}. \tag{3.59}$$

3.4 Results and Discussion

In this section we report some of the results we have obtained by applying our method to the LiHe, LiNe, NaHe and NaNe collisional systems. Energies of interest for the incident alkali atom range from as low as 0.5 keV to greater than 30 keV depending upon the system. The simplest of the alkali-Rg system consisting of Li and He has been used to study in detail the time-dependence of the orbital population, orientation and alignment parameters. Later, we summarize the results of final excitation ICSs.

A careful selection of the initial conditions guarantees the convergence and reproducibility of the final results. Series of test runs ensures the convergence and stability of the numerical procedures for the integration of the equations. These tests involve varying the initial and final separation of the cores, the lower and higher tolerances. Later, in section 3.4.2 we study the effects of the basis set size on the ICSs, where the basis set choice plays an important role in the convergence of the results.

3.4.1 Time-Dependent Study of the Li-He Collision

As discussed in chapter 2, the computational effort taken in the calculation of Hamiltonian matrix rises rapidly with the number of atomic orbitals described by the basis set. Therefore, we have to find an optimal basis set that reduces the computational time without sacrificing the reproducibility and convergence of the results. There are other initial parameters that also affect the final results of the calculations and they need to be investigated as well. We have found that initial and

final distances of 30 au (where the interaction of the two atoms is negligible) are good for most systems. The tolerance set plays an important role in final outcome. It has been found that the pair $10^{-7} - 10^{-5}$ (for lower and higher tolerances respectively) gives accurate results in most cases.

We now report some of the results we have obtained from studies on $LiHe^{71}$:

Figure 3–2 presents the trajectories of the nuclei at different impact parameters (b = 0.5, 0.75, 1.0 au) for a fixed initial laboratory energy (E_{lab}) of 1.0 keV. It is important to note in Figure 3–2 how the He atom (initially at rest) recoils. We also find that the deflection angles are small even for these small impact parameters. This is due to the high collisional energy we have chosen and also the neutral character of the colliding atoms that makes the core-core repulsion significant only when the two nuclei overlap at short distances.

Figure 3–3 shows the population of the Li(2s) and Li(2p) orbitals as a function of time for and E_{lab} of 1 keV. It is always instructive to analyze the temporal change of the orbital populations, to learn about the nature of electronic rearrangement. All populations oscillate over time before coming to a constant asymptotic value that depends on the energy of collision and the impact parameter. The population of the $2p_y$ orbitals is not shown as it is never populated by the chosen geometry of the calculation. The total time intervals over which populations change are about 200.0 au.

Figure 3–4 gives the dependence of the final orbital population on the impact parameter at a E_{lab} of 1 keV. We see how the excitation from the 2s to the 2p orbitals is significant in the region of impact parameters from 0.0-6.0 au. We have found that this feature is repeated at other collisional energies.

Other time-dependent phenomena that are of interest for this system include the alignment parameter presented in figures 3–5-3–7 and orientation parameter

presented in figures 3–8-3–10. These results show that both the alignment and the orientation parameters also oscillates during the collision.

3.4.2 Basis Set Effects

The validity of our method in the study of the electronic rearrangement in alkali-Rg collisions is tested when we compare our ICSs results with those from other theories and experiments.

We turn our attention now to the calculation of the $2s \rightarrow 2p$ integral cross section for Li-He system. Calculations were performed with kinetic energies E_{lab} chosen to be equal to experimental values, and impact parameters in the range $b = 0.0 - 20.0$ au, with eighty values per energy, and a higher density grid at lower impact parameters. Integrals over b converged at an upper limit of 12.0 au. For the detailed calculations we have chosen the basis sets:

Basis I:(6s5p2d/4s4p2d).

Basis II:(6s5p3d/4s4p3d).

Basis III:(7s6p4d/5s5p4d).

Basis IV:(9s9p5d/7s7p5d).

Figure 3–11 gives our integral cross sections for Li-He in the range $E_{lab} = 1.0$-10.0 keV, comparing basis sets I-IV to experimental data.[14] We find that there is a strong dependence of the ICSs on the size of the basis set. The sequences of larger basis sets are found to converge. This comparison shows that our results with basis sets III and IV are in excellent agreement with experiment. The experimental values, which are not measured in absolute terms, have been adjusted to our calculations at a single energy of $E_{lab} = 5.0$ keV. These tests calculations have shown that to correctly obtain the $2s \rightarrow 2p$ ICS it is necessary to include several d-orbitals.

Figure 3–12 shows our calculated ICSs (for basis set III) and compares them with results from calculations using close-coupling equations for a trajectory of constant velocity, and either a model (Baylis) core potential[72] , or atomic pseudopotential.[35] The curves show the same general behavior with energy and the same orders of magnitude of ICSs, but noticeable differences. Our results also allow for close-coupling and use a calculated trajectory, but the different trajectories are not likely to change ICSs much, so that the likely sources of differences are the choice of core potentials and the size of atomic basis sets.

3.4.3 Integral Cross Sections for the Li-Ne, Na-He and Na-Ne Systems

We now move on to ICSs for the Li-Ne, Na-He and Na-Ne collisional systems for energies in the keV range and compare them with experimental data and results from other theories.

Li-Ne: Figure 3–13 shows a comparison of our ICSs with experimental data[14] and theoretical results.[72] The experimental values have been adjusted to our calculations at the single energy of $E_{lab} = 3.0$ keV. Note that the agreement between calculated and experimental results is good through the entire range of energies. Our ICSs are also compared with other theoretical ICSs. We find that the curves have the same general behavior with energy. However, there are pronounced differences in magnitude. These differences may be attributed to the choice of model potential in those calculations.

Na-He: This system has been the subject of extensive experimental and theoretical investigations. Figure 3–14 presents the ICSs we have obtained with the Na (10s10p3d/7s6p3d) basis set. We include experimental[14] and theoretical[35] results. We adjusted the experimental results to our calculation at the single energy of $E_{lab} =$ 15.0 keV. This comparison shows that our theoretical results are in good agreement with both experiment and theory for the entire energy range.

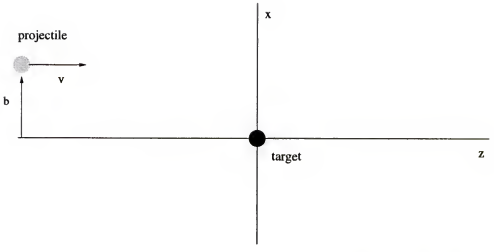

Figure 3–1: The collision is taken to occur in the $x-z$ plane, the alkali atom is chosen to be the projectile and we assume that the rare-gas atom is initially at rest.

Na-Ne: This is the last of the systems we have studied. Figure 3–15 gives the ICSs obtained with the Na (10s10p3d/7s6p3d) basis set. Our results are compared with experimental data from Olsen[14] that we have adjusted at the energy of E_{lab} = 10.0 keV. Both curves present the same behavior at these energies although it is clear that the trends of the two curves at energies greater than 15 keV are different.

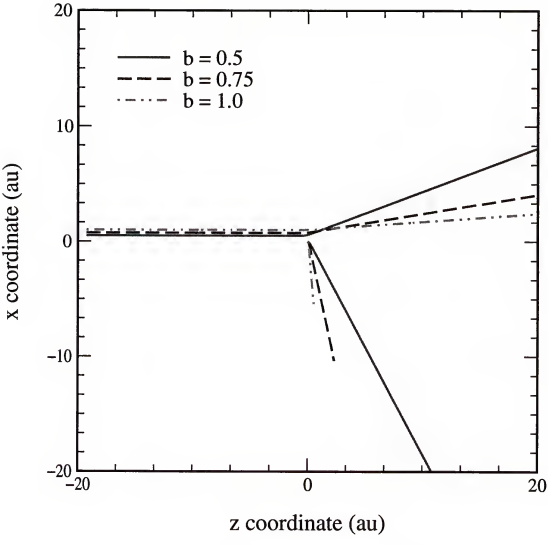

Figure 3–2: Trajectories for a 1.0 keV Li atom incident on a He atom target. Comparison of results for three different impact parameters, b = 0.5, 0.75 and 1.0 au. The He target is initially sitting at rest at the origin of coordinates.

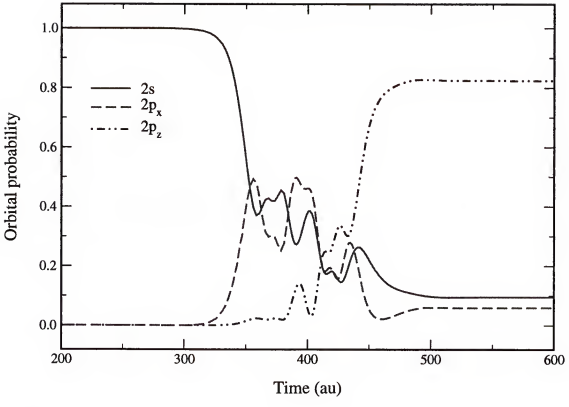

Figure 3–3: Populations of the Li 2s and 2p orbitals vs. time in a 1.0 keV Li-He collision, at $b = 1.0$ au.

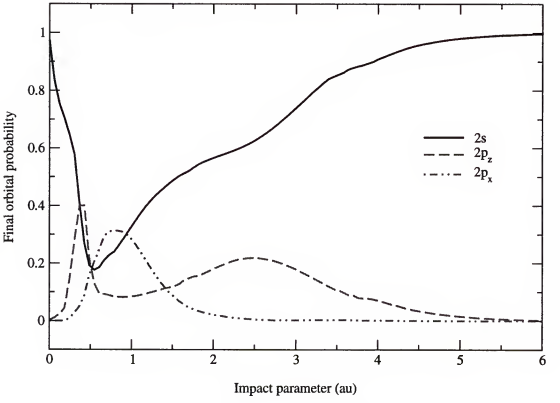

Figure 3–4: Final orbital populations of Li 2s and 2p orbitals vs. impact parameter in 1.0 keV Li-He collisions.

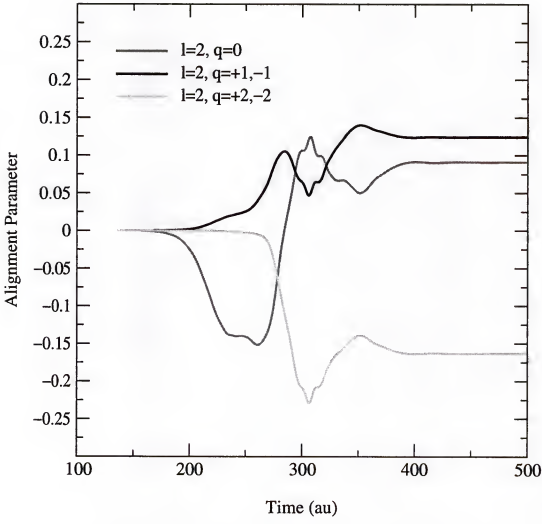

Figure 3–5: Alignment parameter vs. time in a Li-He collision ($E_{lab} = 1.0$ keV, $b = 0.5$ au).

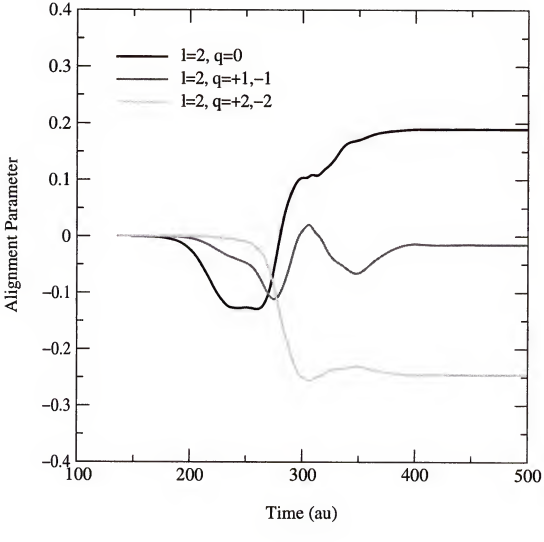

Figure 3–6: Alignment parameter vs. time in a Li-He collision ($E_{lab} = 1.0$ keV, $b = 1.0$ au).

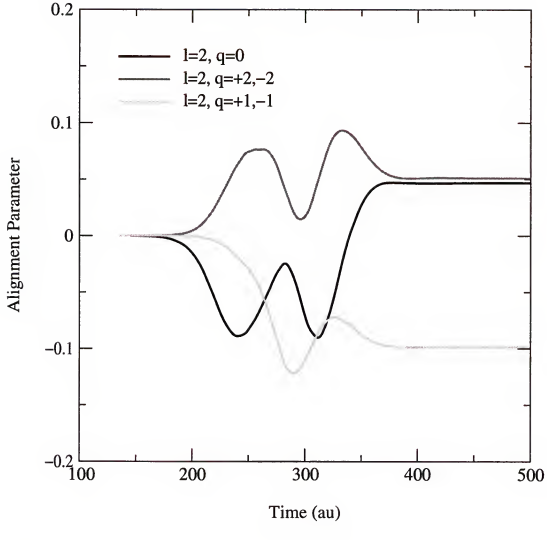

Figure 3–7: Alignment parameter vs. time in a Li-He collision (E_{lab} = 1.0 keV, b = 2.0 au).

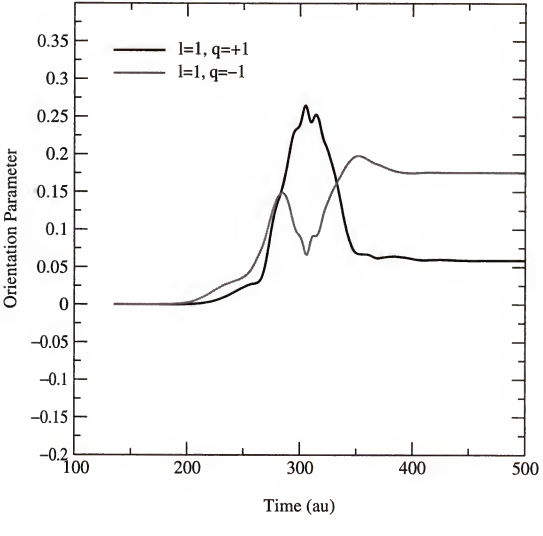

Figure 3–8: Orientation parameter vs. time in a Li-He collision ($E_{lab} = 1.0$ keV, $b = 0.5$ au).

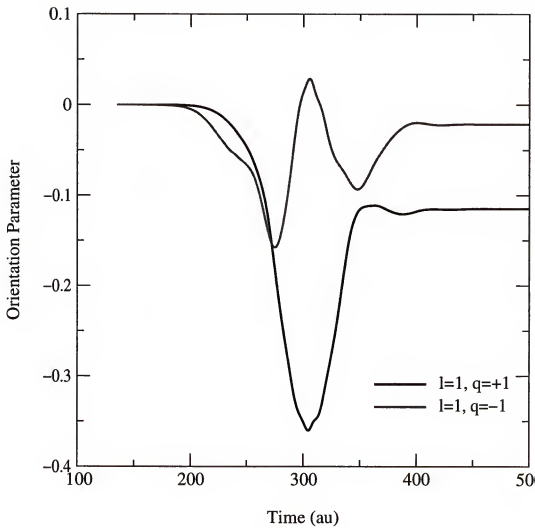

Figure 3–9: Orientation parameter vs. time in a Li-He collision ($E_{lab} = 1.0$ keV, $b = 1.0$ au).

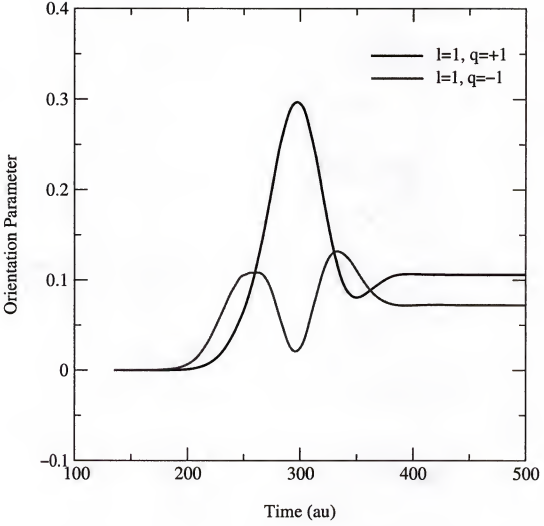

Figure 3–10: Orientation parameter vs. time in a Li-He collision ($E_{lab} = 1.0$ keV, $b = 2.0$ au).

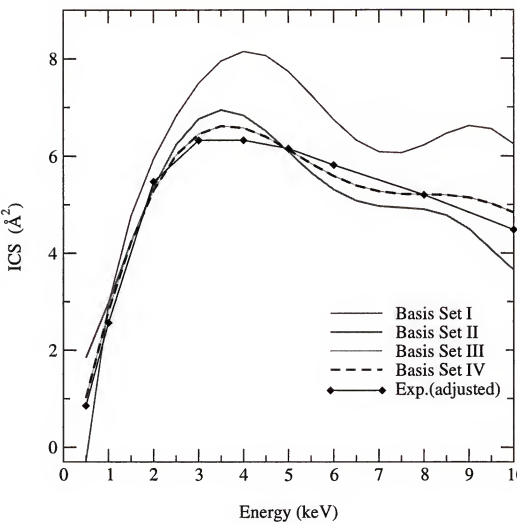

Figure 3–11: $2s \rightarrow 2p$ Integral cross sections vs. E_{lab} for Li-He collisions. Comparison of our results using different basis set choices with experiment.

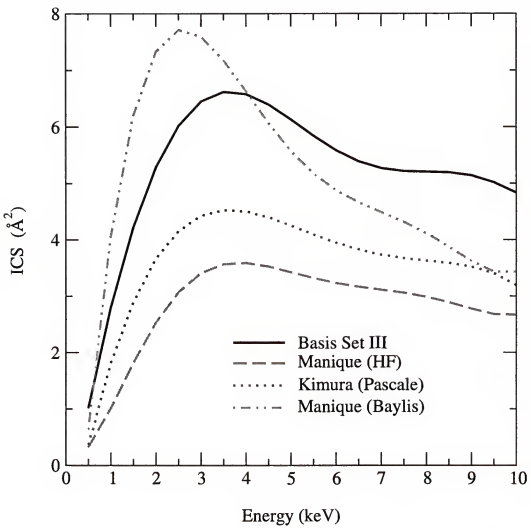

Figure 3–12: $2s \rightarrow 2p$ Integral cross sections for collisions of Li-He (E_{lab} = 1.0-10.0 keV). Our results (using basis set III) compared with other theories.

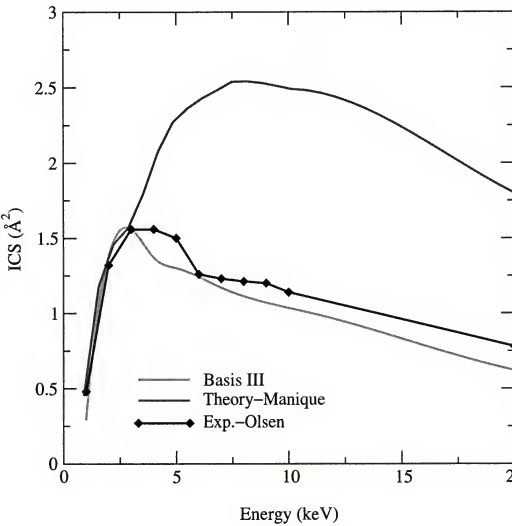

Figure 3–13: $2s \rightarrow 2p$ Integral cross sections in Li-Ne collisions. Comparison of our results with experimental results from Olsen and theoretical results from Manique.

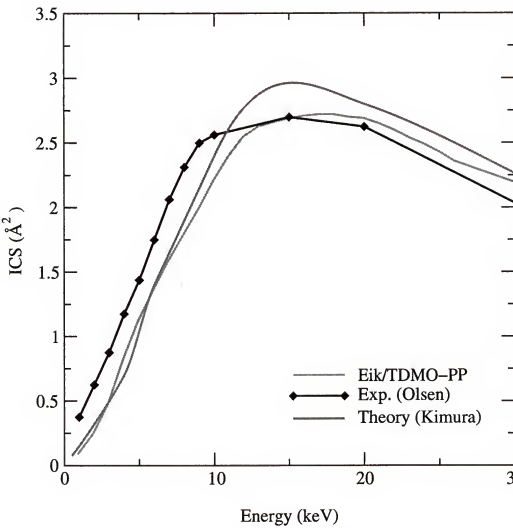

Figure 3–14: $3s \rightarrow 3p$ Integral cross sections in collisions of Na-He. We present our results and those from Olsen (exp.) and Kimura(theory).

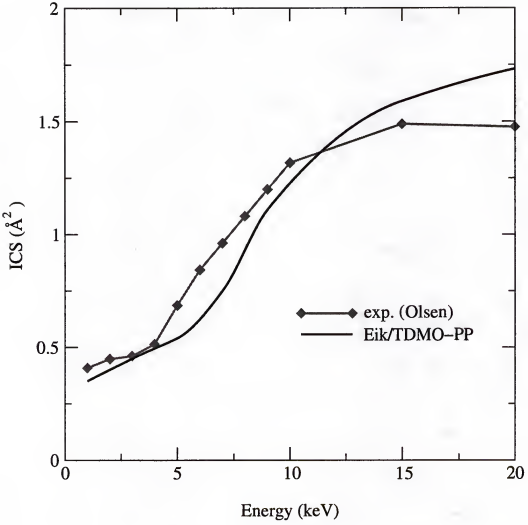

Figure 3–15: $3s \rightarrow 3p$ Integral cross sections for Na-Ne collisions. We show our theoretical results and those from Olsen (exp.).

CHAPTER 4
ALKALI ATOMS FINE-STRUCTURE TRANSITIONS INDUCED BY COLLISIONS WITH RARE GAS ATOMS

4.1 Introduction

In this chapter we are interested in studying the time dependence of the thermal energy collisions of alkali atom with rare-gas atom to gain insight into the mechanism of the fine-structure transitions among fine-structure levels of the alkali atom.

This chapter starts with a general review of the literature since this is the subject of numerous experimental and theoretical investigations. Then, the theory of spin-orbit coupling in atoms is discussed and extended to diatomic interactions. Some computational aspects are discussed including the derivation of the spin-orbit coupling matrix elements in the static basis. Some preliminary results of our calculations including spin-orbit coupling are presented. We then present the Eik/TDMO-PP method and extend it to include spin-orbit coupling (Eik/TDMO-PP-SO). A quick overview of the transformation to atomic eigenstates with spin-orbit coupling is presented, followed by a discussion about the molecular spin-orbitals. Finally, some aspects related to application to the Na^* + He system are discussed.

4.2 Background

The thermal and hyperthermal collisions of excited alkali atoms M^* in a substate ^2P_J with Rg atoms result both in angular momentum reorientation

$$M^*(^2P_{J,M_J}) + Rg \rightarrow M^*(^2P_{J,M'_J}) + Rg \tag{4.1}$$

and in angular momentum recoupling

$$M^*(^2P_J) + Rg \rightarrow M^*(^2P_{J'}) + Rg \tag{4.2}$$

with energy transfer $\Delta E_{JJ'}$. These are the only processes which take place with appreciable probability in the range of energies of a few eV[11] where spin-orbit coupling plays and important role.

These fine-structure transitions have been extensively studied, but more can be learned, especially with regard alignment and orientation effects and the mechanism of the transfer, using a time-dependent description. One of the simplest cases is the process

$$Na(3p\,^3P_{3/2}) + He \rightarrow Na(3p\,^2P_{1/2}) + He. \tag{4.3}$$

A complete and rigorous theory of these processes involves a calculation of the full quantum wave function $\Psi(\mathbf{R}, \mathbf{r})$ describing the motion of the nuclei and active electron. This close-coupling theory begins with an expansion of the wave function in molecular electronic states, and ends with numerical solution of coupled equations for nuclear wave functions and numerical summation over coupled angular momentum states. Accurate cross section have been reported by Reid[27] , Pascale and Olson,[28] Lemoine et al.,[29] Schatz et al.[30] and Leo et al.[73] using this approach. However the formulation of the theory and the long numerical codes are very complex and physical insight can be lost.

A more intuitive, though less rigorous, semiclassical model has successfully been used to study these systems. Nikitin[36] used a strong coupling approximation to obtain analytic formulas for the fine-structure transition cross sections in the Na-Ar system. Masnow-Seeuws,[74] with Roueff[38] numerically solved more exact equations for the Na-He system using a semiclassical impact parameter method; this calculation was later refined by Masnou-Seeuws and McCarroll[39] to take into account trajectory effects. More recently Kovalenko et al.[40] used a semiclassical formalism to monitor the expectation values of the orbital and spin angular momentum vectors. Inspired by the latter we will try to study the mentioned collisional phenomena.

4.3 Spin-Orbit Coupling in Atoms

Spin is of course a relativistic effect, but a classical picture nonetheless does help in the understanding of spin-orbit coupling. The interaction couples together the spin (**s**) and the orbital (**l**) angular momentum vectors, and reduces the degeneracy of spectroscopic terms with a given l and s, but a different value of j, the total angular momentum. The interaction of the electron's magnetic moment $\boldsymbol{\mu}_s$ with a field $\mathbf{B}$ is given by $\boldsymbol{\mu}_s \cdot B$ and, in the absence of an external field, $\mathbf{B}$ is proportional of the vector product of the nuclear field $\mathbf{E}$ and velocity of the electron $\mathbf{v}$

$$\mathbf{B} = \frac{\mathbf{E} \times \mathbf{v}}{c}, \tag{4.4}$$

where c is the speed of light. Now $\boldsymbol{\mu}_s = -(eh/2mc)\boldsymbol{\sigma}$ and $\mathbf{v} = \mathbf{p}/m_e$, where m_e is the electron mass, so that the interaction will be

$$(eh/2m^2c^2)\boldsymbol{\sigma} \cdot (\mathbf{E} \times \mathbf{p}) \tag{4.5}$$

and for a central field

$$\mathbf{E} = -\frac{1}{r}\frac{\partial V}{\partial r}\mathbf{r} \tag{4.6}$$

with V being the potential.

Writing $\mathbf{s} = h\boldsymbol{\sigma}/2$ and $\mathbf{l} = \mathbf{r} \times \mathbf{p}$ for one electron, the expression for the interaction becomes

$$(e^2/m_e^2c^2)\left(\frac{1}{r}\frac{\partial V}{\partial r}\right)\mathbf{l} \cdot \mathbf{s}. \tag{4.7}$$

We have considered the nucleus to be at rest, and so this must be divided by 2 (the Thomas precession factor).

Since spin is a relativistic effect, it is more correct to start with Dirac's relativistic equation for the electron. The reduction of the Dirac equation to non-relativistic form and the use of atomic units ($e = \hbar = m_e = 1$) gives the spin-orbit interaction

energy for a one-electron atom as[75]

$$H^{SO} = \frac{\alpha^2}{2} \frac{1}{r} \frac{\partial V}{\partial r} \mathbf{l} \cdot \mathbf{s}, \tag{4.8}$$

where V is the Coulomb potential due to the nucleus and $\alpha = 1/c$ is the fine-structure constant. This may be rewritten as $\zeta \mathbf{l} \cdot \mathbf{s}$ and this provides a definition of the spin-orbit coupling constant ζ for a one-electron atom. In such case $V = -Z/r$ and so $\partial V/\partial r = Z/r^2$

The generalization of this result to many electron atoms is far from straightforward but following Condon and Shortley[76] it is normal to reinterpret V as the screened potential due to the nucleus and to all the other electrons and the result is then summed over all the outer electrons, giving the spin-orbit Hamiltonian as

$$\begin{aligned} H^{SO} &= \sum_i \frac{\alpha^2}{2} \frac{1}{r_i} \frac{\partial V}{\partial r_i} \mathbf{l}_i \cdot \mathbf{s}_i \\ &= \sum_i \zeta(r_i) \mathbf{l}_i \cdot \mathbf{s}_i. \end{aligned} \tag{4.9}$$

This spin-orbit Hamiltonian does not commute with the operators S_z, L_z, but with S^2, L^2, J^2 and J_z. The latter pair are related to the others by

$$J_z = L_z + S_z \tag{4.10}$$

and its analogues and by

$$J^2 = J_x^2 + J_y^2 + J_z^2. \tag{4.11}$$

If we have a function ψ which is an eigenfunction of these operators, then

$$J_z \psi = M_J \psi \tag{4.12}$$

$$M_J = M_L + M_S \tag{4.13}$$

$$J^2 \psi = J(J+1)\psi \tag{4.14}$$

$$-J \leq M_J \leq J. \tag{4.15}$$

In order to calculate matrix elements of this Hamiltonian including H^{SO} it is convenient to use eigenfunctions of J^2.

4.4 Spin-Orbit Coupling in Diatomic Molecules

There is no rigorous first-principle derivation of the spin-orbit coupling for the two-center many-electron case. Usually, it has been constructed from the additivity of the Breit-Pauli two-particle Hamiltonian.[75,77] For a diatomic molecule one has that

$$H^{SO} = \frac{1}{2c^2}\left[\sum_{i=1}^{N} Z_A \frac{\mathbf{l}_{iA}}{r_{iA}^3}\cdot\mathbf{s}_i + \sum_{i=1}^{N} Z_B \frac{\mathbf{l}_{iB}}{r_{iB}^3}\cdot\mathbf{s}_i - \sum_{i\neq j}^{N}\left(\frac{\mathbf{r}_{ij}\times\mathbf{p}_i}{r_{ij}^3}\right)\cdot(\mathbf{s}_i + 2\mathbf{s}_j)\right], \quad (4.16)$$

where c is the speed of light, $\mathbf{l}_{iX} = \mathbf{r}_{iX}\times\mathbf{p}_i$, $\mathbf{p}_i$ is the momentum of the ith electron, and $\mathbf{r}_{iX}$ is position of the ith electron respective to nuclei X ($X = A,\ B$). The first two terms in Eq. 4.16 are one-electron operators and represent the spin-orbit coupling of each electron in the field of the two bare nuclei with charges Z_A and Z_B, respectively. The third term, the spin-other-orbit interaction, arises from inter-electronic interactions and partially counterbalances the field of the bare nuclei. Its sign is opposite to that of the one-electron term.

The use of Eq. 4.16 gives good agreement with experimental results for the fine-structure splittings,[75] but can not be used within our one-electron formalism. Therefore, we will opt for a different, more convenient approach in terms of pseudopotentials.

4.4.1 Spin-Orbit Coupling in Terms of Pseudopotentials

The potentials obtained directly from relativistic atomic wave functions have the form

$$\hat{U}^{REP} = \sum_{l=0}^{\infty}\sum_{j=|l-1/2|}^{l+1/2} U_{lj}^{REP}(r)\hat{P}_{lj}, \quad (4.17)$$

where we use the notation from Pitzer and Winter.[62] REP denotes relativistic effective potential, and the $\hat{P}_{lj}$ are (spin-dependent) projection operators. The $\hat{P}_{lj}$

are more difficult to work with than the spin-independent projection operators $\hat{P}_l$, but to relate the two, a spin operator must also appear,[78] and it does so in the form $\hat{l} \cdot \hat{s}$:

$$\hat{U}^{REP} = \sum_{l=0}^{\infty} U_l^{AREP}(r)\hat{P}_l + \sum_{l=1}^{\infty} \xi_l(r)\hat{P}_l\, \hat{\mathbf{l}} \cdot \hat{\mathbf{s}}\, \hat{P}_l = \hat{U}^{AREP} + \hat{H}^{SO}, \tag{4.18}$$

where $\hat{U}^{AREP}$ is an averaged (with $2j+1$ weighting) relativistic effective potential and $\xi_l(r)$ depends on the difference of $U_{l,l+1/2}(r)$ and $U_{l,l-1/2}(r)$. These two terms are readily identified[79] as core potentials and spin-orbit (potential) operators respectively.

The core potential is reduced to the potential described in chapter 1. The spin-orbit operator, is reduced to a finite sum by making the approximation that the $\xi_l\, \hat{l} \cdot \hat{s}$ are independent of l for $l \geq L$, where L is one more than the highest quantum number of the core orbitals being replaced. With the use of the completeness relation property of the $\hat{P}_l$, and the truncation of terms higher than $\xi_L(r)$, it yields.

$$\hat{H}^{SO} = \xi_L(r)\hat{l} \cdot \hat{s} + \sum_{l=1}^{L-1} [\xi_l(r) - \xi_L(r)]\, \hat{P}_l\, \mathbf{l} \cdot \mathbf{s} \hat{P}_l, \tag{4.19}$$

but as shown in previous calculations[80,81] the approximate form

$$\hat{H}^{SO} = \sum_{l=1}^{L-1} [\xi_l(r) - \xi_L(r)]\, \hat{P}_l\, \mathbf{l} \cdot \mathbf{s}\, \hat{P}_l \tag{4.20}$$

produces accurate results. Pitzer and Winter[78] have proposed a spin-orbit operator of the form

$$\hat{H}^{SO} = \sum_{l=1}^{l'_{max}} \frac{2\Delta V_{l,\lambda}^{SO}(r_\lambda)}{2l+1} P_{l,\lambda}\, \mathbf{l} \cdot \mathbf{s}\, P_{l,\lambda} \tag{4.21}$$

with $\mathbf{l}$ and $\mathbf{s}$ denoting the orbital angular momentum and spin operators, λ the atomic cores and $P_{l,\lambda}$ are spin-independent projection operator. The difference $\Delta V_{l,\lambda}^{SO}$ of the radial parts of the two-component relativistic pseudopotentials $V_{l,l+1/2}^{PP}$

Table 4–1: Parameters (in au) of the spin-orbit operators for Li and Na.

	l	n_k	ΔB_{lk}	β_{lk}
Li	1	2	0.8078	0.000035
		2	2.5500	-0.000035
		1	7.2535	0.000869
Na	1	2	1.6068	0.000086
		2	22.5231	0.023508
		1	76.2365	0.032039

and $V_{i,l-1/2}^{PP}$ is written (similarly to the radial part of the spin-orbit averaged pseudopotentials) in terms of the Gaussian functions:

$$\Delta V_l^{SO}(r_{i\lambda}) = \sum_k \Delta B_{lk} r^{n_k-2} \exp(-\beta_{lk} r_{i\lambda}^2). \tag{4.22}$$

We have omitted the atomic core index λ index from our notation since the operator is only applied to the alkali atom.

Elimination of the core electrons leads to a molecular valence Hamiltonian (in au)

$$\hat{H} = -\frac{1}{2}\nabla_{r_A}^2 + \hat{V}_{el}^{PP} + \hat{H}^{SO}. \tag{4.23}$$

4.4.2 Choice of Parameters

The exponential parameters β_{lk}, the linear parameters ΔB_{lk} and the exponents n_k from Eq. 4.22 constitute adjustable parameters which are optimized in a least-squares sense to reproduce reference spin-orbit splittings derived form all-electron calculations. Table 4–1 lists the SOC parameters for Li and Na. These numbers were taken from Pacios and Christiansen.[80]

4.5 The Eik/TDMO Method with Spin-Orbit Coupling

We start the TDMO approximation by expressing the spin-orbit coupling states η_λ with $\lambda = (lsjm_j)$ as

$$\eta_\lambda(\mathbf{x}, t) = \sum_j a_{j\lambda}^{in} \psi_j(\mathbf{x}_j, t) \tag{4.24}$$

where the $a_{j\lambda}^{in}$ are taken from the spin-orbit coupling states at initial time t_{in}, and $\mathbf{x}_j = (\mathbf{r}_j, \zeta_j)$ are a collection of position and spin variables.

For a given initial electronic state I and trajectory $\mathbf{R}(t)$, one has that

$$\psi_i(\mathbf{x_i}, t) = \psi_i^\gamma(\mathbf{r}_i, t)\gamma(\zeta_i), \tag{4.25}$$

$$\langle \psi_i^\gamma \mid \psi_j^{\gamma'} \rangle = \delta_{ij}\delta\gamma\gamma', \tag{4.26}$$

where the ψ_i^γ are TDMOs for electron spin $\gamma = \alpha, \beta$. In preparation for the inclusion of spin-orbit coupling in the TDMO approximation, it is convenient to define the electronic density operator for spin projections $\gamma, \gamma' = \alpha, \beta$ as

$$\hat{\rho}^{\gamma\gamma'}(t) = \mid \psi_i^\gamma(t)\gamma\rangle\langle\psi_i^{\gamma'}(t)\gamma' \mid \tag{4.27}$$

satisfying the TDMO equations with spin-orbit coupling (TDMO-SO)

$$\sum_{\gamma''} \left[\hat{H}^{\gamma\gamma''}\hat{\rho}^{\gamma''\gamma'} - \hat{\rho}^{\gamma\gamma''}\hat{H}^{\gamma''\gamma'}\right] = i\hbar\frac{\partial\hat{\rho}^{\gamma\gamma'}}{\partial t} \tag{4.28}$$

with $\hat{H}^{\gamma''\gamma'}$ an operator from the one-electron Hamiltonian.

4.6 Eik/TDMO-SO in Terms of a General Basis Set

In this section a general basis set of electronic orbitals is introduced in which the MOs are expanded as

$$\psi_i^\gamma(\mathbf{r}, t) = \sum_p \phi_p(\mathbf{r}, t)c_{ip}^\gamma(t) \tag{4.29}$$

with the coefficients being complex valued.

In what follows, a general matrix operator for spins $\gamma\gamma'$, $\mathbf{O}^{\gamma\gamma'}$ forms a 2×2 supermatrix $\mathbb{O}$, according to the notation

$$\mathbb{O} = \begin{pmatrix} \mathbf{O}^{\alpha\alpha} & \mathbf{O}^{\alpha\beta} \\ \mathbf{O}^{\beta\alpha} & \mathbf{O}^{\beta\beta} \end{pmatrix}. \tag{4.30}$$

The $\rho^{\gamma\gamma'}$ element of the density superoperator can be written in the basis of Eq. 4.29 as

$$\rho^{\gamma\gamma'}(t) = \sum_{pq} \mid \phi_p\gamma\rangle P^{\gamma\gamma'}_{pq}(t)\langle\phi_q\gamma' \mid \tag{4.31}$$

where $P^{\gamma\gamma'}_{pq}$ is the (pq)-element of the density matrix $\mathbf{P}^{\gamma\gamma'}$. Eq. 4.31 in matrix notation is

$$\rho^{\gamma\gamma'} = \mid \phi\gamma\rangle\mathbf{P}^{\gamma\gamma'}\langle\phi\gamma' \mid \tag{4.32}$$

where $\mid \phi\gamma\rangle$ and $\langle\phi\gamma \mid$ are row and column matrices with spin-orbital elements $\phi_p\gamma$, respectively.

The matrix elements of $\mathbf{P}^{\gamma\gamma'}$ are

$$P^{\gamma\gamma'}_{pq}(t) = \sum_{occ\ i} c^{\gamma}_{pi}(t)c^{\gamma'}_{qi}(t)^*. \tag{4.33}$$

The one-electron Hamiltonian matrix $\mathbf{H}^{\gamma\gamma'}$ is given by

$$\mathbf{H}^{\gamma\gamma'} = \langle\phi\gamma \mid \hat{H} \mid \phi\gamma'\rangle. \tag{4.34}$$

Alternatively, the one-electron Hamiltonian matrix can be written as

$$\mathbf{H}^{\gamma\gamma'} = (\mathbf{K} + \mathbf{V}^{PP}_{el})\delta_{\gamma\gamma'} + \mathbf{H}^{\gamma\gamma'}_{SO} \tag{4.35}$$

with $\mathbf{K}$ being the electron kinetic energy matrix, $\mathbf{V}^{PP}_{el}$ is the pseudopotential matrix described in chapter 2, and $\mathbf{H}^{\gamma\gamma'}_{SO}$ the spin-orbit coupling matrix.

In order to derive the TDMO-SO equations for the density matrix, the matrices Ω and S are defined, respectively, by

$$\mathbf{\Omega}^{\gamma\gamma'} = \langle \boldsymbol{\phi}\gamma \mid \frac{\partial}{\partial t}\boldsymbol{\phi}\gamma' \rangle = \Omega\delta_{\gamma\gamma'}, \tag{4.36}$$

and

$$\mathbf{S}^{\gamma\gamma'} = \langle \boldsymbol{\phi}\gamma \mid \boldsymbol{\phi}\gamma' \rangle = \mathrm{S}\delta_{\gamma\gamma'}. \tag{4.37}$$

Starting from the four differential equations for $\rho^{\gamma\gamma}$ in Eq. 4.28, and multiplying them by $\langle \boldsymbol{\phi}\gamma \mid$ from the left and by $\mid \boldsymbol{\phi}\gamma' \rangle$ from the right, the following four differential equations are obtained

$$i\dot{\mathbb{P}} = \mathbb{S}^{-1}(\mathbb{H} - i\mathbb{\Omega}_s)\mathbb{P} - \mathbb{P}(\mathbb{H} - i\mathbb{\Omega}_s)^{\dagger}\mathbb{S}^{-1}, \tag{4.38}$$

where the supermatrices are defined as

$$\mathbb{P} = \begin{pmatrix} \mathbf{P}^{\alpha\alpha} & \mathbf{P}^{\alpha\beta} \\ \mathbf{P}^{\beta\alpha} & \mathbf{P}^{\beta\beta} \end{pmatrix} \tag{4.39}$$

(4.40)

$$\mathbb{H} = \begin{pmatrix} \mathbf{H}^{\alpha\alpha} & \mathbf{H}^{\alpha\beta} \\ \mathbf{H}^{\beta\alpha} & \mathbf{H}^{\beta\beta} \end{pmatrix} \tag{4.41}$$

(4.42)

$$\mathbb{S} = \begin{pmatrix} \mathbf{S} & \mathbf{0} \\ \mathbf{0} & \mathbf{S} \end{pmatrix} \tag{4.43}$$

and

$$\mathbb{\Omega}_s = \begin{pmatrix} \Omega & \mathbf{0} \\ \mathbf{0} & \Omega \end{pmatrix} \tag{4.44}$$

4.7 Matrix Equations in the Traveling Atomic Basis

As discussed earlier if the molecular orbitals are expanded in terms of a basis of static atomic orbitals $\{\chi_i\}$, it would bring spurious coupling at large internuclear distances. To avoid this problem and to account for translational phase factors, one expands the MOs as linear combinations of traveling atomic orbitals (TAOs) ξ_μ.

$$\psi_i^\gamma(\mathbf{r},t) = \sum_\mu \xi_\mu(\mathbf{r},t) c_{\mu i}^\gamma(t), \tag{4.45}$$

with the TAOs are defined in chapter 3.

Operators can also be expanded in a basis of TAOs. The density operator in this basis is given now in matrix notation by

$$\rho^{\gamma\gamma'} = |\, \boldsymbol{\xi}\gamma\rangle \mathbf{P}^{\gamma\gamma'} \langle \boldsymbol{\xi}\gamma' \,| \tag{4.46}$$

and the Hamiltonian matrix $\mathbf{H}^{\gamma\gamma'}$ is defined as

$$\mathbf{H}^{\gamma\gamma'} = \langle \boldsymbol{\xi}\gamma \mid \hat{H} \mid \boldsymbol{\xi}\gamma' \rangle. \tag{4.47}$$

Evaluating the matrix elements of Ω and of the electron kinetic energy operator $\mathbf{K}$ in the basis of TAOs and canceling terms, Eq. 4.38 becomes

$$i\dot{\mathbb{P}} = \mathbb{S}^{-1}\mathbb{H}_T\mathbb{P} - \mathbb{P}\mathbb{H}_T^\dagger\mathbb{S}^{-1}, \tag{4.48}$$

where the new overlap supermatrix is formed by the elements

$$\mathbf{S}^{\gamma\gamma'} = \langle \boldsymbol{\xi}\gamma \mid \boldsymbol{\xi}\gamma' \rangle = \mathbf{S}\delta_{\gamma\gamma'}, \tag{4.49}$$

and the Hamiltonian

$$\mathbf{H}_T^{\gamma\gamma'} = (\mathbf{K}_T + \mathbf{V}_{el}^{PP}{}_T)\delta_{\gamma\gamma'} + \mathbf{H}_{SO}^{\gamma\gamma'} \tag{4.50}$$

Now it is convenient to define the potential V_{qu}, in Eq. (2.8), in terms of an Ehrenfest potential

$$V_{qu} = V_{cc}(R) + \frac{\mathrm{tr}[\mathbb{PH}]}{\mathrm{tr}[\mathbb{P}]} \tag{4.51}$$

where V_{cc} is the core-core repulsion term.

4.8 Transformation from the Static to the Traveling Basis Set

The calculation of the matrix elements is first carried out in the static basis χ and then transformed to the TAO basis ξ. The transformation is done with the overlap integrals between the two bases. Omitting provisionally the spin indexes γ, γ' and introducing a superscript to discern the χ and ξ bases, one writes

$$\rho = |\,\boldsymbol{\chi}\rangle \mathbf{P}^{(\chi)} \langle\boldsymbol{\chi}\,| = |\,\boldsymbol{\xi}\rangle \mathbf{P}^{(\xi)} \langle\boldsymbol{\xi}\,| \tag{4.52}$$

which yields

$$\mathbf{P}^{(\chi)} = (\mathbf{S}^{\chi})^{-1} \langle\boldsymbol{\chi} \mid \boldsymbol{\xi}\rangle \mathbf{P}^{(\xi)} \langle\boldsymbol{\xi} \mid \boldsymbol{\chi}\rangle (\mathbf{S}^{\chi})^{-1}. \tag{4.53}$$

Here $\mathbf{S}^{\chi}$ is the overlap matrices given in terms of the static basis.

4.9 Physical Properties of Interest

We are interested in monitoring the expectation values of the electronic orbital $\langle \mathbf{l} \rangle$, spin$\langle \mathbf{s} \rangle$ and total $\langle \mathbf{j} \rangle$ angular momentum vectors as functions of time along a particular trajectory. To do that let us introduce first the expression for the expectation value of an general operator $\hat{A}$, given in terms of the density matrix $\hat{\rho}$

$$\langle \hat{A}(t) \rangle = \frac{\mathrm{tr}[\rho(t)\hat{A}]}{\mathrm{tr}[\rho(t)]} \tag{4.54}$$

$$= \frac{\mathrm{tr}[\sum_{\mu\nu} \mid \xi_\mu\gamma\rangle P^{\gamma\gamma'}_{\mu\nu}(t) \langle\xi_\nu\gamma' \mid \hat{A}]}{\sum_{\mu\nu} \mid \xi_\mu\gamma\rangle P^{\gamma\gamma'}_{\mu\nu}(t) \langle\xi_\nu\gamma' \mid} \tag{4.55}$$

$$= \frac{\sum_{\mu\nu} P^{\gamma\gamma'}_{\mu\nu}(t) \langle\xi_\nu\gamma' \mid \hat{A} \mid \xi_\mu\gamma\rangle}{\sum_{\mu\nu} P^{\gamma\gamma'}_{\mu\nu}(t) S^{\gamma\gamma'}_{\nu\mu}}. \tag{4.56}$$

The time evolution of the $\hat{l}_k$ component ($k = x, y, z$) of the angular momentum is given then by

$$\langle \hat{l}_k(t) \rangle = \frac{\sum_{\mu\nu} P_{\mu\nu}^{\gamma\gamma'}(t) \langle \xi_\nu \gamma' \mid \hat{l}_k \mid \xi_\mu \gamma \rangle}{\sum_{\mu\nu} P_{\mu\nu}^{\gamma\gamma'}(t) S_{\nu\mu}^{\gamma'\gamma}}, \tag{4.57}$$

where

$$\hat{l}_x = -i\hbar \left(y \frac{\partial}{\partial z} - z \frac{\partial}{\partial y} \right), \tag{4.58}$$

$$\hat{l}_y = -i\hbar \left(z \frac{\partial}{\partial x} - x \frac{\partial}{\partial z} \right), \tag{4.59}$$

$$\hat{l}_z = -i\hbar \left(x \frac{\partial}{\partial y} - y \frac{\partial}{\partial x} \right). \tag{4.60}$$

In the case of a spin operator, the time evolution of the $\hat{s}_x$ component is given by

$$\langle \hat{s}_x(t) \rangle = \frac{\sum_{\mu\nu} P_{\mu\nu}^{\gamma\gamma'}(t) \langle \xi_\nu \gamma' \mid \hat{s}_x \mid \xi_\mu \gamma \rangle}{\sum_{\mu\nu} P_{\mu\nu}^{\gamma\gamma'}(t) S_{\nu\mu}^{\gamma'\gamma}}, \tag{4.61}$$

$$= \frac{1}{2}\hbar \frac{\sum_{\mu\nu} P_{\mu\nu}^{\gamma\gamma'}(t) \langle \xi_\nu \mid \xi_\mu \rangle (1 - \delta_{\gamma\gamma'})}{\sum_{\mu\nu} P_{\mu\nu}^{\gamma\gamma'}(t) S_{\nu\mu}^{\gamma'\gamma}}, \tag{4.62}$$

for $\hat{s}_y$ we have

$$\langle \hat{s}_y(t) \rangle = \frac{\sum_{\mu\nu} P_{\mu\nu}^{\gamma\gamma'}(t) \langle \xi_\nu \gamma' \mid \hat{s}_y \mid \xi_\mu \gamma \rangle}{\sum_{\mu\nu} P_{\mu\nu}^{\gamma\gamma'}(t) S_{\nu\mu}^{\gamma'\gamma}}, \tag{4.63}$$

$$= \pm\frac{1}{2}\hbar \frac{\sum_{\mu\nu} P_{\mu\nu}^{\gamma\gamma'}(t) \langle \xi_\nu \gamma' \mid \xi_\mu \gamma \rangle (1 - \delta_{\gamma\gamma'})}{\sum_{\mu\nu} P_{\mu\nu}^{\gamma\gamma'}(t) S_{\nu\mu}^{\gamma'\gamma}}, \tag{4.64}$$

where the plus sign is for the case $\gamma' = \beta$ and $\gamma = \alpha$, and the minus sign is for $\gamma' = \alpha$ and $\gamma = \beta$. For $\hat{s}_z$

$$\langle \hat{s}_z(t) \rangle = \frac{\sum_{\mu\nu} P_{\mu\nu}^{\gamma\gamma'}(t) \langle \xi_\nu \gamma' \mid \hat{s}_z \mid \xi_\mu \gamma \rangle}{\sum_{\mu\nu} P_{\mu\nu}^{\gamma\gamma'}(t) S_{\nu\mu}^{\gamma'\gamma}}, \tag{4.65}$$

$$= \pm\frac{1}{2}\hbar \frac{\sum_{\mu\nu} P_{\mu\nu}^{\gamma\gamma'}(t) \langle \xi_\nu \mid \xi_\mu \rangle \delta_{\gamma\gamma'}}{\sum_{\mu\nu} P_{\mu\nu}^{\gamma\gamma'}(t) S_{\nu\mu}^{\gamma'\gamma}}, \tag{4.66}$$

where the plus sign is for the case where $\gamma = \gamma' = \alpha$, and the minus sign for $\gamma = \gamma' = \beta$.

We are also interested in calculating the total cross section for the transition $j \to j'$ at an energy E is given by

$$\sigma_{j\to j'}(E) = \frac{1}{2j+1} \sum_{m_j=-j}^{j} \sum_{m'_{j'}=-j'}^{j'} \sigma_{j,m_j\to j',m'_{j'}}, \tag{4.67}$$

in the above equation $\sigma_{j,m_j\to j',m'_{j'}}$ is the fine-structure cross section calculated with and our integral cross section $\sigma_{jm_j\to j'm'_{j'}}(E)$ is

$$\sigma_{jm_j\to j'm'_{j'}}(E) = 2\pi \int db\, b\, P^{(jm_j)}_{j'm'_{j'},j'm'_{j'}}(E,b) \tag{4.68}$$

for the fine-structure transition from a state jm_j to a final state $j'm'_{j'}$ for the projectile energy E, where b is the impact parameter and $P^{(jm_j)}_{j'm'_{j'},j'm'_{j'}}$ is the transition probability form initial state jm_j to final state $j'm'_{j'}$ at the final time.

Expressions for the fine-structure and total cross sections were derived in Reid.[27] Of greater experimental interest are the multipole relaxation and coherence transfer cross sections which are discussed in detail by Wilson and Shimoni.[82] These cross section can be calculated from the fine-structure cross sections and the total cross sections. For convenience we will only summarize the expressions of those cross sections which have been measured experimentally and theoretically calculated for the Na-He system. Using the notation in Wilson and Shimoni, they are given by

$$\sigma^{\frac{1}{2}}_{\frac{1}{2}} = \sigma_{\frac{1}{2}\to\frac{3}{2}} + 2\sigma_{\frac{1}{2},-\frac{1}{2}\to\frac{1}{2},\frac{1}{2}} \tag{4.69}$$

$$\sigma^{\frac{1}{2}}_{\frac{3}{2}} = \sigma_{\frac{3}{2}\to\frac{1}{2}} + \frac{1}{2}\sigma_{\frac{3}{2},\frac{1}{2}\to\frac{1}{2},\frac{1}{2}} + 2\sigma_{\frac{3}{2},\frac{1}{2}\to\frac{3}{2},\frac{3}{2}} + \frac{3}{2}\sigma_{\frac{3}{2},\frac{3}{2}\to\frac{3}{2},-\frac{3}{2}} \tag{4.70}$$

$$\sigma^{coh\ tr}_{\frac{1}{2}\to\frac{3}{2}} = 5\left[\sigma_{\frac{1}{2},\frac{1}{2}\to\frac{3}{2},\frac{1}{2}} - \sigma_{\frac{1}{2},\frac{1}{2}\to\frac{3}{2},-\frac{3}{2}}\right] \tag{4.71}$$

$$\sigma^{coh\ tr}_{\frac{3}{2}\to\frac{1}{2}} = \frac{1}{3}\left[\sigma_{\frac{3}{2},\frac{3}{2}\to\frac{1}{2},\frac{1}{2}} - \sigma_{\frac{3}{2},-\frac{3}{2}\to\frac{1}{2},-\frac{1}{2}}\right] \tag{4.72}$$

$$\sigma^{dep} = \sigma_{\frac{1}{2},-\frac{1}{2}\to\frac{1}{2},\frac{1}{2}}. \tag{4.73}$$

When making detailed comparisons between theory and experiment, the cross sections above must be averaged over the velocity distribution. The averaged cross sections for a temperature T are given by

$$\sigma(T) = \frac{\int f(v,T)\sigma(v)dv}{\int f(v,T)dv} \tag{4.74}$$

where $f(v,T)$ is the normalized Maxwellian energy distribution given by

$$f(v,T) = 4\pi \left(\frac{\mu}{2\pi k_B T}\right)^{3/2} v^2 \exp[-\mu v^2/(k_B T)], \tag{4.75}$$

and μ is the reduced mass of the system.

4.10 Computational Aspects

4.10.1 Spin-Orbit Integrals

Integrals over the spin-orbit (potential) operator can be factored into (vector) space and spin parts. The computational choice to be made is whether to compute and store integrals over molecular spin-orbitals or to compute and store integrals over molecular orbitals of up to three components of the spatial part of the operator. In a case with no symmetry, the number of the latter would be 3/4 the number of the former. With some amount of spatial symmetry, the ratio would be even smaller. On the other hand, if purely spatial integrals are computed and stored, the spin integrals of $\hat{s}$ must be generated later.

Our atomic functions are expanded in terms of Gaussian atomic orbitals of the form

$$g(\mathbf{r}_X, n_X, l_X, m_X, \alpha_X) = N(n_X, l_X, m_X, \alpha_X) x_X^{n_X} y_X^{l_X} z_X^{m_X} \exp(-\alpha_X r_X^2), \tag{4.76}$$

where the $\mathbf{r}_X$ is the position of electron with respect to center X and the normalization constant is

$$N(n_X, l_X, m_X, \alpha_X) = \frac{(2\alpha_X/\pi)^{3/4}(4\alpha_X)^{(n_X+l_X+m_X)/2}}{[(2n_X-1)!!(2l_X-1)!!(2m_X-1)!!]^{-1/2}}, \tag{4.77}$$

where we have used the label X for the centers A or B.

The spin-orbit matrix elements are of the form

$$\langle g_A\gamma \mid \hat{H}^{SO} \mid g_B\gamma' \rangle =$$

$$\sum_{l=1}^{L}\sum_{j} d_{jl} \overbrace{\sum_{m=-l}^{l}\sum_{m'=-l}^{l} \int r_C^{n_j} \exp^{-\beta_{jl} r_C^2} \langle g_A \mid lm \rangle \langle lm \mid \mathbf{l} \mid lm' \rangle \langle lm' \mid g_B \rangle dr_C}^{\nu_{AB}}$$

$$\cdot \langle \gamma \mid \mathbf{s} \mid \gamma' \rangle, \quad (4.78)$$

where C can be A, B, or a different center.

We describe below the procedure we used to solve the ν_{AB} integral which is based on a procedure developed by Pitzer and Winter:[62]

Transforming the exponentials of g_A and g_B to center C in the following manner:

$$\exp\left(-\alpha_A {r_A}^2\right) = \exp\left(-\alpha_A {r_C}^2 - 2\alpha_A \mathbf{CA} \cdot \mathbf{r_C} - \alpha_A \mid \mathbf{CA} \mid^2\right), \quad (4.79)$$

$$\exp\left(-\alpha_B {r_B}^2\right) = \exp\left(-\alpha_B {r_C}^2 - 2\alpha_B \mathbf{CB} \cdot \mathbf{r_C} - \alpha_B \mid \mathbf{CB} \mid^2\right) \quad (4.80)$$

with

$$\mathbf{CA} = \mathbf{C} - \mathbf{A}, \quad (4.81)$$

$$\mathbf{CB} = \mathbf{C} - \mathbf{B}, \quad (4.82)$$

here $\mathbf{A}$, $\mathbf{B}$ and $\mathbf{C}$ are the position vector of centers A, B and C respectively. Defining

$$D_{ABC} = 4\pi N(n_A, l_A, m_A, \alpha_A) N(n_B, l_B, m_B, \alpha_B)$$

$$\times \exp\left(-\alpha_A \mid \mathbf{CA} \mid^2 - \alpha_B \mid \mathbf{CB} \mid^2\right), \quad (4.83)$$

$$\mathbf{k} = -2(\alpha_A \mathbf{CA} + \alpha_B \mathbf{CB}), \tag{4.84}$$

$$\alpha = \alpha_A + \alpha_B + \beta, \tag{4.85}$$

$$\mathbf{k_A} = -2\alpha_A \mathbf{CA}, \tag{4.86}$$

$$\mathbf{k_B} = -2\alpha_B \mathbf{CB}. \tag{4.87}$$

With the definitions above ν_{AB} in Eq. 4.78 becomes

$$\nu_{AB} = \frac{D_{ABC}}{4\pi} \sum_{m=-l}^{l} \int_0^\infty dr_C \overbrace{\left[\int d\Omega_C x_A^{n_A} y_A^{l_A} z_A^{m_A} \exp(\mathbf{k_A} \cdot \mathbf{r_C}) Y_{lm}(\Omega_C) \right]}^{\boxed{a}} \times \left[\int d\Omega_C x_B^{n_B} y_B^{l_B} z_B^{m_B} \exp(\mathbf{k_B} \cdot \mathbf{r_C}) Y_{lm}(\Omega_C) \right] r_C^{n'} \exp(-\alpha r_C^2) \times \langle lm \mid \mathbf{l} \mid lm' \rangle, \tag{4.88}$$

expanding the exponentials $\exp(\mathbf{k} \cdot \mathbf{r_C})$ in spherical coordinates

$$\exp(\mathbf{k_A} \cdot \mathbf{r_C}) = 4\pi \sum_{\lambda=0}^{\infty} \sum_{\mu=-\lambda}^{\lambda} M_\lambda(k_A r_C) Y_{\lambda\mu}(\theta_{k_A}, \phi_{k_A}) Y_{\lambda\mu}(\theta_C, \phi_C), \tag{4.89}$$

$$\exp(\mathbf{k_B} \cdot \mathbf{r_C}) = 4\pi \sum_{\lambda=0}^{\infty} \sum_{\mu=-\lambda}^{\lambda} M_\lambda(k_B r_C) Y_{\lambda\mu}(\theta_{k_B}, \phi_{k_B}) Y_{\lambda\mu}(\theta_C, \phi_C), \tag{4.90}$$

where M_λ is a modified spherical Bessel function of the first kind:

$$M_\lambda(x) = x^\lambda \left(\frac{1}{x} \frac{d}{dx} \right)^\lambda \frac{\sinh x}{x} \tag{4.91}$$

$$= i^\lambda j_\lambda(-ix). \tag{4.92}$$

Transforming x_A, y_A, z_A in terms of $\mathbf{CA}$, and separating variables of integrations, we have for $\boxed{\text{a}}$ in Eq. 4.88

$$\begin{aligned}
\boxed{\text{a}} &= \int d\Omega_C x_A^{n_A} y_A^{l_A} z_A^{m_A} \exp\left(\mathbf{k_A}\cdot\mathbf{r_C}\right) Y_{lm}(\Omega_C) \\
&= \int d\Omega_C (x_C - CA_x)^{n_A} (y_C - CA_y)^{l_A} (z_C - CA_Z)^{m_A} \\
&\qquad \times \left[4\pi \sum_{\lambda=0}^{\infty} \sum_{\mu=-\lambda}^{\lambda} M_\lambda(k_A r_C) Y_{\lambda\mu}(\theta_{k_A}, \phi_{k_A}) Y_{\lambda\mu}(\theta_C, \phi_C) \right] Y_{l,m}(\Omega_C) \\
&= \sum_{a=0}^{n_A} \sum_{b=0}^{l_A} \sum_{c=0}^{m_A} \binom{n_A}{a} \binom{l_a}{b} \binom{m_a}{c} CA_x^{n_A-a} CA_y^{l_A-b} CA_Z^{m_A-c} \sum_{\lambda=0}^{\infty} M_\lambda(k_A r_C) r_C^{a+b+c} \\
&\qquad \times \sum_{\mu=-\lambda}^{\lambda} Y_{\lambda\mu}(\theta_{k_A}, \phi_{k_A}) \int d\Omega_C \, \bar{x}_C^a \, \bar{y}_C^b \, \bar{z}_C^c \, Y_{\lambda\mu}(\theta_C, \phi_C) \, Y_{lm}(\Omega_C) \qquad (4.93)
\end{aligned}$$

where we have used

$$\bar{x} = \frac{x}{r} \quad \therefore \quad x = r\bar{x}. \qquad (4.94)$$

Calling

$$\Omega_{\lambda lm}^{abc} = \sum_{\mu=-\lambda}^{\lambda} Y_{\lambda\mu}(\theta_{k_A}, \phi_{k_A}) \int d\Omega_C \, \bar{x}_C^a \, \bar{y}_C^b \, \bar{z}_C^c \, Y_{\lambda\mu}(\theta_C, \phi_C) Y_{lm}(\Omega_C), \qquad (4.95)$$

Eq. 4.88 will become

$$\begin{aligned}
\nu_{AB} = \; & 4\pi D_{ABC} \sum_{a=0}^{n_A} \sum_{b=0}^{l_A} \sum_{c=0}^{m_A} \sum_{d=0}^{n_B} \sum_{e=0}^{l_B} \sum_{f=0}^{m_B} \binom{n_A}{a} \binom{l_A}{b} \binom{m_A}{c} \binom{n_B}{d} \binom{l_B}{e} \binom{m_B}{f} \\
& \times CA_x^{n_A-a} CA_y^{l_A-b} CA_z^{m_A-c} CB_x^{n_B-d} CB_y^{l_B-e} CB_z^{m_B-f} \\
& \times \sum_{\lambda=0}^{\infty} \sum_{\bar{\lambda}=0}^{\infty} Q_{\lambda\bar{\lambda}}^{a+b+c+d+e+f+n'}(k_A, k_B, \alpha) \\
& \times \sum_{m=-l}^{l} \sum_{m'=-l}^{l} \Omega_{\lambda lm}^{abc} \Omega_{\bar{\lambda} lm'}^{def} \langle lm \mid \mathbf{1} \mid lm' \rangle, \qquad (4.96)
\end{aligned}$$

where the radial integral $Q_{\lambda\bar{\lambda}}^N$ is given by

$$Q_{\lambda\bar{\lambda}}^N = \int_0^\infty dr r^N \exp\left(-\alpha r^2\right) M_\lambda(k_A r) M_{\bar{\lambda}}(k_B r). \qquad (4.97)$$

Integrals Q^N and Ω^{abc} are solved with the procedures presented in appendix C. The details of the structure of the program are presented in appendix A.

4.10.2 Structure of the Program

We start with the pseudopotential code that includes spin-orbit coupling. There, we do not need to worry much about the basis set given in terms of coupled or uncoupled states since the energy results are independent of this choice.

The implementation of the Eik/TDMO-PP-SO (`eiktdmoppso`) followed the equations presented in previous sections and what we show next is a description of some details that only appeared when implementing the code with spin-orbit coupling.

In appendix A we present a diagram of the algorithm of the current version of the `eiktdmoppso` code along with a detailed explanation of the subroutines invoked.

4.10.3 Choice of Initial Conditions

For the study of fine-structure transitions we need to start our system in one of the fine-structure states given in terms of coupled basis $\mid lsjm_j\rangle$. But, as we mentioned before, our code has been written to propagate the matrices in terms of Cartesian function basis. Therefore, when we initialize our calculations, we first create an initial density matrix in the coupled basis, and we then convert it from that basis to the Cartesian basis (which is the basis of the propagation) and finally when the calculation ends, we follow the opposite by converting the Cartesian density matrix back to the coupled one.

The procedure we created to do the transformation of the density matrix between the basis sets is presented below.

The density matrix of the system can be expressed in terms of the molecular orbitals ψ, the basis of Cartesian atomic functions ξ^c or the basis of coupled atomic functions ξ^j:

$$\hat{\rho} \quad = \quad \mid \psi\rangle \mathbf{P}^{\psi} \langle \psi \mid = \mid \xi^c\rangle \mathbf{P}^{c} \langle \xi^c \mid = \mid \xi^j\rangle \mathbf{P}^{j} \langle \xi^j \mid . \tag{4.98}$$

The first step in a calculation is to select the initial state of the system ψ_i. We do that by assigning 1 to the $\mathbf{P}^{\psi}_{i,i}$ element of the density matrix. We then transform the density matrix from the ψ to ξ^c basis that is the one of the dynamics. Eq. 4.125 shows how it is done. In what comes next we explain how we come up with the relation shown in 4.125.

Let us begin by calling ξ^c, ξ^s, ξ^j the Cartesian, spherical and coupled basis respectively. We can write the matrix relations among them as

$$| \xi^c\rangle = | \xi^s\rangle \mathbf{T}^{sc} \tag{4.99}$$

$$| \xi^j\rangle = | \xi^s\rangle \mathbf{T}^{sj} \tag{4.100}$$

$$| \xi^c\rangle = | \xi^j\rangle \mathbf{T}^{jc} = | \xi^j\rangle (\mathbf{T}^{sj})^{-1} \mathbf{T}^{sc}, \tag{4.101}$$

where $\mathbf{T}^{ab}$ is the transformation matrix from coordinates a to coordinates b.

The density operator $\hat{\rho}$ can be obtained in terms of the ξ^c and the ξ^j basis sets as

$$\hat{\rho} = | \xi^c\rangle \mathbf{P}^c \langle \xi^c | = | \xi^j\rangle \mathbf{P}^j \langle \xi^j | \,. \tag{4.102}$$

Projecting on the left of 4.102 by $\langle \xi^c |$ and on the right by $| \xi^c\rangle$ we get

$$\mathbf{S}^c \mathbf{P}^c \mathbf{S}^c = \langle \xi^c | \xi^j\rangle \mathbf{P}^j \langle \xi^j | \xi^c\rangle \tag{4.103}$$

$$= \langle \xi^c | \xi^c\rangle (\mathbf{T}^{jc})^{-1} \mathbf{P}^j \left[(\mathbf{T}^{jc})^{-1} \right]^{\dagger} \langle \xi^c | \xi^c\rangle \tag{4.104}$$

$$= \mathbf{S}^c (\mathbf{T}^{jc})^{-1} \mathbf{P}^j \left[(\mathbf{T}^{jc})^{-1} \right]^{\dagger} \mathbf{S}^c \tag{4.105}$$

$$\mathbf{P}^c = (\mathbf{T}^{jc})^{-1} \mathbf{P}^j ((\mathbf{T}^{jc})^{-1})^{\dagger} \tag{4.106}$$

$$\mathbf{P}^j = \mathbf{T}^{jc} \mathbf{P}^c (\mathbf{T}^{jc})^{\dagger}. \tag{4.107}$$

The density operator $\hat{\rho}$ can be written in terms of the ξ^j and the ψ basis sets as

$$\hat{\rho} = | \psi\rangle \mathbf{P}^{\psi} \langle \psi | = | \xi^j\rangle \mathbf{P}^j \langle \xi^j | \,. \tag{4.108}$$

Projecting on the left of 4.108 by $\langle \xi^j \mid$ and on the right by $\mid \xi^j \rangle$ we get

$$\langle \xi^j \mid \psi \rangle \mathbf{P}^{\psi} \langle \psi \mid \xi^j \rangle = \mathbf{S}^j \mathbf{P}^j \mathbf{S}^j \tag{4.109}$$

with $\mid \psi \rangle = \mid \xi^j \rangle \mathbf{C}^j$

$$\mathbf{S}^j \mathbf{C}^j \mathbf{P}^{\psi} \mathbf{C}^{j\dagger} \mathbf{S}^j = \mathbf{S}^j \mathbf{P}^j \mathbf{S}^j \tag{4.110}$$

$$\mathbf{C}^j \mathbf{P}^{\psi} \mathbf{C}^{j\dagger} = \mathbf{P}^j \tag{4.111}$$

using in 4.106 the relation for $\mathbf{P}^j$ in 3.56 we have

$$\mathbf{C}^j \mathbf{P}^{\psi} \mathbf{C}^{j\dagger} = \mathbf{T}^{jc} \mathbf{P}^c (\mathbf{T}^{jc})^{\dagger} \tag{4.112}$$

and solving for $\mathbf{P}^c$ we get

$$\mathbf{P}^c = (\mathbf{T}^{jc})^{-1} \mathbf{C}^j \mathbf{P}^{\psi} \mathbf{C}^{j\dagger} ((\mathbf{T}^{jc})^{-1})^{\dagger}. \tag{4.113}$$

To obtain $\mathbf{C}^j$ we start with the time independent Schrödinger equation

$$\hat{H} \mid \psi \rangle = \mid \psi \rangle \mathbf{E}, \tag{4.114}$$

and expanding ψ in Eq. 4.114 in terms of $\mid \xi^j \rangle$ as shown in 3.52, and projecting on the right by $\langle \xi^j \mid$ we obtain

$$\langle \xi^j \mid \hat{H} \mid \xi^j \rangle \mathbf{C}^j = \langle \xi^j \mid \xi^j \rangle \mathbf{C}^j \mathbf{E} \tag{4.115}$$

$$\mathbf{H}^j \mathbf{C}^j = \mathbf{S}^j \mathbf{C}^j \mathbf{E} \tag{4.116}$$

multiplying on both sides of Eq. 4.116 by $(\mathbf{S}^j)^{-1}$

$$(\mathbf{S}^j)^{-1} \mathbf{H}^j \mathbf{C}^j = \mathbf{C}^j \mathbf{E} \tag{4.117}$$

$$\mathbf{W}^j \mathbf{C}^j = \mathbf{C}^j \mathbf{E} \tag{4.118}$$

giving the eigenvalue matrix equation in the coupled basis set. Therefore $\mathbf{C}^j$ is obtained diagonalizing $\mathbf{W}^j$ in Eq. 4.118. The matrices $\mathbf{S}^j$ and $\mathbf{H}^j$ can be obtained

easily from the corresponding matrix calculated in the Cartesian basis ξ^c, to obtain

$$\mathbf{W}^j = (\mathbf{S}^j)^{-1}\mathbf{H}^j \tag{4.119}$$

$$= (\langle \xi^j \mid \xi^j \rangle)^{-1}\langle \xi^j \mid \hat{H} \mid \xi^j \rangle \tag{4.120}$$

$$= \left[((\mathbf{T}^{jc})^{-1})^\dagger \langle \xi^c \mid \xi^c \rangle (\mathbf{T}^{jc})^{-1}\right]^{-1} ((\mathbf{T}^{jc})^{-1})^\dagger \langle \xi^c \mid \hat{H} \mid \xi^c \rangle (\mathbf{T}^{jc})^{-1} \tag{4.121}$$

$$= \left[\mathbf{T}^{jc}(\mathbf{S}^c)^{-1}(\mathbf{T}^{jc})^\dagger\right] ((\mathbf{T}^{jc})^{-1})^\dagger \mathbf{H}^c (\mathbf{T}^{jc})^{-1} \tag{4.122}$$

$$= \mathbf{T}^{jc}(\mathbf{S}^c)^{-1}\mathbf{H}^c(\mathbf{T}^{jc})^{-1} \tag{4.123}$$

$$= \mathbf{T}^{jc}(\mathbf{W}^c)(\mathbf{T}^{jc})^{-1}. \tag{4.124}$$

Once the propagation in the Cartesian basis ends, we use the following transformation to analyze the results,

$$\mathbf{P}^\psi = \mathbf{C}^{j^{-1}}\mathbf{T}^{jc}\mathbf{P}^c(\mathbf{T}^{jc})^\dagger(\mathbf{C}^{j^\dagger})^{-1}. \tag{4.125}$$

4.11 Results and Discussion

4.11.1 Pseudopotential Results

To test the validity of the method and the accuracy of the computer code we have calculated the spin-orbit coupling splitting of Li and Na. Results are reported in table 4–2.

Table 4–2: Spin-orbit splitting for ^2P states (cm^{-1}).

Atom	H^{SO}	Exp.[38]
Li	0.4	0.3
Na	16	17

We have also calculated the diatomic potential energy curve for Li-He, Li-Ne , Na-He and Na-Ne. Figure 4–1 shows our results for Na-He and a comparison with the ab-initio results.

Energies for both the atomic and molecular energies were obtained with the small (4s4p/2s2p) basis. Despite the small size of this basis set, the results are in good agreement with the experimental and theoretical data.

4.11.2 Pictures of the Evolution of Electronic Angular Momenta

To get a complete picture of the collisional process, we examine the orbital probabilities as functions of time. In figure 4–2 we show the time evolution of $\mathrm{Na}(^2P_{j,m_j})$ states for a particular trajectory that corresponds to the initial state $\mid j, m_j\rangle = \mid 3/2, 3/2\rangle$, $v = 9 \times 10^4$ au, and an impact parameter of 10 au. All the populations oscillate in the time region of 20000-45000 au until they come to a constant value.

A simpler picture of the collision process can be obtained by monitoring the expectation values of the electronic angular momentum vectors $\langle \mathbf{l} \rangle$, $\langle \mathbf{s} \rangle$, and $\langle \mathbf{j} \rangle$ as functions of time along a trajectory. Each element of these vectors is given by the expectation values in Eqs. 4.9,4.62-4.66, where l_x is the matrix representing the component of the electronic angular momentum operator along the rotating x axis in the Born-Oppenheimer basis. Using the density matrix expression these matrices are easy to derive and expectation values can be computed at regular time steps along the trajectory.

The exact evolution of the angular momentum vectors is complicated, because it is determined by the relative magnitudes of three competing effects: the electrostatic fields of He, spin-orbit coupling in Na, and the rotation of the internuclear coordinates over the course of the collision.

In figures 4–3-4–5 we present typical trajectories. The He atom is located at the origin of the space-fixed coordinate system. The Na atom is traveling in the z

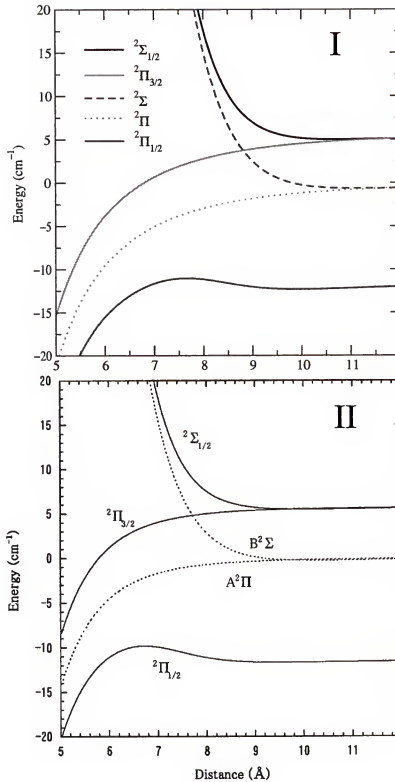

Figure 4–1: Diatomic potential energy curves of Na(^2P)-He, including(solid line) and neglecting (dotted line) spin-orbit interactions. Energies are relative to the asymptotic values neglecting spin-orbit interactions. I: Our results, II: Ab initio results.

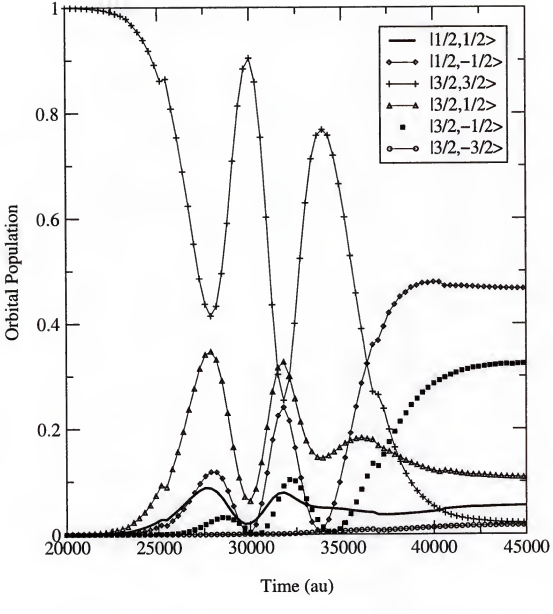

Figure 4–2: Population of the $\mathrm{Na}(^2P_{j,m_j})$ states as a function of time.

direction. We chose initial conditions so that we could easily see the time evolution of $\langle \mathbf{l} \rangle$, $\langle \mathbf{s} \rangle$, and $\langle \mathbf{j} \rangle$. We have used a moderately large impact parameter ($b = 10$ au), $v = 9 \times 10^4$ au and straight line trajectory. The collision begins with excited Na in the $^2P_{3/2,3/2}$ state. Our initial conditions do not necessarily correspond to any easily attained experimental situation. In figure 4–3 we see the evolution of $\langle \mathbf{l} \rangle$ which seems to undergo precession about the internuclear axis, while during the same time as shown in figure 4–4 $\langle \mathbf{s} \rangle$ rotates slowly by around 90^0. This results in an overall change in the relative orientation of the two vectors and thus a change in $\langle \mathbf{j} \rangle$ as shown in figure 4–5. Therefore a fine-structure transition has taken place.

In the Na*-He system $jm_j \rightarrow j'm'_j$, transitions occur by the following mechanism. As shown in the figure the system begins in the j=3/2 state, in which $\langle \mathbf{l} \rangle$ and $\langle \mathbf{s} \rangle$ are aligned to each other. Then as a result of the collision, the orientation of both have changed. It follows that both the magnitude and direction of $\langle \mathbf{j} \rangle$ are also changed by the collision. Change in the orientation of $\langle \mathbf{j} \rangle$ corresponds to $m_j \rightarrow m'_j$ transitions. Usually a change of the magnitude of $\langle \mathbf{j} \rangle$ represents a $j \rightarrow j'$ transitions. However, we must be a little cautious with this last statement: actually it is the change of $\langle j^2 \rangle$ that corresponds to $j \rightarrow j'$; since $\langle j^2 \rangle \neq \langle \mathbf{j} \rangle^2$, it is sometimes possible for the magnitude of $\langle \mathbf{j} \rangle$ to change even when $\langle j^2 \rangle$ does not change.

4.12 Fine-Structure Cross Sections

In tables 4–3 and 4–4 we present results for the partial cross sections $\sigma_{j,m_j \rightarrow j'm'_j}$ for velocities corresponding to two different temperatures 400 K and 450 K. The calculations were done at the most probable velocity v^* for the temperature T, given by the expression

$$v^* = \sqrt{\frac{2k_B T}{\mu}}, \tag{4.126}$$

where μ is the reduced mass of the Na-He system. These cross sections were obtained by numerical integration over a grid of 80 impact parameters from 0.0 au to 20 au

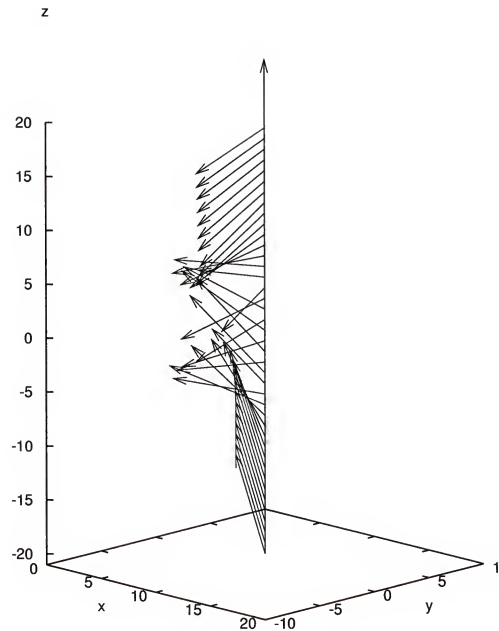

Figure 4–3: Evolution of $\langle \mathbf{l} \rangle$ for a straight line trajectory. The initial state is $\mathrm{Na}(^2P_{3/2,3/2})$

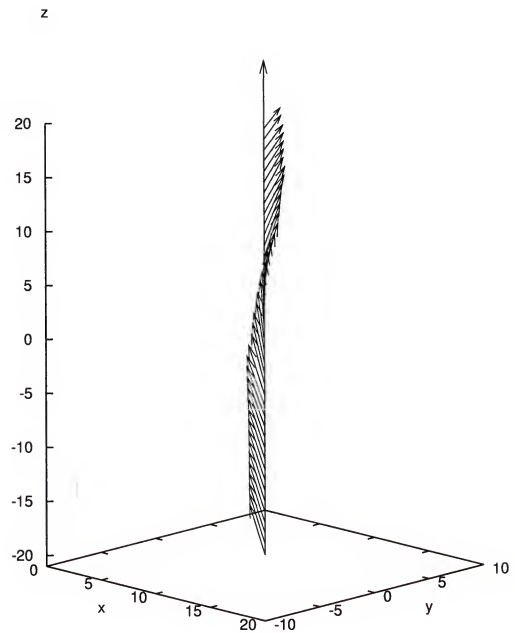

Figure 4–4: Evolution of $\langle \mathbf{s} \rangle$ for a straight line trajectory. The initial state is $\mathrm{Na}(^2P_{3/2,3/2})$

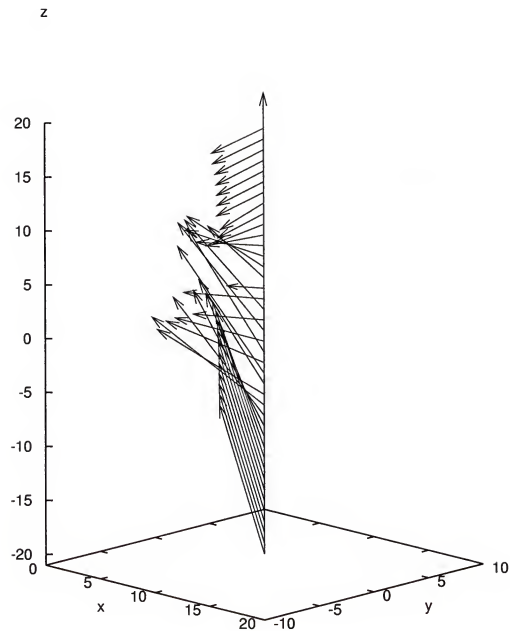

Figure 4–5: Evolution of $\langle \mathbf{j} \rangle$ for a straight line trajectory. The initial state is $\mathrm{Na}(^2P_{3/2,3/2})$

Table 4–3: Calculated fine-structure cross sections $\sigma_{j,m_j \to j',m'_{j'}}$ at $v^*(400\ \mathrm{K})$

	$j',m'_{j'}$					
j,m_j	1/2,1/2	1/2,-1/2	3/2,3/2	3/2,1/2	3/2,-1/2	3/2,-3/2
1/2,1/2	668.93	15.61	9.84	13.12	20.47	18.81
1/2,1/2-1/2	13.37	636.17	37.07	17.30	37.23	3.84
3/2,3/2	16.19	26.44	635.48	26.85	15.50	25.98
3/2,1/2	17.52	28.98	22.59	632.24	9.28	7.66
3/2,-1/2	18.40	17.11	6.82	18.21	660.89	14.86
3/2,-3/2	26.12	20.23	15.91	16.36	22.68	641.85

with different step sizes. The tolerance set $10^{-7} - 10^{-5}$ for low and high respectively seemed to converge.

In figure 4–6 we present the final populations of some of the $\mathrm{Na}(^2P_{j,m_j})$ states as a function of the impact parameter for an initial velocity $v^*(450\mathrm{K}) = 6.74 \times 10^4$ au.

We have also calculated the total, multipole relaxation and coherence cross sections. To compare our results with experimental and theoretical results we have averaged our cross sections over a Maxwell distribution for temperatures of 400 and 450 K. In table 4–5 our calculated thermally averaged total, multipole relaxation and coherence cross sections are compared with experimental data and past theoretical results including recent ones from Leo et al.[73] Our results are similar in many cases to the past theoretical results but lie above most of the calculations of Leo and below most measurements.

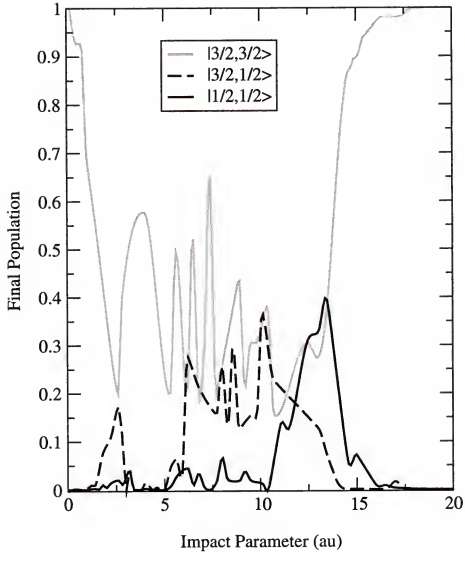

Figure 4–6: Transition probabilities vs. impact parameter in a $Na_{3/2.3/2}$+He collision, $v * (450K) = 6.74 \times 10^4$ au

Table 4–4: Calculated fine-structure cross sections $\sigma_{j,m_j \to j'm'_{j'}}$ at v^*(450 K)

	$j',m'_{j'}$					
j,m_j	1/2,1/2	1/2,-1/2	3/2,3/2	3/2,1/2	3/2,-1/2	3/2,-3/2
1/2,1/2	665.24	16.16	17.96	14.02	22.06	24.72
1/2,1/2-1/2	16.13	653.74	11.58	35.85	11.75	35.85
3/2,3/2	19.22	39.44	625.79	27.70	19.47	21.92
3/2,1/2	18.59	33.94	20.38	662.23	6.40	4.84
3/2,-1/2	28.88	223.22	14.96	16.30	643.52	25.27
3/2,-3/2	27.66	15.19	16.60	16.84	17.40	642.43

Table 4–5: Theoretical and experimental results for the total and multipole relaxation cross sections (in $\AA^2$) at 400 and 450 K

σ	$T(K)$	Experiment	Past theory	Past theory[73]	Present
$\sigma_{1/2\to3/2}$	450	106.9 ± 11^{83}	75.2^{27}	85.4	77.55
	400	86 ± 8^{84}	78^{38}	81.5	77.05
$\sigma_{3/2\to1/2}$	450	46 ± 4^{84}	43.6^{27}	44	46.46
	400	57 ± 5^{83}	43.8^{38}	44.5	46.39
σ^{dep}	450	13.2 ± 1.8^{83}	12.55^{85}	10.8	16.07
	400	15.6 ± 1.6^{86}	10.9^{82}	11.0	16.12
$\sigma^1_{\frac{1}{2}}$	450	133 ± 7^{83}	119.7^{85}	103.1	108.87
	400	90 ± 9^{86}	112^{82}	103.5	108.45
$\sigma^1_{\frac{3}{2}}$	450	112 ± 6^{83}	110.0^{85}	88.6	90.84
	400	128 ± 13^{87}	98^{82}	90.2	90.89
$\sigma^{coh\ tr}_{\frac{1}{2}}$	450	-66.3 ± 10.3^{83}	-75^{85}	-57.5	-60.39
	400	-64 ± 6.4^{86}	-62.4^{82}	-56.5	-59.83
$\sigma^{coh\ tr}_{\frac{3}{2}}$	450	-6.5 ± 1.1^{83}	-6.9^{85}	-5.77	-10.36
	400				-10.15

CHAPTER 5
CONCLUSION

The purpose of this study has been to develop a time-dependent methodology to explore in detail the dynamics of alkali atoms colliding with rare-gas atoms at two very different energy regimes:

- A high energy (0.5 to 30 keV) regime to study the time-dependence of the electronic excitation of the alkali atom.
- A low energy (hyperthermal) regime with energies of the order of fractions of one eV to study the spin-orbit recoupling of an initially excited alkali atom.

A new formalism which combines pseudopotentials, spin-orbit coupling potentials and the eikonal time-dependent molecular orbital method has been developed to study the dynamics of the active electron and nuclei by reducing our many electron systems into one active electron systems. The conclusions of this work are given in the same order as that of the preceeding chapters.

5.1 Pseudopotentials

An overview of the pseudopotential theory has been presented. The approach we chose in this work was the l-dependent pseudopotential method including core-polarization suggested by Preuss and collaborators.[58] This choice was based on the following premises: a) it reproduces accurately the interatomic potentials of the molecular systems of interest; b) all the pseudopotential parameters and basis sets were available in the literature; c) the pseudopotential operators are expanded in terms of standard functions, for which efficient analytical methods to solve the integrals are available in the literature.

We successfully reproduced the experimental ionization energies of the Li and Na atoms. We calculated the potential energy curves of the Li-He, Li-Ne, Na-He

and Na-Ne diatomic systems and found them to compare very well with electronic structure calculations.[3,4,31,41,67] We have them available for a series of alkali and rare-gas atoms.

We found that the basis set size has an important impact on the calculations and that convergence with respect to potential energies versus distances is reached only when basis sets containing several d-functions are used.

We conclude from our results that l-dependent atomic pseudopotentials are very convenient and accurate for studies of an alkali atom with a rare-gas atom. Our present results showed that they give excellent potential curves, by comparison with previous work, and also led to the correct non-adiabatic couplings between electronic states. The potentials we obtain are of sufficient quality so that they could also be used to describe the spectra of alkali atoms in a rare-gas environment

5.2 The Eikonal-Time Dependent Molecular Orbital Method Including Pseudopotentials

A novel treatment based on the Eik/TDMO method in terms of pseudopotentials was introduced to study the time evolution of electronic excitation in collisions of alkali atoms with rare-gas atoms, and was called the Eik/TDMO-PP method.

The calculation of time-dependent properties such electronic populations and polarization parameters for these systems provided a unique insight into the electronic rearrangement mechanism. It was noted that electronic populations tended to fluctuate during collisions and to settle at a final value. We found that the final value of the electronic populations was a function of the projectile energy and the impact parameter.

We calculated the integral cross sections for the electronic excitation from the ground state of Li and Na to their first excited state in collisions with He and Ne in the range from 0.5 to 30 keV depending upon the system. We obtained reasonable agreement with measurements for those systems. From our results we conclude that

several atomic d-orbitals were needed to describe 2s to 2p transitions of Li and the 3s to 3p transitions of Na and that a large basis set was necessary for obtaining accurate integral cross sections. We found that the basis set size also affected probabilities versus impact parameters and therefore the differential cross sections.

5.3 Spin-Orbit Recoupling

We extended the Eik/TDMO-PP formalism to include spin-orbit coupling for the study of angular momenta recoupling during hyperthermal alkali-rare-gas atom collisions. The work involved the use of pseudopotentials and it also required the construction of the molecular spin-coupled states from atomic spin-coupled states.

The calculation of the spin-orbit Hamiltonian was possible using a modified version of a procedure available in the literature.[62] We calculated the spin-orbit coupling splittings for Li and Na, and our results compared well with experimental data. We generated the potential energy curves of Na-He including spin-orbit and they were in good agreement with other theoretical results.

We presented pictures of the evolution of the expectation values of angular momentum vectors $\langle \mathbf{l} \rangle$, $\langle \mathbf{s} \rangle$ and $\langle \mathbf{j} \rangle$. They allowed us to interpret the results and to obtain information about the mechanism leading to the fine-structure transitions. We found that the evolution of $\langle \mathbf{l} \rangle$ underwent precession about the internuclear axis while $\langle \mathbf{s} \rangle$ rotated slowly. The change of orientation of $\langle \mathbf{l} \rangle$ relative to $\langle \mathbf{s} \rangle$ resulted in a change of $\langle \mathbf{j} \rangle$, i.e., a fine-structure transition.

Finally, we calculated the fine-structure cross sections of Na-He at 400 and 450 K. Our calculated total, multipole relaxation and coherence cross section were compared with experimental and theoretical data. Our results were similar in many cases to theoretical results and showed correct magnitudes and trends compared to experiment. Theoretical results are consistent among themselves but generally they were below most measurements. The agreement in general was acceptable.

5.4 Computational Aspects

We coded a new pseudopotential program entitled `eiktdmoppso` entirely in Fortran 90. We presented a complete derivation of the hamiltonian integrals in the chapter 2 and in the appendices A,B and C. We rewrote in Fortran 90 The `eiktdmo` to efficiently calculate all the necessary components appearing in the integration of the equations of the time-dependent density matrix formalism including pseudopotential and spin-orbit coupling. We included in appendix A a flow diagram of the time-dependent density matrix computer code.

It is remarkable that our theoretical and computational treatment of the electronic and nuclear dynamics can provide the information needed for optical transition phenomena at both hyperthermal and high collision energies.

5.5 Future Work

The formalism and computer implementation of the method are suitable for completing studies similar to the ones presented above, on other alkali-rare-gas atom pairs, as well as the alkaline-earth-rare-gas atom pairs. The present work will allow us to study spectra and dynamics in clusters containing an alkali atom or alkaline-earth ions and several rare-gas atoms.

APPENDIX A
FLOW CHART FOR THE EIKTDMOPPSO PROGRAM

A.1 Program Features

The program `eiktdmoppso` is the latest extension of the original `eiktdmo` program (written by Keith Runge[70]). Most of the subroutines of the original code have been upgraded into fortran 90, some have been rewritten and many more have been added. As a result the `eiktdmoppso` code contains several new options.

The type of calculation the program will perform is controlled by a single option number (read from the input) called 'task'. These task numbers go from [1-15]; task numbers [1-9] tell the program to run the dynamics of the system using a particular potential choice, as given below (task numbers [1-5] are the options from the old `eiktdmo` program):

1. Straight lines (V_{qu}=0).
2. Coulomb trajectory (no electronic contribution).
3. Screened coulomb potential.
4. Average effective potential.
5. Ehrenfest potential.
6. Pseudopotential calculation.
7. Spin-orbit coupling calculation.
8. Pseudopotential calculation using parameterized hamiltonian.
9. No available yet.

Task numbers [10-15] tell the program to diagonalize the **W** matrix and depending on the number it will:

10. Print eigenvectors and eigenvectors of the **W** matrix.
11. Print electronic energies neglecting core-core repulsion contribution.

12. Print electronic energies including core-core repulsion contribution.
13. Print electronic energies including core-core repulsion contribution and spin-orbit coupling.
14. Print electronic energies using parameterized Hamiltonian
15. Print eigenvalues and eigenvectors from calculation including spin-orbit coupling.

A.2 Subroutine Description

In this section we turn our attention to the description of the features of the main subroutines.

- `read_input.f90`: Read the input in either the old (`eiktdmo`) style or the new (`eikdtmoppso`) one. Calculate factors to be used throughout the calculation and also the normalization constants of the gaussian primitives. If requested, print out the information read from the input.
- `get_overlap.f90`: Calculate the overlap matrix $\mathbf{S}$ at t_0 as well as the matrices $\mathbf{S}^{1/2}$ and $\mathbf{S}^{-1}$ which are needed for the transformation between basis sets.
- `init.f90`: Allocate matrices and initialize them as well as the other variables.
- `print_energies.f90`: (Invoked only when task ≥ 10) Print electronic energies as explained above.
- `set_p0.f90`: At t_0 construct the density matrix in terms of the basis set and transform it to the cartesian set.
- `set_t0.f90`: Save the information of the variables at t_0 in case the current step is rejected.
- `buildq.f90`: Compute the change in the density matrix $\mathbf{Q}$.
- `get_p0.f90`: Calculate the current value of the reference density $\mathbf{P0}$.
- `test_step.f90`: Compute the quotient $\| \mathbf{Q} \| / \| \mathbf{P0} \|$ and compare it to the tolerances. Then decide whether to accept or reject the step.
- `update.f90`: Update the variables and matrices if step is accepted.

- `pot.f90`: Calculate the current potential.
- `props.f90`: If requested, calculate and print time-dependent properties (e.g. Löwdin populations, alignment parameters, etc.).
- `out.f90`: Report final results.

A.3 `eiktdmoppso` Flow Diagram

We present now the flow diagram of the program; it has been split in three parts for convenience.

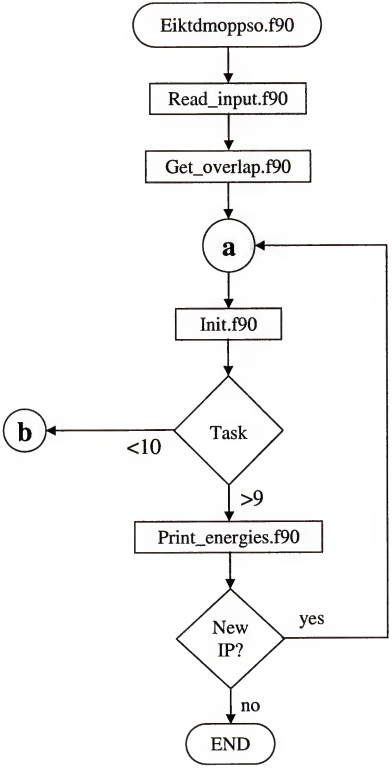

Figure A–1: Cycle for printing energies and initializing dynamics.

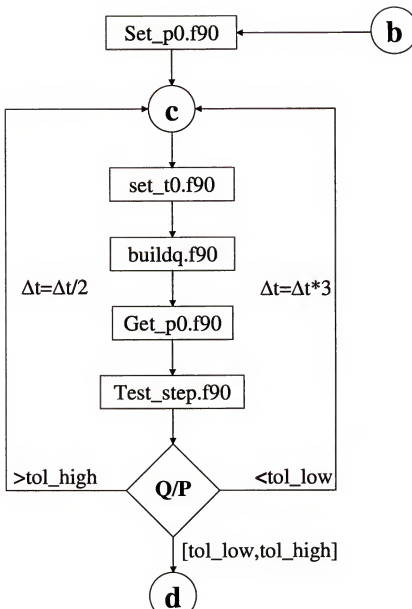

Figure A–2: Relax-and-drive cycle.

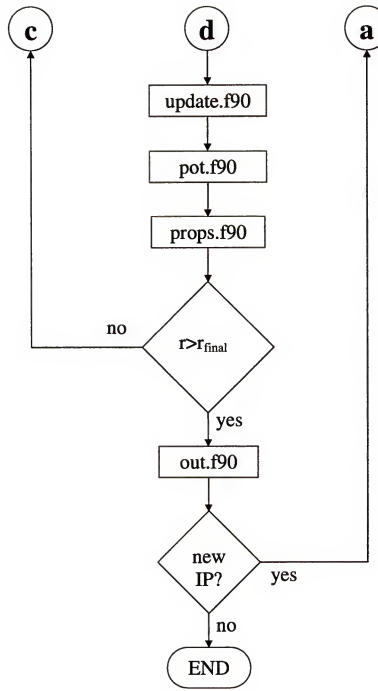

Figure A–3: Update and continue.

APPENDIX B
SUBROUTINE POLAR.F90

B.1 Subroutine polar.f90

This program evaluates the matrix elements of the polarization V_{pol} and cross terms V_{ec} of the potential energy operators in terms of cartesian gaussian functions using a procedure presented by Schwerdtfeger and Silberbach .[63]

The procedure has the advantage of reducing the integral to standard functions, including the error function $erf(x)$, the Dawson function $d(x)$, and the Dawson-error hybrid function $m(x)$:

$$\begin{aligned} erf(x) &= \int_{[0,x]} e^{-t^2} dt, \\ d(x) &= e^{-x^2} \int_{[0,x]} e^{t^2} dt, \\ m(x) &= \int_{[0,x]} e^{t^2} erf(t) dt. \end{aligned} \tag{B.1}$$

B.1.1 Evaluation of the r^K Integral

Without loss of generality, we want to solve the integral

$$I_{102} = \langle g_1 \mid x^{m_1} y^{m_2} z^{m_3} r^{-k} (1 - e^{-\alpha r^2})^q \mid g_2 \rangle \tag{B.2}$$

with CGTO's g_1 and g_2 at centers 1 and 2:

$$g_j = (x - x_j)^{n_{1j}} (y - y_j)^{n_{2j}} (z - z_j)^{n_{3j}} \exp\left(-\beta_j (\mathbf{r} - \mathbf{r}_j)^2\right), \; j = 1, 2. \tag{B.3}$$

Here $k > 2$, $\mathrm{q} \in \mathbb{N}, n_{ij} \in \mathbb{N}_0$, α, $\beta_j \in \mathbb{R}_+$, the angular indexes i = 1,2,3, and the center indexes j = 1,2. The three different centers are also denoted in the indices of I_{102} with 0 representing the origin. For the following we omit the subscripts of I.

Let us start by applying the binomial formula to the cutoff function, as well as to the x, y and z factors of the CGTO's:

$$(1 - e^{-\alpha r})^q = \sum_{\mu=0}^{q} \binom{q}{\mu} (-1)^\mu e^{-\mu\alpha r^2} \tag{B.4}$$

$$(x - x_j)_{ij}^{n} = \sum_{\eta_{ij}=0}^{n_{ij}} \binom{n_{ij}}{\eta_{ij}} (-1)^{n_{ij}-\eta_{ij}} x_j^{n_{ij}-\eta_{ij}} x^{\eta_{ij}}. \tag{B.5}$$

We can rewrite Eq. B.2 as

$$I = \sum_{\eta} f(\eta, n)$$
$$\times \int_{\mathbb{R}^3} x_1^{l_1^\eta} y_2^{l_2^\eta} z^{l_3^\eta} \exp[-\beta_1(\mathbf{r} - \mathbf{r}_1)^2 - \beta_2(\mathbf{r} - \mathbf{r}_2)^2] \sum_{\mu=0}^{q} \binom{q}{\mu} (-1)^\mu e^{\mu\alpha r^2} d\mathbf{r}.$$

Note that the first summation is taken over six indices $\eta_{ij} \in \{0, 1, \ldots, n_{ij}\}$:

$$\sum_{\eta} = \sum_{\eta_{11}=0}^{n_{11}} \sum_{\eta_{21}=0}^{n_{21}} \cdots \sum_{\eta_{32}=0}^{n_{32}} \tag{B.6}$$

and f is defined as

$$f(\eta, n) = \prod_{i,j} \binom{n_{ij}}{\eta_{ij}} (-1)^{n_{ij}-\eta_{ij}} \xi_{ij}^{n_{ij}-\eta_{ij}}, \tag{B.7}$$

where

$$(\xi_{1j}, \xi_{2j}, \xi_{3j}) = (x_j, y_j, z_j) \tag{B.8}$$

and $l_i^\eta = \eta_{i1} + \eta_{i2} + m_i \in \mathbb{N}_0$. Defining the Laplace transformation to remove the denominator $r^{-k} (k \in \mathbb{N})$:

$$r^k = \Gamma^{-1}(k/2) \int_{\mathbb{R}_+} e^{-tr^2} t^{k/2-1} dt, \tag{B.9}$$

where Γ is the gamma function. Using this transformation the above integral can be written as

$$I = \Gamma^{-1}(k/2) \sum_{\eta} f(\eta, n) \sum_{\mathbb{R}^3 \times \mathbb{R}_+} \int x^{l''_1} y^{l''_2} z^{l''_3} t^{k/2-1} \sum_{\mu=0}^{q} \binom{q}{\mu} (-1)^{\mu} \times \exp[-\beta_1(\mathbf{r}-\mathbf{r}_1)^2 - \beta_1(\mathbf{r}-\mathbf{r}_2)^2 - (\mu\alpha + t)r^2] dt d\mathbf{r}. \quad \text{(B.10)}$$

Using the lemma of Fubini for infinite intervals

$$\int_{\mathbb{R}^3 \times \mathbb{R}_+} \cdots dt d\mathbf{r} = \int_{\mathbb{R}_+ \times \mathbb{R}^3} \cdots d\mathbf{r}\, dt\,, \quad \text{(B.11)}$$

we can first take the integration over the range $\mathbf{r} \in \mathbb{R}^3$. Before doing so, we transform the exponent in B.10

$$\beta_1(\mathbf{r}-\mathbf{r}_1)^2 + \beta_2(\mathbf{r}-\mathbf{r}_2)^2 + (\mu\alpha + t)r^2 = \left[\sqrt{a_{t\mu}}\mathbf{r} - \frac{\mathbf{b}}{\sqrt{a_{t\mu}}}\right]^2 - \frac{b^2}{a_{t\mu}} + \beta_1 r_1^2 + \beta_2 r_2^2, \quad \text{(B.12)}$$

using the shorthand notations

$$a_{t\mu} = a_\mu + t = \beta_1 + \beta_2 + \mu\alpha + t,\ \mathbf{b} = (b_1, b_2, b_3)^T = \beta_1 \mathbf{r}_1 + \beta_2 \mathbf{r}_2,\ b = \mid \mathbf{b} \mid . \quad \text{(B.13)}$$

By formal rearrangement we get

$$I = \Gamma^{-1}(k/2) e^{-\beta_1 r_1^2 - \beta_2 r_2^2} \sum_{\eta} f(\eta, n) \int_{\mathbb{R}_+} \sum_{\mu=0}^{q} \binom{q}{\mu} (-1)^{\mu} t^{k/2-1} e^{b^2/a_{t\mu}} \times \underbrace{\int_{\mathbb{R}^3} x^{l''_1} y^{l''_2} z^{l''_3} \exp\left[-\left[\sqrt{a_{t\mu}}\mathbf{r} - \frac{\mathbf{b}}{\sqrt{a_{t\mu}}}\right]^2\right] d\mathbf{r}}_{\boxed{\text{a}}} dt. \quad \text{(B.14)}$$

We try now to solve the integral $\boxed{\text{a}}$ on $\mathbf{r}$ in Eq.

$$\int_{\mathbb{R}^3} x^{l''_1} y^{l''_2} z^{l''_3} \exp\left[-\left[\sqrt{a_{t\mu}}\mathbf{r} - \frac{\mathbf{b}}{\sqrt{a_{t\mu}}}\right]\right]^2 d\mathbf{r}. \quad \text{(B.15)}$$

Let us split the last integral in its x, y, z components. Substituting $\omega = \sqrt{a_{t\mu}}\mathbf{r} - \mathbf{b}/\sqrt{a_{t\mu}}$, if we take the x component we get (calling it $\boxed{\text{a,x}}$:

$$\boxed{\text{a,x}} = \frac{1}{\sqrt{a_{t\mu}}} \int \left(\frac{\omega_x}{\sqrt{a_{t\mu}}} + b_x \right)^{l_1^n} e^{-\omega_x^2} d\omega_x \tag{B.16}$$

calling $\omega_x = \omega,\ b_x = b,\ l_1^n = l,\ \sqrt{a_{t\mu}} = a$ we have:

$$\boxed{\text{a,x}} = \frac{1}{a} \int \left(\frac{\omega}{a} + b \right)^{l} e^{-\omega^2} d\omega. \tag{B.17}$$

Using the binomial theorem

$$\boxed{\text{a,x}} = \frac{1}{a} \int \sum_{i=0}^{l} \binom{l}{i} \left(\frac{\omega}{a} \right)^{i} (b)^{l-i} e^{-\omega^2} d\omega \tag{B.18}$$

being ω an axis, when i is odd the integral goes to zero, so for even values of i we get

$$\boxed{\text{a,x}} = \frac{1}{a} \sum_{i=0}^{l} \binom{l}{i} (b)^{l-i} \left(\frac{1}{a} \right)^{i} \underbrace{\int \omega^i e^{-\omega^2} d\omega}_{\frac{(i-1)!!}{2^{i/2}}\sqrt{\pi}} \tag{B.19}$$

therefore

$$\boxed{\text{a,x}} = \frac{\sqrt{\pi}}{a} \sum_{i=0}^{l} \binom{l}{i} (b)^{l-i} \left(\frac{1}{a} \right)^{i} \frac{(i-1)!!}{2^{i/2}} \tag{B.20}$$

valid for $l_x^n \neq 0$. Using the convention $(-1)!! = 1$, this leads to

$$\begin{aligned} I = \Gamma^{-1}(k/2)\pi^{3/2} e^{-\beta_1 r_1^2 - \beta_2 r_2^2} \sum_{\eta} f(\eta, n) \sum_{\zeta} g(\zeta, l^n) \\ \times \int_{\mathbb{R}_+} \sum_{\mu=0}^{q} \binom{q}{\mu} (-1)^{\mu} e^{-b^2/a_{t\mu}} a_{t\mu}^{-s_{lc}''} {}^{-3/2} t^{k/2-1} dt. \end{aligned} \tag{B.21}$$

The second summation is taken over the three indices $\zeta_i \in \{0, \ldots, l_i^n\}, i = 1, 2, 3$:

$$\sum_{\zeta} = \sum_{\zeta_1=0}^{l_1^n} \sum_{\zeta_2=0}^{l_2^n} \sum_{\zeta_3=0}^{l_3^n},\ (\zeta_1, \zeta_2, \zeta_3 \text{ even}), \tag{B.22}$$

and g is defined as

$$g(\zeta, l^\eta) = \prod_{i=1}^{3} \binom{l_i^\eta}{\zeta_i} \frac{(\zeta_i - 1)!!}{2^{\zeta_i/2}} b_i^{l_i^\eta - i}. \tag{B.23}$$

The l_i^η are defined in Eq. B.1.1, and $s_{l\zeta}^\eta = l_1^\eta + l_2^\eta + l_3^\eta - (\zeta_1 + \zeta_2 + \zeta_3)/2 \in \mathbb{N}_0$. Now we turn to the last integral over $t \in \mathbb{R}_+$. As we will see below, the integral and sum (over μ) are interchangeable only for the conditions mentioned before. For the general case (2s - $k \in \mathbb{Z}$) we have to solve the integral

$$\begin{aligned} J &= \int_{\mathbb{R}_+} \sum_{\mu}^{q} \binom{q}{\mu} (-1)^\mu (a_\mu + t)^{-s-3/2} t^{k/2-1} e^{b^2/(a_\mu + t)} dt \\ &= \lim_{\epsilon \to \infty} \sum_{\mu}^{q} \binom{q}{\mu} (-1)^\mu \int_{[0,\epsilon]} (a_\mu + t)^{-s-3/2} t^{k/2-1} e^{(b^2/a_\mu + t)} dt, \end{aligned} \tag{B.24}$$

where $s = s_{l\zeta}^\eta \in \mathbb{N}_0, a_\mu, b \in \mathbb{R}_+$. We must consider two cases whether the power of k of r_k is even or odd.

Case 1. $k = 2j, j \in \mathbb{N}$. We substitute $\omega = b^2/(a_\mu + t)$, and make use of the binomial theorem for the factor t:

$$\begin{aligned} J_1 = b^{-2s+2j-3} \lim_{\epsilon \to \infty} \sum_{\mu}^{q} \binom{q}{\mu} (-1)^\mu \sum_{\nu=0}^{j-1} \binom{j-1}{\nu} (-1)^\nu \left(\frac{a_\mu}{b^2}\right)^\nu \\ \times d_\eta \left(s - j + \nu + \frac{3}{2}, \frac{b^2}{a_\mu}\right), \eta = \frac{b^2}{a_\mu + \epsilon} \end{aligned} \tag{B.25}$$

with

$$d_\eta(a, x) = \int_{[\eta, x]} w^{a-1} e^\omega d\omega. \tag{B.26}$$

For positive first arguments of d_η, the limit and sum in Eq. B.25 are interchangeable and the d function may also be written as an incomplete γ function [$d(a, x) = d_0(a, x)$ if $a > 0$]

$$\gamma(a, x) = \int_{[0,x]} e^{-t} t^{a-1} dt = (-1)^a d(a, -x) \tag{B.27}$$

with $a \in \mathbb{R}_+$. From a p-fold integration by parts we get the general formula ($p = a - 1/2 \in \mathbb{N}_0$)

$$d(p+1/2,x) = \frac{(2p-1)!!}{2^{p-1}}(-1)^p e^x \left(d(\sqrt{x}) - \sum_{i=0}^{p-1} (-1)^i x^{i+1/2} \frac{2^i}{(2i+1)!!} \right), \quad \text{(B.28)}$$

where $d(x)$ is the Dawson function introduced in Eq. B.1. By convention the sum in B.28 vanishes if $p = 0$. To find a formula for the d function with negative first arguments we set $p = j - s - \nu - 1$ and integrate by parts p times using the equation

$$\int_{[\eta,x]} t^{-p-1/2} e^t dt = \left. \frac{t^{-p+1/2} e^t}{-p+1/2} \right|_\eta^x - \frac{1}{-p+1/2} \int_{[\eta,x]} t^{-p+1/2} e^t dt. \quad \text{(B.29)}$$

For the first term on the right hand side in B.29 we have to evaluate the limit $\eta \to 0$, where $\eta = b^2/(a_\mu + \epsilon)(\epsilon \to \infty)$:

$$\lim_{\epsilon \to \infty} S_q(x) = \lim_{\epsilon \to \infty} \sum_{\mu=0}^{q} \binom{q}{\mu} (-1)^\mu \left(\frac{b^2}{a_\mu + \epsilon} \right)^{-p+1/2}. \quad \text{(B.30)}$$

Substituting $\alpha x = \epsilon + a_\mu - \mu\alpha$ leads to

$$\lim_{x \to \infty} S_q(x) = \left(\frac{\alpha}{b^2} \right)^{p-1/2} \lim_{x \to \infty} \sum_{\mu=0}^{q} \binom{q}{\mu} (-1)^\mu (\mu + x)^{p-1/2}. \quad \text{(B.31)}$$

Expression B.31 tends to zero with x approaching infinity only if $q > p - 1/2$ or $q \geq k/2 - s - 1$ for all ν. From this we derive the formula

$$d(1/2-p,x) = e^x \left(2C_{pp} d(\sqrt{x}) - \sum_{i=1}^{p} C_{ip} x^{i-p-1/2} \right) \quad \text{(B.32)}$$

with coefficients

$$C_{ip} = \prod_{\nu=1}^{i} (p + 1/2 - \nu)^{-1} = 2^i \frac{(2p-2i-1)!!}{(2p-1)!!}. \quad \text{(B.33)}$$

Case 2. $k = 2j+1, j \in \mathbb{N}$. We rearrange B.24 and substitute $z = b^2/a_\mu - b^2/(a_\mu + t)$:

$$J_2 = \lim_{\eta\to\infty} \sum_{\mu=0}^{q} \binom{q}{\mu} (-1)^\mu \left(\frac{a_\mu}{b^2}\right)^{s+3/2} \int_{[0,\eta]} \left(\frac{b^2}{a_\mu} - \frac{b^2}{a_\mu + t}\right)^{s+3/2} t^{j-s-2} e^{b^2/(a_\mu+t)} dt$$

$$= \lim_{\epsilon\to 1} \sum_{\mu=0}^{q} \binom{q}{\mu} (-1)^\mu a_\mu^{j-s-1} \left(\frac{a_\mu}{b^2}\right)^{s+1/2} e^{b^2/a_\mu}$$

$$\times \int_{[0,(b^2/a_\mu)\epsilon]} \left(\frac{b^2}{a_\mu} - z\right)^{s-j} z^{j-1/2} e^{-z} dz, \quad \text{(B.34)}$$

where ϵ comes from the left to 1. We must consider two cases, whether $s-j$ is positive (including zero) or not.

Subcase 1. $s - j \in \mathbb{N}_0$. We make use of the binomial theorem, set $\epsilon = 1$ (which is allowed in this case) and write

$$J_2 = \sum_{\mu=0}^{q} \binom{q}{\mu} (-1)^\mu a_\mu^{j-s-1} \left(\frac{a_\mu}{b^2}\right)^{j+1/2} e^{b^2/(a_\mu+t)}$$

$$\times \sum_{\nu=0}^{s-j} \binom{s-j}{\nu} (-1)^\nu \left(\frac{a_\mu}{b^2}\right)^\nu \gamma\left(j+\nu+\frac{1}{2}, \frac{b^2}{a_\mu}\right). \quad \text{(B.35)}$$

The incomplete γ function was defined previously and we can use B.27 and B.28 to derive the γ function from the $erf(x)$ B.1:

$$\gamma(p+\frac{1}{2}, x) = \frac{(2p-1)!!}{2^{p-1}} \left(erf(\sqrt{x}) - e^x \sum_{\mu=0}^{p-1} x^{\mu+1/2} \frac{2^\mu}{(2\mu+1)!!} \right) \quad \text{(B.36)}$$

with $p \in \mathbb{N}_0$. By convention, the second sum in B.36 vanishes if $p = 0$.

Subcase 2. $s - j \in \mathbb{Z} \neq 0$. We have to solve the integral

$$\frac{1}{2} \left(\frac{b^2}{a_\mu}\right)^{p-j-1/2} \int_{[0,\epsilon]} z^{j-1/2} (b^2/a_\mu - z)^{-p} e_{-z} dz, \epsilon < \frac{b^2}{a_\mu},$$

$$\int_{[0,\epsilon]} \frac{x^{2j}}{(1-x^2)^p} e^{(b^2/a_\mu)x^2} dx = h_\epsilon(j, p, b^2/a_\mu), \epsilon < 1 \quad \text{(B.37)}$$

with $p = j - s$. As a first step, we extend the numerator in B.37

$$\begin{aligned} h_\epsilon(j,p,a) &= \int_{[0,\epsilon]} \frac{x^{2j} - x^{2(j-1)} + x^{2(j-1)}}{(1-x^2)^p} e^{-\alpha x^2} \\ &= h_\epsilon(j-1,p,a) - h_\epsilon(j-1,p-1,a),\ j \in \mathbb{N},\ p \in \mathbb{Z}. \end{aligned} \tag{B.38}$$

This is a recursive definition of the general h_ϵ function and we get the h_ϵ function of the zeroth order, which we denote by $H_\epsilon(p,a) = h_\epsilon(0,p,a)$ by multiple application of B.38

$$h_\epsilon(j,p,a) = \sum_{\eta=0}^{j} \binom{j}{\eta} (-1)^\eta H_\epsilon(p-\eta,a). \tag{B.39}$$

Note that this integral exists only for $\epsilon < 1$ if $p < 0$ and we cannot exchange the limit and the sum in B.34 recursively in the limit $\epsilon = 1$ if $q \geq j - 2$:

$$\begin{aligned} H(p,a) &= \frac{2(p+a)-3}{2(p-1)} H(p-1,a) - \frac{a}{p-1} H(p-2,1), \\ H(0,a) &= a^{-1/2} erf(\sqrt{a}), \\ H(1,a) &= 2e^{-a} m(\sqrt{a}). \end{aligned} \tag{B.40}$$

We can either use B.40 for the defining the function H or we must write

$$\sum_{\mu=0}^{q} \binom{q}{\mu} (-1)^\mu H(p,a) = \lim_{\epsilon \to 1} \sum_{\mu=0}^{q} \binom{q}{\mu} (-1)^\mu H_\epsilon(p,a). \tag{B.41}$$

The function $m(x)$ is defined in B.1. $p - \eta$ can become negative, and therefore we define the H function also for negative first arguments similar to the d function in B.1:

$$\begin{aligned} H(-p,a) &= \int_{[0,1]} (1-x^2)^p e^{-ax^2} dx \\ &= \frac{1}{2} \sum_{\nu=0}^{p} \binom{p}{\nu} (-1)^\nu a^{-\nu-1/2} \gamma(\nu + 1/2, a). \end{aligned} \tag{B.42}$$

We can now write down the solution for negative values of $(s-j)$:

$$J_2 = 2\sum_{\mu=0}^{q}\binom{q}{\mu}(-1)^{\mu}a_{\mu}^{j-s-1}e^{b^2/a_{\mu}}\sum_{\eta=0}^{j}\binom{j}{\eta}(-1)^{\eta}H(j-s-\eta,b^2/a_{\mu}). \quad \text{(B.43)}$$

Now, the integral is completely solved and we summarize the results using Eqs. B.21, B.25, B.35, B.43:

$$I = \Gamma^{-1}(k/2)\pi^{3/2}e^{-\beta_1\mathbf{r}_1^2-\beta_2\mathbf{r}_2^2}\sum_{\eta}f(\eta,n)\sum_{\zeta}g(\zeta,l^n)\sum_{\mu=0}^{q}\binom{q}{\mu}(-1)^{\mu}u_{k_2}^{e^{\eta}\iota_{\zeta}}(k_1,a_{\mu},b) \quad \text{(B.44)}$$

with $k = 2k_1+k_2$, $k_1 \in \mathbb{N}$, $k_2 \in \{0,1\}$, $q \in \mathbb{N}$, $q \geq \kappa(k)-\sum_{i=1}^{3}\kappa(m_i)-1, \kappa(n) = n/2$ if n is even, and $\kappa(n) = (n+1)/2$ if n is odd, $a_{\mu} = \beta_1+\beta_2+\mu\alpha, b = \mid \beta_1\mathbf{r}_1+\beta_2\mathbf{r}_2 \mid$, the functions

$$u_0^s(j,a,b) = b^{-2s+2j-3}\sum_{\nu=0}^{j-1}\binom{j-1}{\nu}(-1)^{\nu}\left(\frac{a}{b^2}\right)^{\nu}d\left[s-j+\nu+\frac{3}{2},\frac{b^2}{a}\right], \quad \text{(B.45)}$$

$$u_1^s(j,a,b) = a^{j-s-1}e^{b^2/a}\sum_{\nu=0}^{s-j}\binom{s-j}{\nu}(-1)^{\nu}\left(\frac{a}{b^2}\right)^{j+\nu+1/2}\gamma\left[j+\nu+\frac{1}{2},\frac{b^2}{a}\right] \quad \text{(B.46)}$$

for $s-j \in \mathbb{N}_0$, and

$$u_1^s(j,a,b) = 2a^{j-s-1}e^{b^2/a}\sum_{\nu=0}^{j}\binom{j}{\nu}(-1)^{\nu}H(j-s-\nu,\frac{b^2}{a}) \quad \text{(B.47)}$$

for $j-2 \in \mathbb{N}$. The Γ function is defined in B.27, the H function in B.40 and B.42, the erf, d, and m functions in B.1, and the f and g function and appropriate sum-conventions in B.7 and B.23.

B.1.2 Special Case b=0

This case occurs when both CGTO's and the operator are placed at the origin:

$$I_{000} = \lim_{b\to 0} I_{Eq.B.2}, \quad \text{(B.48)}$$

which is equivalent to solving the integral

$$\int_{\mathbb{R}^3} x^{p_1}y^{p_2}z^{p_3}r^{-k}\sum_{\mu=0}^{q}\binom{q}{\mu}(-1)^{\mu}e^{-(\beta_1+\beta_2+\mu\alpha)r^2}d\mathbf{r} \quad \text{(B.49)}$$

with $p_i = n_{i1} + n_{i2} + m_i, i \in \{1,2,3\}$.

Case 1. $k = 2j,\ b = 0$. The sums over η *and* ζ in B.21 break down to just one term and the integral is reduced to an elementary one. The result is

$$I_{000} = \Gamma^{-1}(j)\pi^{3/2} \sum_{\mu=0}^{q} \binom{q}{\mu} (-1)^{\mu} a_{\mu}^{j-s-3/2} \sum_{\nu=0}^{j-1} (-1)^{\nu} \binom{j-1}{\nu} (s-j+\nu+\frac{3}{2})^{-1}. \quad \text{(B.50)}$$

Using the formula

$$\sum_{\nu=0}^{j} \frac{(-j)_{\nu}}{\nu!(x+\nu)} = \frac{j!}{x(x+1)_j},\ x \in \mathbb{R}, \quad \text{(B.51)}$$

where $(-z)_{\nu},\ z \in \mathbb{R}$, and $\nu \in \mathbb{N}_0$ is the factorial function, we get

$$I_{000} = \pi^{3/2} \prod_{i=0}^{j-1} (s-i+\frac{1}{2})^{-1} \sum_{\mu=0}^{q} \binom{q}{\mu} (-1)^{\mu} a_{\mu}^{j-s-3/2}. \quad \text{(B.52)}$$

Case 2. $k = 2j+1,\ b = 0$. Using the mixed Gaussian-Laplace transformation

$$r^{-2j-1} = \frac{2}{\sqrt{\pi}} \Gamma^{-1}(j) \int_{\mathbb{R}_+^2} e^{-(t_1+t_2^2)r^2} t_1^{j-1} d(t_1, t_2) \quad \text{(B.53)}$$

instead of B.9, the first integration leads to Eq. B.50 substituting only $a_{\mu} \to a_{\mu} + t_2^2$. We now integrate B.50 over $t_2 \in \mathbb{R}_+$. Two cases have to be considered, whether or not $j - s \leq 0$. In the first case we use the expression

$$\int_{[0,\infty)} (a+x^2)^{-p-3/2} = \frac{2^p p!}{a^{p+1}(2p+1)!!},\ p = s-j \quad \text{(B.54)}$$

and get

$$I_{000} = \pi \frac{2^s (s-j)!}{(2s+1)!!} \sum_{\mu=0}^{q} \binom{q}{\mu} (-1)^{\mu} a_{\mu}^{j-s-1} \quad \text{(B.55)}$$

APPENDIX C
SUBROUTINE SHORT_RANGE.F90

C.1 Subroutine short_range.f90

This program has been written to evaluate the matrix elements of the short-range operator in terms of cartesian gaussian functions[61] for any l in either the operator or the gaussian functions.

The semi-local (l-dependent) short-range operator has the form

$$V_C^{sr}(\vec{r}_C) = \sum_{l,i} B_{l,i} \exp(-\beta_{l,i} r_C^2) P_{l,C}, \tag{C.1}$$

where $B_{l,i}$ and $\beta_{l,i}$ are pseudopotential parameters adjusted to experimental data and $P_{l,C}$ stands for the projection operator on angular symmetry l

$$P_{l,C} = \sum_m |Y_{lm}(\hat{r}_C)\rangle\langle Y_{lm}(\hat{r}_C)|. \tag{C.2}$$

Here $|Y_{lm}(\hat{r}_C)\rangle$ represents a real orthonormal spherical harmonic function centered on the core C ($\hat{r}_C = \vec{r}_C/r_C$).

The integral between gaussian functions g_A, g_B and the short range can be written as

$$\gamma_{AB} = \sum_{m=-l}^{l} \int_0^\infty dr_C \left[\int d\Omega_C g_A Y_{lm}(\Omega_C) \right] r_C^2 \exp(-\xi r_C^2) \left[\int d\Omega_C Y_{lm}(\Omega_C) g_B \right]. \tag{C.3}$$

The derivation of the solution of the above equation is similar to the one presented in the chapter on spin-orbit coupling. After following the steps 4.78-4.96, we

get

$$\gamma_{AB} = 4\pi D_{ABC} \sum_{a=0}^{n_A} \sum_{b=0}^{l_A} \sum_{c=0}^{m_A} \sum_{d=0}^{n_B} \sum_{e=0}^{l_B} \sum_{f=0}^{m_B} \binom{n_A}{a}\binom{l_A}{b}\binom{m_A}{c}\binom{n_B}{d}\binom{l_B}{e}\binom{m_B}{f}$$
$$\times C A_x^{n_A-a} C A_y^{l_A-b} C A_z^{m_A-c} C B_x^{n_B-d} C B_y^{l_B-e} C B_z^{m_B-f}$$
$$\times \sum_{\lambda=0}^{\infty} \sum_{\bar{\lambda}=0}^{\infty} Q_{\lambda\bar{\lambda}}^{a+b+c+d+e+f+2}(k_A, k_B, \alpha) \sum_{m=-l}^{l} \Omega_{\lambda lm}^{abc} \Omega_{\bar{\lambda} lm}^{def}, \quad \text{(C.4)}$$

the angular integral $\Omega_{\lambda lm}^{abc}$ is given by

$$\Omega_{\lambda lm}^{abc} = \sum_{\mu=-\lambda}^{\lambda} Y_{\lambda\mu}(\Omega_k) \int \frac{d\Omega}{4\pi} \hat{x}^a \hat{y}^b \hat{z}^c Y_{\lambda\mu}(\Omega) Y_{lm}(\Omega), \quad \text{(C.5)}$$

and the radial integral $Q_{\lambda\bar{\lambda}}^N$ is given by

$$Q_{\lambda\bar{\lambda}}^N = \int_0^\infty dr r^N \exp(-\alpha r^2) M_\lambda(k_A r) M_{\bar{\lambda}}(k_B r). \quad \text{(C.6)}$$

The only nonzero terms in the sum over λ are

$$max(l-a-b-c, 0) \leq \lambda \leq l+a+b+c \quad \text{(C.7)}$$

and likewise for $\bar{\lambda}$. Also $l+a+b+c-\lambda$ must be even.

C.2 Special Cases

C.2.1 $k_A, k_B = 0$

The exponential terms for both A and B is reduced to

$$\exp(\vec{0}.\vec{r}_C) = 1, \quad \text{(C.8)}$$

and the short range integral is reduced to

$$\gamma_{AB} = \frac{D_{ABC}}{4\pi} \sum_{m=-l}^{l} \int_0^\infty dr_C \left[\int d\Omega_C x_A^{n_A} y_A^{l_A} z_A^{m_A} Y_{lm}(\Omega_C) \right] \times r_C^2 \exp\left(-\alpha r_C^2\right) \left[\int d\Omega_C x_B^{n_B} y_B^{l_B} z_B^{m_B} Y_{lm}(\Omega_C) \right]$$

$$= \frac{D_{ABC}}{4\pi} Q^{n_A+l_A+m_A+n_B+l_B+m_B+2}(\alpha) \sum_{m=-l}^{l} \Omega_{lm}^{n_A+l_A+m_A} \Omega_{lm}^{n_B+l_B+m_B}. \quad \text{(C.9)}$$

The radial integral takes the form

$$Q^N(\alpha) = \int_0^\infty dr r^N \exp\left(-\alpha r^2\right), \quad \text{(C.10)}$$

and the angular integral

$$\Omega_{lm}^{abc} = \int \frac{d\Omega}{4\pi} \hat{x}^a \hat{y}^b \hat{z}^c Y_{lm}(\Omega) = \sum_{r,s,t}^{l} Y_{r,s,t}^{lm} \int d\Omega \hat{x}^{a+r} \hat{y}^{b+s} \hat{z}^{c+t} \quad \text{(C.11)}$$

C.2.2 k_A or $k_B = 0$

Let's choose $k_B = 0$ for the moment, the short range integral becomes

$$\gamma^{AB} = \frac{D_{ABC}}{4\pi} \sum_{m=-l}^{l} \int_0^\infty dr_C \left[\int d\Omega_C x_A^{n_A} y_A^{l_A} z_A^{m_A} \exp\left(\mathbf{k_A} \cdot \mathbf{r_c}\right) Y_{lm}(\Omega_C) \right] \times r_C^2 \exp\left(-\alpha r_C^2\right) \left[\int d\Omega_C x_B^{n_B} y_B^{l_B} z_B^{m_B} Y_{lm}(\Omega_C) \right]. \quad \text{(C.12)}$$

Expanding the exponential $\exp\left(\mathbf{k_A} \cdot \mathbf{r_C}\right)$ in spherical coordinates and transforming x_A, y_A, z_A to point C and separating variables of integration we obtain

$$\gamma_{AB} = D_{ABC} \sum_{a=0}^{n_A} \sum_{b=0}^{l_A} \sum_{c=0}^{m_A} \binom{n_A}{a} \binom{l_A}{b} \binom{m_A}{c} C A_x^{n_A-a} C A_y^{l_A-b} C A_z^{m_A-c} \times \sum_{\lambda=0}^{\infty} \sum_{\bar{\lambda}=0}^{\infty} Q_\lambda^{a+b+c+d+e+f+2}(k_A, \alpha) \sum_{m=-l}^{l} \Omega_{\lambda lm}^{abc} \Omega_{lm}^{def}, \quad \text{(C.13)}$$

and the radial integral Q_λ^N is given by

$$Q_\lambda^N(k_A,\alpha) = \int_0^\infty dr r^N \exp(-\alpha r^2) M_\lambda(k_A r). \tag{C.14}$$

C.3 Evaluation of the Integrals

C.3.1 Angular Integrals

Expanding the real orthonormal spherical polynomials $Y_{\lambda\mu}$ in terms of $\hat{x}$,$\hat{y}$ and $\hat{z}$:

$$Y_{\lambda\mu} = \sum_{r,s,t}^{\lambda} y_{rst}^{\lambda\mu} \hat{x}^r \hat{y}^s \hat{z}^t, \quad r+s+t=\lambda \tag{C.15}$$

the complete angular integral will be

$$\Omega_{\lambda m}^{abc} = \sum_{\mu=-\lambda}^{\lambda} \left[\sum_{r,s,t}^{\lambda} y_{rst}^{\lambda\mu} \hat{k}_x^r \hat{k}_y^s \hat{k}_z^t \right] \sum_{r,s,t}^{\lambda} \sum_{u,v,w}^{l} y_{rst}^{\lambda\mu} y_{uvw}^{lm} \int d\Omega \hat{x}^{a+r+u} \hat{y}^{b+s+v} \hat{z}^{c+t+w}. \tag{C.16}$$

The evaluation of the integral is straightforward

$$\begin{aligned} 4\pi \int d\Omega \hat{x}^i \hat{y}^j \hat{z}^k &= 0, && \text{i,j,k odd,} \\ &= \frac{(i-1)!!(j-1)!!(k-1)!!}{(i+j+k+1)!!}, && \text{i,j,k even.} \end{aligned} \tag{C.17}$$

C.3.2 Radial Integral

Single Power Series

We start with

$$Q_{\lambda\tilde{\lambda}}^N = \int_0^\infty dr r^N \exp(-\alpha r^2) M_\lambda(k_A r) M_{\tilde{\lambda}}(k_B r), \tag{C.18}$$

and doing a change of variables $r = r/\sqrt{\alpha}$ and $dr = dr/\sqrt{\alpha}$ we get

$$Q_{\lambda\tilde{\lambda}}^N = \frac{1}{\sqrt{\alpha}} \int_0^\infty dr (\frac{r}{\sqrt{\alpha}})^N \exp(-\alpha r^2) M_\lambda(\frac{k_A r}{\sqrt{\alpha}}) M_{\tilde{\lambda}}(\frac{k_B r}{\sqrt{\alpha}}). \tag{C.19}$$

Replacing only $M_\lambda(k_A r/\sqrt{\alpha})$ by its expansion in a power series we get

$$Q^N_{\lambda\tilde{\lambda}} = \frac{1}{\alpha^{\frac{N+1}{2}}}\int_0^\infty dr r^N \exp(-r^2)\left(\left[\frac{k_A r}{\sqrt{\alpha}}\right]^\lambda \sum_{j=0}^\infty \frac{\left(\frac{k_A r}{\sqrt{\alpha}}\right)^{2j}}{j!(2\lambda+1+2j)!!}\right) M_{\tilde{\lambda}}(k_B r)$$

$$= \frac{{k_A}^\lambda}{\alpha^{\frac{N+1+\lambda}{2}}}\int_0^\infty dr r^{N+\lambda}\exp(-r^2)\left(\sum_{j=0}^\infty \frac{\left(\frac{k_A^2 r^2}{2\alpha}\right)^j}{j!(2\lambda+1+2j)!!}\right) M_{\tilde{\lambda}}(k_B r)$$

$$= \frac{{k_A}^\lambda}{\alpha^{\frac{N+1+\lambda}{2}}}\sum_{j=0}^\infty \frac{\left(\frac{k_A^2}{2\alpha}\right)^j}{j!(2\lambda+1+2j)!!}\int_0^\infty dr r^{N+\lambda+2j}\exp(-r^2)M_{\tilde{\lambda}}(k_B r). \qquad \text{(C.20)}$$

Knowing that

$$Q^N_\lambda(k,\alpha) = \int_0^\infty dr r^N \exp(-\alpha r^2) M_\lambda(kr) \qquad \text{(C.21)}$$

we get

$$Q^N_{\lambda\tilde{\lambda}}(k_A,k_B,\alpha) = \frac{{k_A}^\lambda}{\alpha^{\frac{N+1+\lambda}{2}}}\sum_{j=0}^\infty \frac{\left(\frac{k_A^2}{2\alpha}\right)^j}{j!(2\lambda+1+2j)!!} Q^{N+\lambda+2j}_{\tilde{\lambda}}\left(\frac{k_B}{\sqrt{\alpha}},1\right)$$

$$= \frac{k_A^\lambda}{\alpha^{(N+\lambda+1)/2}}\sum_{j=0}^\infty \frac{(k_A^2/2\alpha)^j}{j!(2\lambda+1+2j)!!} Q^{N+\lambda+2j}_{\tilde{\lambda}}(k_B/\sqrt{\alpha},1). \qquad \text{(C.22)}$$

We only need to calculate $Q^{N+\lambda}_{\tilde{\lambda}}$ and $Q^{N+\lambda+2}_{\tilde{\lambda}}$ the others are obtained by recursion (type 1 integral is given at the end of document)

$$Q^n_l(k,\gamma) = \frac{1}{\gamma}\left[\left(\frac{k^2}{4\gamma}+\frac{2n-5}{2}\right)Q^{n-2}_l + \frac{(l-n+4)(l+n-3)}{4}Q^{n-4}_l\right]. \qquad \text{(C.23)}$$

The upper limit to the utility of this method is found to be $(k_A+k_B)^2/2\alpha = 100$ when approximately 70 terms are required to give an accuracy of 10^{-13}.

Gaussian Points and Weights Method

Writing the modified spherical Bessel function $M_l(z)$ in exponential for as

$$M_l(z) = \frac{1}{2z}\left[R_l(-z)\exp(z) - (-1)^l R_l(z)\exp(-z)\right] \tag{C.24}$$

$$R_l(z) = \sum_{k=0}^{l} \frac{(l+k)!}{k!(l-k)!}(2z)^{-k}. \tag{C.25}$$

For large z , $M_l(z)$ becomes simply the first term in the Eq. C.24. Thus when $k_A/\sqrt{\alpha}$ and $k_B/\sqrt{\alpha}$ are large,

$$M_l(z) \approx= \frac{1}{2z}R_l(-z)\exp(z); R_l(z) \approx 1 \approx \frac{1}{2z}\exp(-z), \tag{C.26}$$

therefore

$$\begin{aligned} Q^N_{\lambda\bar{\lambda}}(k_A, k_B, \alpha) &= \int_0^\infty dr r^N \exp(-\alpha r^2)\frac{\exp(k_A r)}{2k_A r}\frac{\exp(k_B r)}{2k_B r} \\ &= \frac{1}{4k_A k_B}\int_0^\infty dr r^{N-2}\exp(-\alpha r^2 + k_A r + k_B r). \end{aligned} \tag{C.27}$$

The radial integral can be approximated (after a change of variables $r \to r/\sqrt{\alpha}$

$$Q^N_{\lambda\bar{\lambda}}(k_A, k_B, \alpha) \approx \frac{1}{4\sqrt{\alpha}k_A k_B}\int_0^\infty dr \left(\frac{r}{\sqrt{\alpha}}\right)^{N-2}\exp\left(-r^2 + \frac{k_A}{\sqrt{\alpha}}r + \frac{k_B}{\sqrt{\alpha}}r\right), \tag{C.28}$$

this suggest gaussian integration. Finding the maximum by differentiating the integrand

$$\begin{aligned} (N-2)\left(\frac{r}{\sqrt{\alpha}}\right)^{N-3}\frac{1}{\sqrt{\alpha}}\exp\left(-r^2 + \frac{k_A}{\sqrt{\alpha}}r + \frac{k_B}{\sqrt{\alpha}}r\right) \\ + \left(\frac{r}{\sqrt{\alpha}}\right)^{N-2}\left(-2r + \frac{k_A}{\sqrt{\alpha}} + \frac{k_B}{\sqrt{\alpha}}\right) = 0 \end{aligned} \tag{C.29}$$

$$\begin{aligned} -2r = r\left(\frac{(k_A + k_B)^2}{\alpha}\right) + (N-2) = 0 \\ r_C = \frac{1}{4}\frac{(k_A + k_B)}{\sqrt{\alpha}} \pm \frac{1}{2}\left[\frac{1}{4}\frac{(k_A + k_B)^2}{\alpha} + 2(N-2)\right]^{1/2} \end{aligned} \tag{C.30}$$

for the range of $\frac{1}{2}(k_A + k_B)/\sqrt{\alpha}$ for which the method is practical, the effect of the term $2(N-2)$ is very small. Therefore, keeping r_c independent of N the maximum is approximated as

$$r_C = \frac{1}{2}\frac{k_A + k_B}{\sqrt{\alpha}}. \tag{C.31}$$

A change of variables $t = r - r_C$ minimize the number of points in the numerical integration:

$$Q^N_{\lambda\bar{\lambda}} = \int_{-r_C}^{\infty} dt f(t, r_C, k_A, k_B, \alpha) \exp(-t^2), \tag{C.32}$$

where

$$f(t, r_C, k_A, k_B, \alpha) = \frac{1}{\sqrt{\alpha}}\left(\frac{t + r_C}{\sqrt{\alpha}}\right)^N M_\lambda\left[\frac{k_A}{\sqrt{\alpha}}(t + r_C)\right] \times M_{\bar{\lambda}}\left[\frac{k_B}{\sqrt{\alpha}}(t + r_C)\right] \exp[-2r_C t - r_C^2]. \tag{C.33}$$

Extracting

$$\exp\left(\frac{k_A}{\sqrt{\alpha}}(t + r_C)\right) \text{ and } \exp\left(\frac{k_B}{\sqrt{\alpha}}(t + r_C)\right) \tag{C.34}$$

from M_λ and $M_{\bar{\lambda}}$ in Eq. C.33 and the operating exponents

$$-2r_C t - r_C^2 + \frac{k_A}{\sqrt{\alpha}}(t + r_C) + \frac{k_B}{\sqrt{\alpha}} \rightarrow -2r_C t - r_C^2 + \frac{k_A + k_B}{\sqrt{\alpha}}(t + r_C) \rightarrow -2r_C t - r_C^2 + 2r_c(t + r_C) = r_C^2 \tag{C.35}$$

then f in Eq. C.33 reduces to

$$f(t, r_C, k_A, k_B, \alpha) = \frac{1}{\sqrt{\alpha}}\left(\frac{t + r_C}{\sqrt{\alpha}}\right)^N M'_\lambda\left[\frac{k_A}{\sqrt{\alpha}}(t + r_C)\right] \times M'_{\bar{\lambda}}\left(\frac{k_B}{\sqrt{\alpha}}(t + r_C)\right) \exp(r_C^2), \tag{C.36}$$

where

$$M_l'(z) = \frac{1}{2z}\left[R_l(-z) - (-1)^l R_l(z)\exp(-2z)\right]. \tag{C.37}$$

The number of integration points required for a given accuracy decreases with increasing $(k_A + k_B)^2/2\alpha$.

Range of $(k_A + k_B)^2/2\alpha$	Number of points
$[10^2, 10^3]$	20
$10^3, 10^5$	10
$> 10^5$	5

Finite Sum

This method can be applied to many, but not all of the needed integrals. A tabulated integral of Bessel function in the present notation gives

$$Q^2_{\lambda\lambda}(k_A, k_B, \alpha) = \frac{\pi^{1/2}}{(4\alpha^{3/2})}\exp\left(\frac{(k_A^2 + k_B^2)}{4\alpha}\right) M_\lambda\left(\frac{k_A k_B}{2\alpha}\right). \tag{C.38}$$

By differencing this expression with respect to k_A and k_B various numbers of times, using the Bessel function recursion relation and using the binomial coefficient summation relations , a moderately general form is obtained:

$$\begin{aligned} Q^{\lambda+\mu+2-2\nu}_{\lambda\mu} = & \frac{\pi^{1/2}}{(4\alpha^{3/2})}\exp\left(\frac{k_A^2 + k_B^2}{4\alpha}\right)\sum_{t=0}^{\lambda-\nu}\sum_{u=0}^{\mu-\nu}\binom{\lambda-\nu}{t}\binom{\mu-\nu}{u} \\ & \times \frac{(\lambda+\mu-\nu+\frac{1}{2})!(\mu+\nu-\frac{1}{2})!(t+u+\nu+\frac{1}{2})}{(\mu+t+\frac{1}{2})!(\lambda+u+\frac{1}{2})!(\nu-\frac{1}{2})!} \\ & \times \left(\frac{k_A}{2\alpha}\right)^{\lambda-\nu-t+u}\left(\frac{k_B}{2\alpha}\right)^{\mu-\nu+t-u} M_{u+t+\nu}\left(\frac{k_A k_B}{2\alpha}\right). \end{aligned} \tag{C.39}$$

To avoid underflows and overflows a scaled form of the Bessel function is used

$$M_\lambda(x) = \frac{x^\lambda}{(2\lambda+1)!!}\exp(x) M^s_\lambda(x). \tag{C.40}$$

We then obtain

$$\begin{aligned} Q_{\lambda\mu}^{\lambda+\mu+2-2\nu} =& \frac{\pi^{1/2}}{(4\alpha^{3/2})}\left(\frac{1}{2\alpha}\right)^{\nu}\left(\frac{k_A}{2\alpha}\right)^{\lambda}\left(\frac{k_B}{2\alpha}\right)^{\mu}\frac{(2(\lambda+\mu-\nu)+1)!!}{(2\nu-1)!!} \\ &\times \exp\left(\frac{(k_A+k_B)^2}{(4\alpha)}\right)\sum_{t=0}^{\lambda-\nu}\sum_{u=0}^{\mu-\nu}\binom{\lambda-\nu}{t}\binom{\mu-\nu}{u} \\ &\times \frac{(2(t+\nu)-1)!!(2(u+\nu)-1)!!}{(2(\mu+t)+1)!!(2(\lambda+u)+1)!!}\left(\frac{k_A^2}{2\alpha}\right)^{u}\left(\frac{k_B^2}{2\alpha}\right)^{t} \\ &\times M_{t+u+\nu}^{s}\left(\frac{k_Ak_B}{2\alpha}\right)\frac{1}{(2(t+u+\nu)-1)!!} \end{aligned}$$

where we have used M' in terms of M^s

$$M_l(x) = \exp(x)M_l'(x) = \frac{x^l}{(2l+1)!!}\exp(x)M_l^s(x) \tag{C.41}$$

$$M_l^s = \frac{(2l+1)!!}{x^l}M_l'(x) = \frac{(2(t+u+\nu)+1)!!}{\left(\frac{k_Ak_B}{2\alpha}\right)^{t+u+\nu}}M_l'(x). \tag{C.42}$$

The integral Q is reduced now to

$$\begin{aligned} Q_{\lambda\mu}^{\lambda+\mu+2-2\nu} =& \frac{\pi^{1/2}}{4\alpha^{3/2}}\left(\frac{1}{2\alpha}\right)^{2\nu}\left(\frac{k_A}{2\alpha}\right)^{\lambda-\nu}\left(\frac{k_B}{2\alpha}\right)^{\mu-\nu}\frac{(2(\lambda+\mu-\nu)+1)!!}{(2\nu-1)!!} \\ &\times \exp\left(\frac{(k_A+k_B)^2}{4\alpha}\right)\sum_{t=0}^{\lambda-\nu}\sum_{u=0}^{\mu-\nu}\binom{\lambda-\nu}{t}\binom{\mu-\nu}{u} \\ &\times \frac{(2(t+\nu)-1)!!(2(u+\nu)-1)!!}{(2(\mu+t)+1)!!(2(\lambda+u)+1)!!}\left(\frac{k_B}{k_A}\right)^{t-u} \\ &\times (2(t+u+\nu)+1)M_{t+u+\nu}^{r}\left(\frac{k_Ak_B}{2\alpha}\right) \end{aligned} \tag{C.43}$$

Type 1 Radial Integral

$$Q_l^n(k,\alpha) = \sqrt{\pi}k^l 2^{-l-2}\alpha^{-\frac{(l+n+1)}{2}}R(l,n)\phi\left(\frac{(l+n+1)}{2}; l+\frac{3}{2}; \frac{k^2}{4\alpha}\right), \tag{C.44}$$

here R is the ratio of gamma functions

$$R(l,n) = \frac{\Gamma((l+n+1)/2)}{\Gamma(l+\frac{3}{2})} = \frac{(l+n-1)!!}{(2l+1)!!} 2^{\frac{l}{2}+1-\frac{n}{2}}, \quad n+l \text{ even} \tag{C.45}$$

$$= \frac{(\frac{l+n-1}{2})!!}{\sqrt{\pi}(2l+1)!!} 2^{(l+1)}, \quad n+l \text{ odd.} \tag{C.46}$$

In Eq. C.44 ϕ is the degenerate hypergeometric function. The confluent hypergeometric series for ϕ is

$$\phi(a,b,c) = 1 + \frac{a}{b}\frac{z}{1!} + \frac{a(a+1)}{b(b+1)}\frac{z^2}{2!} + \cdots \tag{C.47}$$

REFERENCE LIST

[1] K. M. Sando and S. I. Chu. *Adv. At. Mol. Phys.*, 25:133, 1988.

[2] B. J. Archer, N. F. Lane, and M. Kimura. *Phys. Rev. A*, 42:6379, 1990.

[3] E. Czuchaj, F. Rebentrost, H. Stoll, and H. Preuss. *Chem. Phys.*, 196:37, 1995.

[4] W. Behmenburg, A. Makonnen, A. Kaiser, F. Rebentrost, V. Staemmler, M. Jungen, G. Peach, A. Devdariani, S. Tserkovnyi, A. Zagrebin, and E. Czuchaj. *J. Phys. B*, 29:3891, 1996.

[5] N. Andersen, J. T. Broad, E. E. Campbell, J. W. Gallagher, and I. V. Hertel. *Phys. Reports*, 278:107, 1997.

[6] F. Stienkemeier, J. Higgins, W. E. Ernst, and G. Scoles. *Z. Phys. B.*, 98:413, 1995.

[7] J. P. Toennies and A. F. Vilesov. *Ann. Rev. Phys. Chem.*, 49:1, 1998.

[8] J. Reho, J. Higgins, C. Callegari, K. K. Lehmann, and G. Scoles. *J. Chem. Phys.*, 113:9694, 2000.

[9] J. P. Toennies, A. F. Vilesov, and K. B. Whaley. *Phys. Today*, 31:31, 2001.

[10] M. Kimura and N. F. Lane. *Adv. At. Mol. Opt. Phys.*, 26:79, 1990.

[11] E. E. Nikitin and S. Y. Umanskii. *Theory of Slow Atomic Collisions.* Springer-Verlag, Berlin, 1984.

[12] R. B. Bernstein. *Atom-Molecule Collision Theory.* Plenum Press, New York, 1979. R. B. Bernstein (editor).

[13] R. W. Anderson, V. Aquilanti, and D. R. Herschbach. *Chem. Phys. Lett.*, 4:5, 1969.

[14] J. Ostgaard Olsen, N. Andersen, and T. Andersen. *J. Phys. B*, 10:1727, 1977.

[15] S. E. Nielsen, N. Andersen, T. Andersen, J. Ostgaard Olsen, and J. S. Dahler. *J. Phys. B*, 11:3187, 1978.

[16] W. Mecklenbrauck, J. Schon, E. Speller, and V. Kempter. *J. Phys. B*, 10:3271, 1977.

[17] P. J. Dagdigian and M. L. Campbell. *Chem. Rev.*, 87:1, 1987.

[18] P. J. Dagdigian. *Selectivity in Chemical Reaction.* Kluwer Acad. Publ., Dordrecht, 1988. J. C. Whitehead (editor).

[19] C. J. Smith, E. M. Spain, M. J. Dalberth, S. Leone, and J. P. J. Driessen. *J. Chem. Soc. Faraday Trans.*, 89:1401, 1993.

[20] H. Ferkel, A. Koch, and R. Feltgen. *J. Chem. Phys.*, 100:2690, 1994.

[21] K. Runge, D. A. Micha, and E. Q. Feng. *Intern. J. Quantum Chem. Symposium*, 24:781, 1990.

[22] E. Q. Feng, D. A. Micha, and K. Runge. *Intern. J. Quantum Chem.*, 40:545, 1991.

[23] D. A. Micha and K Runge. *Phys. Rev. A.*, 50:322, 1994.

[24] K. Runge and D. A. Micha. *Phys. Rev. A*, 53:1388, 1996.

[25] E. Deumens, A. Diz, R. Longo, and Y. Öhrn. *Rev. Mod. Phys*, 66:917, 1994.

[26] C. Courbin and V. Sidis. *J. Phys. B*, 18:699, 1985.

[27] R. H. Reid. *J. Phys. B*, 6:2018, 1973.

[28] J. Pascale and R. E. Olson. *J. Chem. Phys.*, 64:3358, 1976.

[29] D. Lemoine, J. M Robbe, and B. Poully. *J. Phys. B*, 27:1007, 1988.

[30] G. C. Schatz, L. J. Kovalenko, and S. R. Leone. *J. Chem. Phys.*, 91:6961, 1989.

[31] W. Behmenburg, A. Kaiser, F. Rebentrost, M. Jungen, M. Smit, M. Luo, and G. Peach. *J. Phys. B*, 31:689, 1998.

[32] N. Andersen and S. E. Nielsen. *Adv. At. Mol. Phys.*, 18:265, 1982.

[33] C. Bottcher. *J. Phys. B*, 4:1140, 1971.

[34] W. E. Baylis. *J. Chem. Phys.*, 51:2665, 1969.

[35] M. Kimura and J. Pascale. *J. Phys. B*, 18:2719, 1985.

[36] E. E. Nikitin. *J. Chem. Phys.*, 43:744, 1965.

[37] F. Masnou-Seeuws and E. Roueff. *Chem. Phys. Lett.*, 16:593, 1972.

[38] F. Masnou-Seeuws. *J. Phys. B*, 3:1437, 1970.

[39] F. Masnou-Seeuws and R. McCarrol. *J. Phys. B*, 7:2230, 1974.

[40] L. J. Kovalenko, S. R. Leone, and J. B. Delos. *J. Chem. Phys.*, 91:6948, 1989.

[41] E. Czuchaj, F. Rebentrost, H. Stoll, and H. Preuss. *Chem. Phys.*, 136:79, 1989.

[42] J. Pascale. *Phys. Rev. A*, 28:632, 1983.

[43] H. Hellmann. *J. Chem. Phys.*, 3:61, 1935.

[44] H. Hellmann and W. Kassatotschkin. *Acta Fizicochem. USSR*, 5:23, 1936.

[45] P. Gombas. *Z. Phys*, 94:473, 1935.

[46] L. Szasz. *Pseudopotential Theory of Atoms and Molecules.* John Wiley and Sons, New York, 1985.

[47] J. C. Phillips and L. Kleinman. *Phys. Rev.*, 116:287, 1959.

[48] L. R. Kahn, P. Baybutt, and D. G. Truhlar. *J. Chem. Phys.*, 65:3826, 1976.

[49] P. J. Hay, W. R. Wadt, , and L. R. Kahn. *J. Chem. Phys.*, 68:3059, 1978.

[50] J. N. Bardsley. *Case Stud. At. Phys.*, 4:299, 1974.

[51] J. Pascale and J. Vandeplaque. *J. Chem. Phys.*, 60:2278, 1974.

[52] R. Duren and G. Moritz. *J. Chem. Phys.*, 73:5155, 1980.

[53] R. Duren. *Adv. At. Mol. Phys.*, 16:55, 1980.

[54] G. Peach. *Comments At. Mol. Phys.*, 14:101, 1982.

[55] E. Czuchaj, F. Rebentrost, H. Stoll, and H. Preuss. *Chem. Phys. Lett.*, 173:573, 1990.

[56] Y. S. Kim and R. G. Gordon. *J. Chem. Phys.*, 61:1, 1974.

[57] S. H. Patil. *J. Chem. Phys.*, 86:7000, 1987.

[58] P. Fuentealba, H. Press, H. Stoll, and L. V. Szentpaly. *Chem. Phys. Lett.*, 89:418, 1982.

[59] C. E. Moore. *US Natl. Bur. Stds. Circular No. 467, Vols. 1, 2, 3.* US Govt. Printing Office, Washington, 1958.

[60] S. Obara and A. Saika. *J. Chem. Phys.*, 89:1540, 1988.

[61] L. E. McMurchie and E. R. Davidson. *J. Computat. Phys.*, 44:289, 1981.

[62] R. M. Pitzer and N. W. Winter. *Intern. J. Quantum Chem.*, 40:773, 1991.

[63] P. Schwerdtfeger and H. Silberbach. *Phys. Rev. A*, 37:2834, 1988.

[64] H. J. Werner and P. J. Knowles. *MOLPRO.* University of Birmingham, Birmingham, 2000.

[65] H. Lischka, R. Shepard, I. Shavitt, R. M. Pitzer, M. Dallos, Th. Müller, P. G. Szalay, F. B. Brown, R. Ahlrichs, H. J. Bvhm, A. Chang, D. C. Comeau, R. Gdanitz, H. Dachsel, C. Ehrhardt, M. Ernzerhof, P. Hvchtl, S. Irle, G. Kedziora, T. Kovar, V. Parasuk, M. J. M. Pepper, P. Scharf, H. Schiffer, M. Schindler, M. Schler, M. Seth, E. A. Stahlberg, J. G. Zhao, S. Yabushita, and Z. Zhang. *COLUMBUS, an ab initio electronic structure program, release 5.8.* Ohio State University, Colombus, 2001.

[66] C. J. Lee, M. D. Havey, and R. P. M. Meyer. *Phys. Rev. A*, 43:77, 1991.

[67] G. Theodorakopoulos and I. Petsalakis. *J. Phys. B*, 26:4367, 1993.

[68] K. Runge and D. A. Micha. *Phys. Rev. A*, 62:22703, 2000.

[69] R. N. Zare. *Angular Momentum.* J. Wiley, New York, 1988.

[70] K. Runge. *A Time-Dependent Many-Electron Approach to Atomic and Molecular Interactions.* PhD dissertation, University of Florida, Physics Department, 1993.

[71] A. Reyes, D. A. Micha, and K. Runge. *Chem. Phys. Lett.*, 363:441, 2002.

[72] J. Manique, S. E. Nielsen, and J. S. Dahler. *J. Phys. B*, 10:1703, 1977.

[73] P. J. Leo, G. Peach, and I. B. Whittingham. *J. Phys. B*, 33:4779, 2000.

[74] A. Nakayama and K. Yamashita. *J. Chem. Phys.*, 114:780, 2001.

[75] W. G. Richard, H. P. Trivedi, and D. L. Cooper. *Spin-Orbit Coupling in Molecules.* Oxford Univ. Press, Oxford, 1981.

[76] E. U. Condon and G. H. Shortley. *The Theory of Atomic Spectra.* Cambridge University Press, London, 1935.

[77] R. McWeeny. *Methods of Molecular Quantum Mechanics.* Academic Press, San Diego, CA, 2nd edition, 1989.

[78] R. M. Pitzer and N. W. Winter. *J. Phys. Chem.*, 92:3061, 1988.

[79] W. C. Ermler, Y. S. Lee, P. A. Christiansen, and K. S. Pitzer. *Chem. Phys. Lett.*, 81:70, 1981.

[80] L. F. Pacios and P. A. Christiansen. *J. Chem. Phys.*, 82:2665, 1984.

[81] A. Nicklass, M. Dolg, H. Stoll, and H. Preuss. *J. Chem. Phys.*, 102:8942, 1995.

[82] A. D. Wilson and Y. Shimoni. *J. Phys. B*, 8:2415, 1975.

[83] J. C Gay and W. B. Schneider. *Z. Phys.*, 278:211, 1976.

[84] J. Pitre and L. Krause. *Can. J. Phys.*, 45:2671, 1969.

[85] J. Pascale. *XIII Summer School on Quantum Optics.* Plenum Press, New York, 1985. J. Fiutak and J. Mizerski (editors).

[86] W. B. Schneider. *Z. Phys.*, 248:387, 1971.

[87] M. Elbel, B. Kamke, and W. B. Schneider. *Physica*, 77:146, 1974.

BIOGRAPHICAL SKETCH

Andrés Reyes, the third child of Luz Nancy Velasco and Miguel Reyes, was born on the 11th of March of 1974 in Cali, Colombia. His life as a child was other than typical since when he was very young his mother came to the United States to work to support his family.

Although his life was not easy, he found comfort in reading. He loved as a child watching TV series like *Cosmos*, *Nova* and *Planet Earth*. He thought that maybe one day he could be the one on the other side of the screen.

During his years at school he excelled in math and when applying to college he wanted to be an engineer. Fortunately he was not accepted in engineering but in chemistry. After spending a little more than five years at Universidad del Valle (Cali) he came in 1997 to the prestigious QTP group at the University of Florida to pursue graduate studies under the supervision of David A. Micha to work on computational aspects of atomic collisions.

He is now looking for a postdoctoral position on the computational aspects of systems with more than two atoms.

He has a strong sentimental bond with his country, Colombia, and expects that one day he may go back with his family to live a humble life there happily ever after.

I certify that I have read this study and that in my opinion it conforms to acceptable standards of scholarly presentation and is fully adequate, in scope and quality, as a dissertation for the degree of Doctor of Philosophy.

D. A. Micha, Chairman
Professor of Chemistry

I certify that I have read this study and that in my opinion it conforms to acceptable standards of scholarly presentation and is fully adequate, in scope and quality, as a dissertation for the degree of Doctor of Philosophy.

A. Rettberg
Assistant Scientist

I certify that I have read this study and that in my opinion it conforms to acceptable standards of scholarly presentation and is fully adequate, in scope and quality, as a dissertation for the degree of Doctor of Philosophy.

Y. N. Öhrn
Professor of Chemistry

I certify that I have read this study and that in my opinion it conforms to acceptable standards of scholarly presentation and is fully adequate, in scope and quality, as a dissertation for the degree of Doctor of Philosophy.

N. Richards
Professor of Chemistry

I certify that I have read this study and that in my opinion it conforms to acceptable standards of scholarly presentation and is fully adequate, in scope and quality, as a dissertation for the degree of Doctor of Philosophy.

S. B. Trickey
Professor of Physics

This dissertation was submitted to the Graduate Faculty of the Department of Chemistry in the College of Liberal Arts and Sciences and to the Graduate School and was accepted as partial fulfillment of the requirments for the degree of Doctor of Philosophy.

May 2003

Dean, Graduate School